2019

Investigating Anions and Hydrophobicity of Deep Eutectic Solvents by Experiment and Computational Simulation

Amos Kwabena Dwamena
South Dakota State University

INVESTIGATING ANIONS AND HYDROPHOBICITY OF DEEP EUTECTIC SOLVENTS BY EXPERIMENT AND COMPUTATIONAL SIMULATION

BY

AMOS KWABENA DWAMENA

A dissertation submitted in partial fulfilment of the requirements for the

Doctor of Philosophy

Major in Chemistry

South Dakota State University

2019

INVESTIGATING ANIONS AND HYDROPHOBICITY OF DEEP EUTECTIC SOLVENTS BY EXPERIMENT AND COMPUTATIONAL SIMULATION

AMOS KWABENA DWAMENA

This dissertation is approved as a creditable and independent investigation by a candidate for the Doctor of Philosophy in Chemistry degree and is acceptable for meeting the dissertation requirements for this degree. Acceptance of this dissertation does not imply that the conclusions reached by the candidate are necessarily the conclusions of the major department.

Douglas E. Raynie, Ph. D. Date

Dissertation Advisor

Department Head, Chemistry & Biochemistry

Dean, Graduate School Date

I dedicate this dissertation to my wife and son.

ACKNOWLEDGEMENTS

To God be the glory for all things He has done. I am grateful to God for taking the front seat of my education in the United States. To my wife, Mercy Adoma Fosu, I am forever thankful to you for your unflinching support, love, and care all this while. I couldn't have gone through this journey alone without you. To my lovely son, Josiah Nhyiraba Dwamena, your presence made everything joyful. I thank you Dr. Douglas Raynie, my academic and dissertation advisor for the mentorship, training, guidance, and tutelage throughout the course of my studies. To my academic committee members, Dr. Matthew Miller, Dr. Surtaj Iram, and Dr. Robert Fourney, I am grateful for your useful feedback, reviews, and overall assistance during my studies. I am forever indebted to my parents Mr. Stephen K.A. Fosu and Mrs. Lucy Boatemaa for their encouragement, prayers, and support throughout my education. I am thankful to my siblings Antwi, Nimoh, Boateng, Rose, Sekyere, Augustine, and Addo for your support. I am grateful to my past and present labmates for their love, support, and motivation. I would also want to thank the Department of Chemistry and Biochemistry of the South Dakota State University for giving me the chance and supporting me financially throughout my studies. Also, I appreciate the Pharmacy and Ag. Engineering Departments for granting me access to their instruments. Last but not the least, I would like to thank the Holy Life Tabernacle Church, Brookings for feeding me spiritually through their constant prayers. A special thanks to SGS North America, Brookings and Raven Industries, Sioux Falls (especially the late Dr. Harry Harlow) for giving me practical training through internships. A special thanks to Joey and Angela Johnson for opening their doors for me during my stay in Sioux Falls. ALL GLORY BE TO GOD.

CONTENTS

LIST OF FIGURES

LIST OF TABLES

LIST OF EQUATIONS

LIST OF ABBREVIATIONS

α……..…Hydrogen bond donor acidity

β……..…….Hydrogen bond accepter basicity

π*……..……...Dipolarity/polarizability parameter

mg ……..…….Milligram

μL ……..…….Microliter

°C ……..…….Degree Celsius

% ……..…….…….Percentage

cm……..…….…….Centimeter

DES……..……..…….Deep eutectic solvent

HDES……..…….Hydrophobic deep eutectic solvent

FTIR……..…….……..…Fourier transformed infrared

g ……..……..……. Gram

λ_{max}……..……...….Maximum absorption wavelength

GLP……..……...….Good laboratory practices

kg……..……...Kilogram

HBA ……..…….Hydrogen bond acceptor

HBD ……..…….Hydrogen bond donor

cP……..……..…….Centipoise

kcal ……..……..…….kilocalories

M ……..…….…….Molar

aw……..…….…….Water activity

ΔHvap ……..…….……. Enthalpy of vaporization

kJ …….…….…….kilojoules

mp…….…….…….Melting point

K_{OW} …….……..…….Octanol/water partition coefficient

mg…….…….…….Milligram

SS …….…….Shear stress

VOCs…….…….Volatile organic compounds

mL…….…….Milliliter

SR…….…….…….Shear rate

^{1}H-NMR…….. ……..…….Proton nuclear magnetic resonance

Pa …….……. Pascal

RI …….…….…….Refractive Index

rpm …….……..……. Revolution per minute

T_d …….……. Decomposition temperature

T_{onset}…….……...Onset decomposition temperature

T_f …….…….……. Freezing temperature

T_g …….……. Glass transition temperature

T_m …….…….…….Melting temperature

EPA…….……..……Environmental Protection Agency

COSMO…….…….…….....Conductor-like screening model

QAS …….……...…...Quaternary ammonium salts

LCA…….…….……...…..Life-cycle analysis

UV-Vis …….…….....Ultra violet-visible

wt. …….……...….Weight

w% …….……Weight percent

ILs …….……..... Ionic liquids

DMSO-d6 …….…….....Deuterated dimethyl sulfoxide

[Ch]Cl…….…….…...Choline chloride

[Ch]Br…….…….…..Choline bromide

[Ch]I…….…….….Choline iodide

[Ch]Cl:BA…….…….…....Choline chloride/butyric acid mixture

[Ch]Cl:VA …….……. …….....Choline chloride/valeric acid mixture

[Ch]Cl:HA…..……....….Choline chloride/hexanoic acid mixture

[Ch]Cl:CA…….……Choline chloride/caprylic acid mixture

DFT …….…….…… Density functional theory

ABSTRACT

INVESTIGATING ANIONS AND HYDROPHOBICITY OF DEEP EUTECTIC SOLVENTS BY EXPERIMENT AND COMPUTATIONAL SIMULATION

AMOS KWABENA DWAMENA

2019

Deep eutectic solvents are a new generation of ionic liquid-like solvents formed by combining hydrogen bond acceptor with hydrogen bond donor which result in the depression of the melting point of the solvent. Like ionic liquids, anions play a critical role in tuning the polarity, physicochemical properties, and thermodynamic behavior of deep eutectic solvent (DES). Choline chloride is the most widely used quaternary ammonium salt (QAS) in the literature and has remarkable advantages from reduced cost to low toxicity and volatility. Choline bromide and choline iodide are other QAS that have not been used often for DES synthesis and applications, probably with the opinion that chlorides form stronger hydrogen bonds. Developing new DES from these anions will broaden the scope of green solvents selection for diverse applications.

The first objective of this dissertation looked into the synthesis and characterization of DES from choline chloride, choline bromide, and choline iodide with malic acid, malonic acid, and urea. Also, we studied the thermodynamic behavior of the solvents by measuring their vapor pressure, density, and infinite activity coefficient in polar and

nonpolar solvents. The results show that choline bromide can sometimes be used to replace choline chloride because both QAS share comparable physicochemical behavior. In most cases, choline iodide forms weaker hydrogen bonding with the donors leading to the formation of a solid at room temperature. Nevertheless, all the solvents have melting temperature below 100℃. In summary, DES can be synthesized from the choline cation bonded with the halides, with the melting point and nature of the solvent dependent on the hydrogen bond donor (HBD).

Secondly, despite the rapid rise in publications and applications since their inception in 2001, most of the DES synthesized are generally hydrophilic. The low cost, low toxicity, and bioavailability of DES make the solvent green and sustainable for diverse applications. Conversely, the hydrophilicity of DES practically limits their application to only polar compounds, which is a major drawback of the solvent. For the past three years, hydrophobic deep eutectic solvents (HDES) have emerged as alternative extractive media capable of extracting nonpolar molecules from aqueous environments. In chapter three of this dissertation, the general objective was to design a cost-effective hydrophobic DES from choline chloride and fatty acids. Varying the alkyl chain of the fatty acid broadened our understanding about the role of HBD in DES and also helped in the tunability of the HDES polarity. Due to the infancy of HDES, for the first time, this dissertation expands on the design, synthesis, and physicochemical characterization of HDES developed from choline chloride and fatty acids. To understand the hydrogen-bonding pattern of HDES, a multivariate unsupervised principal component analysis was used to cluster HDES by using known DES as a control. The HDES was able to extract about 70% of piperine, a bioactive

compound from *Piper nigrum*. In the future, it is believed that HDES could replace the majority of toxic organic solvents used for analytical purposes.

Lastly, the electronic and molecular properties of the HDES synthesized were studied by using a solvatochromic molecular probes and a hybrid density functional theory at 6-31G (d) basis set. The empirical polarity assay and quantum theoretical calculations showed that decreasing the alkyl chain length of the hydrogen bond donor increases viscosity of the DES. Optimization of the DES molecular geometry indicates a reduced bond angle between the C15-O16-H17 atoms in choline chloride, signifying a change in electronegativity of the central atom (O16) during DES formation. From our results, we predict a possible molecular reorientation between the donor and the acceptor molecules during DES formation. The combined theoretical calculations and experimental approaches are useful to establish clear correlations between electronic parameters and physiochemical parameters like polarity, viscosity, and stability of carboxylic acid-DES and can be extended to other conventional solvents.

CHAPTER ONE

INTRODUCTION

1.1. Background

Solvents are substances, mostly a liquid, in which other materials dissolve to form a solution. Solvents are integral part of everyday activities and can serve in an array of applications including media for chemical synthesis, pharmaceuticals, agrochemicals, paints, inks, coatings, extraction, and industrial cleaning. About three decades ago, most of these applications employed the use of organic solvents. For example, during the first four decades of the 20th century, benzene was used as a hand-cleanser and also as an aftershave until its carcinogenic properties were brought to light[1-2]. The lack of precaution and increased exposure to benzene was in part due to inadequate data on benzene toxicity and its cheaper price compared to other alternatives[1]. Organic solvents, also known as carbon-bonded solvents[3], are typically volatile compounds which often vaporize even at room temperature. These volatile organic compounds (VOCs) have numerous environmental and health concerns. The increasing demand for solvents has been forecasted to reach about 9.6 billion pounds by 2020 in the United States (Coatings World, last accessed 4-19-19). This growth is driven by a strict US Environmental Protection Agency (EPA) regulations to shift solvents toward a more eco-friendly and biodegradable alternatives with reduced emissions and toxicity.

The concept of green chemistry emerged during the early works by Trost and Sheldon about economical use of mass (atom economy[4] and synthesis efficiency[5]) and E-factor[6], respectively. The field of green chemistry revamped after the 12 principles by

Warner and Anastas were stipulated in 1998[7]. Since then, a number of industries and pharmaceutical companies like Pfizer have laid down a restrictive guideline to help in the selection of solvents and reagents. According to the Pfizer solvent selection guide for medicinal chemistry (Table 1.1)[2], if one is to choose any solvent, water is preferred rather than cyclohexane and pentane. Nevertheless, in chemical synthesis and processing, cyclohexane is usable compared to pentane. Due to the environmental, health, and safety implications of some organic solvents, the impetus in solvent replacement is growing globally.

Table 1.1 Pfizer solvent selection table for medicinal chemistry[2]

Preferred	Usable	Undesirable
Water	Cyclohexane	Pentane
Acetone	Heptane	Hexane(s)
2-Propanol	Toluene	Diethyl ether
1-Propanol	Methylcyclohexane	Dichloromethane (DCM)
Ethyl acetate	Methyl *t*-butyl ether	Chloroform
Isopropyl acetate	Isooctane	Dimethyl formamide
Methyl ethyl ketone	Acetonitrile	*N*-Mehtylpyrrolidonone

Table 1.2 Pfizer solvent replacement table

Solvent	Concerns/Issues	Alternatives
Pentane	Lower flash point than other similar solvents	Heptane
Diethyl ether	Lower flash point than other similar solvents	2-MeTHF, TBME
Diisopropyl ether	Powerful peroxide formation agent	2-MeTHF, TBME
Hexane(s)	More toxic than other similar solvents	Heptane
Benzene	Carcinogen	Toluene
Chloroform	Carcinogen	DCM

According to the Pfizer solvent replaceable table (Table 1.2)[2, 8], it is preferable to use dichloromethane (DCM) instead of chloroform or carbon tetrachloride when a process or a reaction requires a chlorinated solvent. Solvent substitution with similar structural

alternatives may present many of the same health, environmental, and safety concerns of the primary solvent (i.e., the solvent to be substituted)[8]. With reference to the above example, DCM is regarded as a greener solvent compared to chloroform or carbon tetrachloride. On the contrary, DCM has high vapor pressure and is an occupational health threat[9]. Also, solvent replacement should be done without compromising the compatibility and process functionality of the primary solvent. Due to the increasing regulatory measures and continues amendments of the EPA regulations, especially concerning VOCs, the exponential rise in market demand for green solvents in the 21st century is not shocking.

A common question that often surfaces is "how green is a green solvent?" A green solvent should encompass the environmental and health safety (EHS), life cycle analysis (LCA), energy demand, and toxicity of the solvent in question[8]. A detailed assessment of solvents for these parameters is invaluable in the call for environmental sustainability. The concept of green chemistry and green solvents is actively under research in the quest to design and develop new solvents to replace conventional organic solvents. Ionic liquids and deep eutectic solvents are among the new generation of solvents under study due to their tunability and lower volatility.

1.2. Green solvents

1.2.1. Green solvents emergence: Ionic liquids and deep eutectic solvents

Ionic liquids (ILs) are salts with melting temperature lower than the boiling point of water (< 100 °C)[10]. ILs are completely ionic consisting of organic cations and organic or inorganic polyatomic anions[10-11]. The first report of ionic liquids date back in 1914 during the preparation of ethylammonium nitrate from a concentrated nitric acid and

ethylamine followed by water removal by distillation[10]. The resulting pure salt remained liquid at room temperature. Most importantly, the formation of the desired cation and the anion exchange process are key steps to ILs formation. In 1948, Hurley and Weir found that an anion exchange reaction between Lewis acid ($AlCl_3$, 67% by mole) dissolved in fused ethyl pyridinium bromide forms a very low melting eutectic with a melting point at -40 °C[12-13]. The addition of Lewis acid to a halide salt is by far one of the most simple methods of synthesizing ionic liquids[10].

1.2.2. Synthesis of ILs

The first step in the synthesis of ILs is the quaternization of a pyridine, sulfide, imidazole, phosphine, or amine by using an alkylating agent (choice depends on the desired anion required in the ILs) to form the cation[14]. From Figure 1.1, quaternization of NR_3 with alkylating agent (+R'X) leads to the formation of ILs ($[R'R_3N]^+X^-$). Anion exchange reactions can occur by using a Lewis acid (MX_y) to form $[R'R_3N]^+[MX_{y+1}]^-$ (Equation 1.1) as seen in the synthesis of ethylammonium nitrate. A reaction between $[R'R_3N]^+ Cl^-$ and $AlCl_3$ (Lewis acid) by a series of equilibria is shown (Equations 1.2-1.4). The availability of excess Lewis acid in ILs synthesis can lead to the formation of unwanted by-products, hence, ensuring purity at each reaction step is critical. From Figure 1.1 step 2b, the addition of a metal salt $M^+[A]^-$ or a strong acid $H^+[A]^-$ can displace or exchange the anion in the initial step. This displacement process is called anion metathesis. A notable example of anion metathesis is the formation of water-insoluble ILs, $[EMIM][PF_6]$, from [EMIM]Cl and HPF_6 in aqueous solution[14].

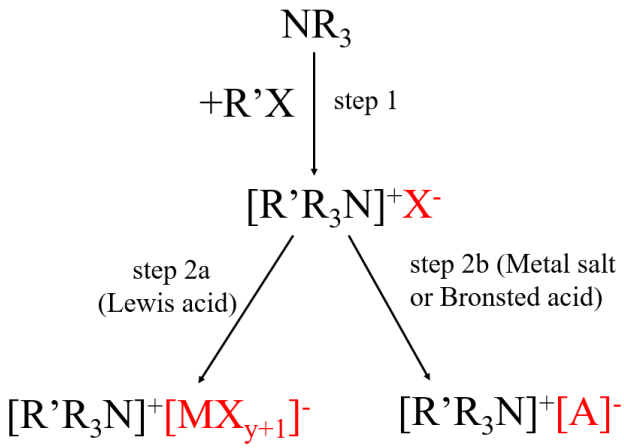

Figure 1.1. Schematic pathway for preparation of ammonium salt-based ionic liquids[14].

$$[R'R_3N]^+ X^- + MX_y \longleftrightarrow [R'R_3N]^+ [MX_{y+1}]^- \quad \text{(Equation 1.1)}$$

$$[R'R_3N]^+ Cl^- + AlCl_3 \longleftrightarrow [R'R_3N]^+ AlCl_4^- \quad \text{(Equation 1.2)}$$

$$[R'R_3N]^+ AlCl_4^- + AlCl_3 \longleftrightarrow [R'R_3N]^+ Al_2Cl_7^- \quad \text{(Equation 1.3)}$$

$$[R'R_3N]^+ Al_2Cl_7^- + AlCl_3 \longleftrightarrow [R'R_3N]^+ Al_3Cl_{10}^- \quad \text{(Equation 1.4)}$$

The precipitate, M^+X^-, is an impurity which needs to be cleaned before applying the solvent especially for pharmaceutical or clinical purposes. The thriving interest in ionic liquids stem from its nonvolatile nature with several advantages making them suitable candidates to replace VOCs[15-18]. Compared to conventional organic solvents, ionic liquids are still expensive. The synthesis coupled with extensive cleaning or purification steps, make ionic liquids expensive for industrial applications. Several recycling procedures have been outlined in literature including using supercritical CO_2[19], palladium coupling[20], and membrane techniques look promising[10]. The density, viscosity, solvation, solubility, density, melting, and other physicochemical properties of ILs have been comprehensively

reviewed[14]. Ionic liquids in biomedical and pharmaceutical applications[21-22], protein analysis[23], water treatment[24], textiles[25], biomass[26], and metal dissolution and extraction[27] has been reviewed recently. The ability to tune ILs to suit a particular process condition and functionality is one of the many driving forces for the continued research into these room-temperature solvents. For instance, changing the anion on imidazolium cation ([EMIM]) ILs influences the melting point of the liquid. [EMIM]Cl has a mp of 87 °C[14, 28], [EMIM]NO_2 has mp of 55 °C[14, 29], [EMIM]NO_3 has mp of 38 °C[14, 29], [EMIM]$AlCl_4$ has mp of 7 °C[30], [EMIM]BF_4 has *T*g of 6 °C[31], [EMIM]CF_3SO_3 has mp of -9 °C[14, 32], and [EMIM]CF_3CO_2 has mp of -14 °C[14, 32]. Changing the anion size of the imidazolium ILs decreases or increases the mp of the resulting liquid. A hydrophobic ILs from 1,3-dialkyl imidazolium cations and hydrophobic anions have been reported[32]. ILs can be tailored by modifying the cations or anions depending on the required application of the solvent.

1.2.3. Emergence of DES

Concerning the issues of cost and impurities, especially water, associated with ILs, a new generation of ILs called deep eutectic solvents (DES) has surfaced a little over a decade ago. As an extension of ILs, DES share similar characteristics like ILs and are formed from eutectic mixture of Brønsted or Lewis acids and bases[33]. The formation of DES depends on the magnitude of interaction that happen between the individual components involved[34]. Fig. 1.2 depicts a binary interaction between component A and component B to form a binary mixture A + B. Unlike theoretical ideal mixtures, this interaction results in a larger value of ΔT_f[34]. The eutectic point is reached when the correct molar fraction (ratio) of component A interacts with component B. At this point, a melting

point depression is observed as shown in the phase diagram. Typically, deep eutectic solvents are classified into 4 categories (Table 1.3) with type III as a focus of attention in most research. The Cat^+ in DES is usually quaternary ammonium, phosphonium, or sometimes sulfonium salt[34]. The X^- is the anionic moiety often involved in hydrogen bonding with protons from the donor RZ group. Choline chloride is the most used QAS for DES synthesis due to its low cost, availability, biocompatibility, and low toxicity.

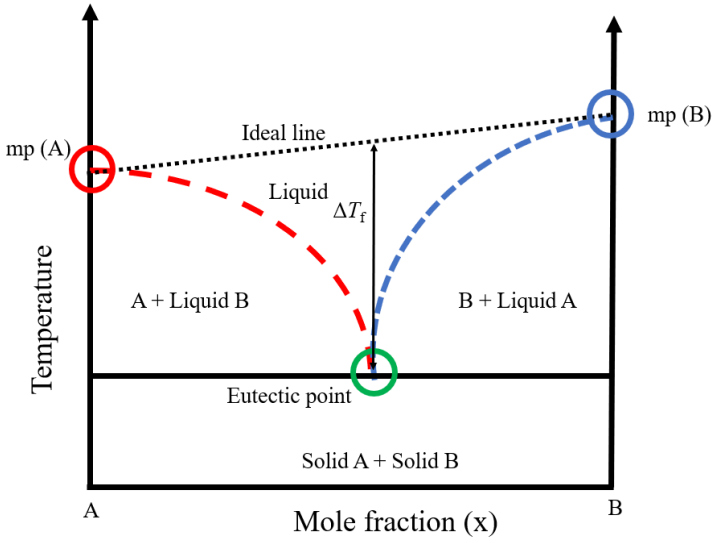

Figure 1.2. A eutectic point of two-component phase diagram.

Table 1.3. General Formula for DES classification[34].

Type	General formula	Terms
type I	$Cat^+X^-zMCl_x$	M = Zn, Sn, Al, Ga, In
type II	$Cat^+X^-zMCl_x.yH_2O$	M = Cr, Co, Cu, Ni, Fe
type III	Cat^+X^-zRZ	Z = $CONH_2$, COOH, OH
type IV	$MCl_x + RZ = MCl_{x-1}^+ \cdot RZ + MCl_{x+1}^-$	M = Al, Zn and Z = $CONH_2$, OH

The chloride anion is readily available to interact with diverse proton donors through hydrogen bonding. Abbott and co-workers found that choline chloride (mp = 302 ℃) and urea (mp = 133 ℃) interact to form a liquid at room temperature with a freezing point of 12 ℃ at 1:2 molar ratio[34]. DES is synthesized by combining a hydrogen-bond acceptor (HBA) and a hydrogen-bond donor (HBD)[35-37]. DES physicochemical properties like conductivity, viscosity, polarity, and thermal properties can easily tuned by varying the molar ratios of the constituent materials. Most of the synthesized DES reviewed[34, 38-39] are hydrophilic. The type III DES are categorized into low-transition-temperature mixtures (LTTMs), natural deep eutectic solvents (NADES), carboxylic acid-based deep eutectic solvents[35, 40-41], and therapeutic deep eutectic solvents (THEDES)[42-43].

Since most DES are synthesized by combining naturally occurring proton donors like fatty acids, urea, glucose, or glycerol with acceptor molecules like choline chloride. The combined mixture is environmentally benign, safe, and sustainable[34-36, 39, 44-46]. The advantages of using DES for extraction goes beyond its simple preparation procedures, greener nature, and easy tunability [40, 46-47] but also is bioavailable and low toxicity. DES chemical and physical properties are flexible to adjust by simply changing the molar ratio of the constituents.

1.3. Scope of research

1.3.1. Problem Statement

Scientists continue to search for greener solvents capable of replacing conventional toxic VOCs in their daily activities[15, 48-50]. The challenge emanates when it becomes difficult to acquire a more sustainable greener alternative to toxic chemicals with desired

chemical and physical properties[48]. In most cases, ensuring the availability of greener solvents tunable to replace nongreen solvents is problematic for most scientists[51]. Despite the numerous publications about DES since its first inception in 2001[33-34], most research work has concentrated mainly on hydrophilic DES which limits the solvents utilization to polar environments[34, 52]. In an application that requires hydrophobic media, the common truth is that most scientists still resort to toxic organic chemicals due to the scarcity of greener hydrophobic alternatives. This is a major drawback to the call for environmental sustainability. The availability of greener solvents in all of the four solvent categories (high basicity-low polarity, low basicity-low polarity, high basicity-high polarity, and low basicity-high polarity) is pivotal to ensuring sustainability[51]. A hydrophobic ILs involving $[NTf_2]$ anion, ([Bmim][NTf_2]), was reported to be more efficient in the enzymatic synthesis of biodiesel compared to the hydrophilic $[PF_6]$ and $[BF_4]$ anionic counterparts[53]. A review of the application of hydrophobic ILs in biodiesel synthesis is available[54]. To date, nearly all deep eutectic solvents are hydrophilic and are limited in applications that require high basicity and low water content. In Figure 1.3., a Web of Science search of the phrase "deep eutectic solvents" shows an increasing number of publications since 2004. Out of the 1860 hits, over 88 % of DES articles are from 2013 to 2018. The skyrocketing numbers have only been biased to hydrophilic DES rather than their hydrophobic counterparts. Till now, PubMed, Elsevier, Google Scholar, and Web of Science search for the phrase " hydrophobic deep eutectic solvent" result in less than forty publications.

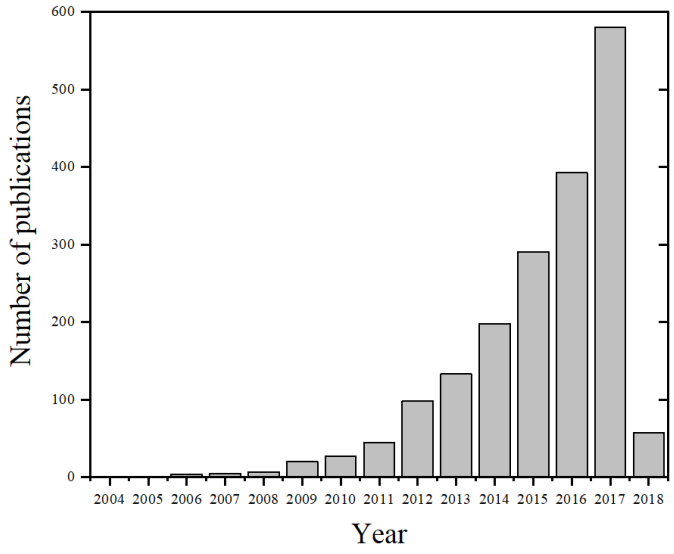

Figure 1.3. Number of publications based on a Web of Science search for the phrase "deep eutectic solvent". Date accessed: 2/10/18.

1.3.2. Objectives of this study

The main objective of this study is to design cost effective and greener solvents which are capable of replacing volatile organic compounds.

In Chapter 2, we investigate how different anions (Cl^-, Br^-, and I^-) impact the QAS in forming DES. Specifically, nine different DES were synthesized using choline chloride ([Ch]Cl), choline bromide ([Ch]Br), and choline iodide ([Ch]I) as hydrogen bond acceptor with malic acid, malonic acid, and urea as hydrogen bond donor. The DES were characterized to find their chemical composition, viscosity, conductivity, density, melting, thermal stability, and chemical shifts. These experimental data were coupled with theoretical quantum calculations using COSMO-RS simulations to estimate the surface charge density, vapor pressure, and density. In significance, a new DES with diverse

physicochemical properties has been developed, which in essence can be applied to electroplating or for extraction due to their unique properties.

In Chapter 3, we synthesized a hydrophobic deep eutectic solvent (HDES) from choline chloride and fatty acids (butyric acid, BA; valeric acid, VA; hexanoic acid, HA; and caprylic acid, CA). Specifically, we evaluated how increasing alkyl chain length affects the hydrophobicity and hydrogen-bonding potential of the solvent. Also, a multivariate unsupervised statistical approach called chemometrics was adopted to study the hydrogen-bonding capabilities of the newly designed solvent. In a broader scope, the solvent was applied to extract piperine, a bioactive compound, from black pepper.

In chapter 4, we investigated the electronic and molecular properties of the synthesized DES by employing solvatochromic molecular probes and density functional theory. This chapter significantly enhances our understanding on how charge transfer impacts hydrogen bonding and other thermodynamic properties of the solvent. The hydrogen bonding acidity, hydrogen bonding basicity, and the polarizability/dipolarity of the HDES was studied at different temperatures. Also, by fitting the DES into the Snyder's selectivity triangle, we showed that the synthesized HDES can be used to replace some of the conventional volatile organic solvents.

1.3.3. Justification of the study

The concept of hydrophobic DES (HDES) was introduced by van Osch and co-workers[55] in 2015 when diverse quaternary ammonium salts (QAS) were combined with decanoic acid (DecA). The water-immiscible solvent was applied to extract water-insoluble

volatile organic compounds, which they reported high extraction yield and efficiency[55]. Since then, active research has been ongoing to investigate how HDES are synthesized and their application in diverse fields. The concept of DES in analytical extraction is still in its infancy[56] compared to ionic liquids, nonetheless, the increasing number of yearly publications make the field very promising. Until now, almost all QAS used for HDES synthesis are derivatized or have large alkyl groups attached to the cation, hence making it expensive and uncompetitive to VOCs. Figure 1.6 and Figure 1.7 show the most used salts and HBD for HDES synthesis, respectively. This study employs [Ch]Cl and fatty acids at different molar ratios to synthesize HDES. The solvent is easy to prepare, starting materials are biodegradable, and the solvents have diverse polarity range.

1.3.4. Choline chloride

Choline chloride (Figure 1.4), also known as cholinium cation, (2-hydroxyethyl)-trimethylammonium cation or $HOCH_2CH_2N^+(CH_3)_3$ is the most widely used QAS for DES synthesis[34]. Choline is a dietary component, precursor for acetylcholine (a neurotransmitter), and can appear in esterified forms such as phosphatidylcholine and glycerophosphocholine. Choline chloride is non-toxic, biodegradable, and is cheap, making it possible to implement industrially.

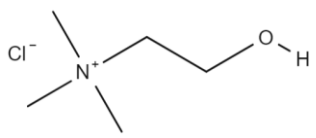

Figure 1.4. Structure of choline chloride.

1.3.5. Fatty acids

Fatty acids (FA) are carboxylic acids with the general formula $H(CH_2)_nCOOH$. FA are important structural components of animals. FA differ from each other based on the alkyl chain length. Short-chained fatty acids have fewer than 5 carbons, medium-chained FA have between 6 to 12, and longer-chain FA has greater than or equal to 13 carbons.

1.4. Hydrophilic DES and Applications

The LTTMs are synthesized mostly by mixing natural high-melting-point starting materials, which form a liquid by hydrogen-bond interactions with notable applications in organic synthesis[57-59], biofuel processing[60-61], and catalysis[39, 62]. Some of the underexplored fields of DES include biomass processing and liquid-liquid extractions or extractive distillation[38]. Nonetheless, a few reviews on DES for analytical extraction have surfaced recently[37, 56, 63-67]. Hizaddin et al.[68] screened 94 DES solvents by applying conductor-like screening model for realistic solvents (COSMO-RS) and evaluated their potential usage for extractive denitrification of diesel. A comprehensive review of deep eutectic solvents and its application in modifying electrode surfaces for electrochemical sensing and biosensors has been published[69-70]. The use of DES as a media for *Candida antartica* B lipase transesterification reactions is explained in details[71].

Apart from LTTMs, other forms of DES from natural raw materials have evolved over the past decade in the form of natural deep eutectic solvents (NADES). NADES was introduced when cellular constituents like fructose, glucose, citric acid, proline, and other metabolites formed viscous liquids at defined molar ratios[72]. NADES synthesis, types, characterization, and applications, including its use in analytical extraction and

lignocellulosic biomass pretreatment, are reviewed[67, 73-80]. A recent review by Vanda et al.[81] looked into the evolution of NADES from ionic liquids and DES, and further expanded on the applications of NADES in pharmaceuticals, cosmetics, food and agricultural. NADES can be used as a solubilization agent for macromolecules and as a media for enzymatic reactions[81]. Unlike LTTMs and NADES, THEDES is another subgroup of DES with one of the components as a pharmaceutically active ingredient (API). Commonly used API include acetylsalicylic acid, benzoic acid, ibuprofen, and phenylacetic acid[42-43]. Developmental research is ongoing to develop THEDES which will be effective for drug delivery. Compared to water, choline chloride-urea and choline chloride-malonic acid DES improved the solubility of benzoic acid, danazol, griseofulvin, AMG517, and itraconazole by 5 to 22,000 fold[82]. This notable feature of DES makes it promising for pharmaceutical applications and drug delivery. In view of this, developing HDES is important not only for analytical extraction but also as vehicles for drug solubilization.

1.5. Hydrophobic DES synthesis

The synthesis of HDES is similar to hydrophilic DES. As shown in Figure 1.5., HDES is synthesized by mixing DL-menthol (HBA) and DecA (HBD) at 1:1 molar ratio followed by heating. The polarity surface of both the donor and the acceptor molecules show three regions; blue = proton-donating region with negative charge density, red = proton-acceptor region with positive charge density, and green = hydrophobic region. Among the HBAs, DL-menthol is gaining popularity for its use in solvents for analytical extraction whereas decanoic acid (DecA) is the most used HBD in HDES synthesis. There is no single way for HDES synthesis since this depends on the starting raw materials.

HDES can be synthesized by simply mixing the constituents at ambient temperature[83] or by heating at as high as 80 ℃ with or without stirring[84-85]. Figure 1.6 and Figure 1.7 list a number of hydrogen bond donors and hydrogen bond acceptors commonly used for HDES, respectively. The physical appearance of most HDES depends on the nature of the constituents. However, most HDES form clear and transparent liquids, and are stored in a desiccator. In designing HDES for analytical extraction, a careful consideration of the molar ratio and the alkyl-chain length of the HBA and HBD are critical. HDES physical and chemical properties were tailored for pyrethroids[86] and polycyclic aromatic hydrocarbons (PAH)[87] extraction by modifying the molar ratio of the constituents. In the extraction of bisphenol A, Florindo et al.[88] showed that octanoic acid (C_8), nonanoic acid (C_9), decanoic acid (C_{10}), and dodecanoic acid (C_{12}) can act as either HBA (due to the carbonyl group) or HBD (due to the hydroxyl group) to form HDES.

A moderately high extraction efficiency of 76.04 %, 88.32 %, and 81.81 % was obtained by using C_8−C_{12} HDES, C_9−C_{12} HDES, and C_{10}−C_{12}, respectively. Low alkyl-chain carboxylic acids like acetic acid, butyric acid, levulinic acid, hexanoic acid, and pyruvic acid have been used together with DL-menthol or N_{4444}–Cl for HDES synthesis[89]. Varying the alkyl chain of either the HBA or the HBD is necessary to tune the polarity of the HDES for a defined application. Martins et. al[90] recently synthesized and designed HDES from the terpenes thymol and L (-) menthol and monocarboxylic acids and characterized the solvent through density measurements, viscosity, solid-liquid equilibria, and Kamlet-Taft solvatochromic parameters. Thymol-based HDES were found to be less viscous (1.3−50.6 mPa.s) and denser than L (-) menthol-based eutectic mixtures[90]. As expected, despite the similarities between thymol and L (-) menthol, the physical and

chemical properties of their resulting solvent differ with thymol having higher hydrogen-bonding acidity character and menthol having high basicity behavior[90].

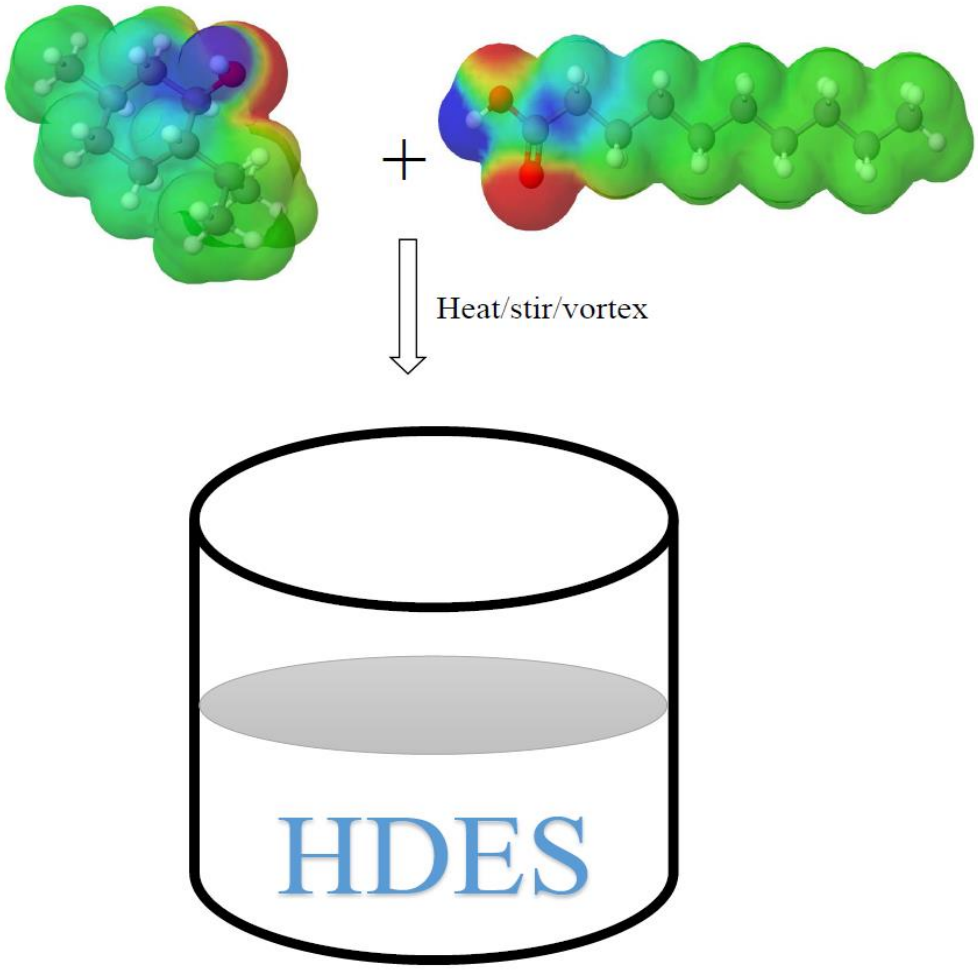

Figure 1.5. Synthesis of HDES from DL-menthol (HBA) and decanoic acid (HBD) at 1:1 molar ratio. Molecular structure graphics by MolView version 2.4.

1.6. Applications of HDES in analytical extraction

DES hydrophobicity was introduced in 2015 by van Osch and co-workers, although, the authors acknowledged earlier work involving hydrophobic menthol-based eutectic mixtures[55, 91]. The first application of HDES involved liquid-liquid extraction of volatile fatty acids (VFAs) comprising of acetic, propionic, and butyric acid from the aqueous environment. The extraction efficiency of the VFAs was found to increase with increasing alkyl chain length. For example, N8881-Cl: DecA 1:2 efficiently extracted 38 % acetic acid, 70.5 % propionic acid, and 89.8 % butyric acid[55]. The high extraction efficiency compared to similar VFAs extraction with amine-based extractants could be attributed to the hydrophobicity of the HDES[55, 92].

Since then, active research is ongoing to investigate how HDES are synthesized and their possible applications in diverse fields. Four different HDES synthesized from trioctylmethylammonium chloride and DecA 1:2, trioctylmethylammonium chloride and octanoic acid, tetrabutylammonium chloride and DecA, and tetrabutylammonium chloride and octanoic acid found the latter as an effective solvent to efficiently extract eight synthetic pigments in beverages with recoveries between 74.5−102.5 % and RSD less than 5.4 %[93]. Recently, a low cost, highly porous, and ultralight HDES was synthesized (combined techniques from nanofibrillation, silylation, and freeze-drying) capable of squeezing oil (superabsorbing agents) with an absorption capacity of 65−205 (g/g)[94]. Another liquid-liquid separation of metal uranyl nitrate ($[UO_2]^{2+}$) from aqueous acid using low viscosity hydrophobic eutectic solvent from trioctylphosphine and phenol has been reported[95]. The presence of phenol in the mixture was reported to be crucial for generating

the eutectic mixture composition rather than having a role in the uranyl complexation and extraction[96].

A menthol-based HDES with acetic acid (1:1) showed efficient extraction of phytocannabinoids with yields ranging from 118.6 % to 132.6 %, which is higher than using terpenol, borneol, geraniol, and linalool as HBA[97]. This HDES has higher extraction efficiency for phytocannabinoids than traditional liquids like methanol and ethanol[97]. Apart from acetic acid, other transparent liquid-based HDES formed with menthol include hydrogen-bond donors like formic, propionic, butyric, hexanoic, octanoic, dodecanoic, lactic, phenylacetic, and mandelic acid at 1:1 molar ratio[97]. Menthol with oxalic, malonic, tartaric, phthalic, glycolic, malic, hippuric, pyruvic, and aspartic acid (1:1) form solid-liquid mixture after heat treatment at 80−95 °C[97]. A tailor-made HDES with methyltrioctyl ammonium chloride (N_{81}−Cl) and 18 different alcohols or aliphatic acids was able to extract between 13 mg/g to 23 mg/g of polyprenyl acetates from *Ginkgo biloba* leaves powder[98]. Lastly, reports on using HDES for In^{3+} [99] and Co^{3+} [100] extraction from aqueous solutions has been established. For quantification purposes, HPLC coupled with UV/Vis is the most used separation and quantification technique. A low limit of detection (LOD) for amphetamine and methamphetamine is between 2 ng/mL to 5 ng/mL[83].

In the next chapters, the role of anions in DES by experimental and COSMO-RS simulation was investigated. Moreover, the synthesis, characterization, and application of HDES from choline chloride and fatty acids were studied. These solvents were applied to isolate piperine, a bioactive compound, from black pepper was evaluated. Also, the electronic and molecular properties of HDES by solvatochromic molecular probes and density functional theory were studied.

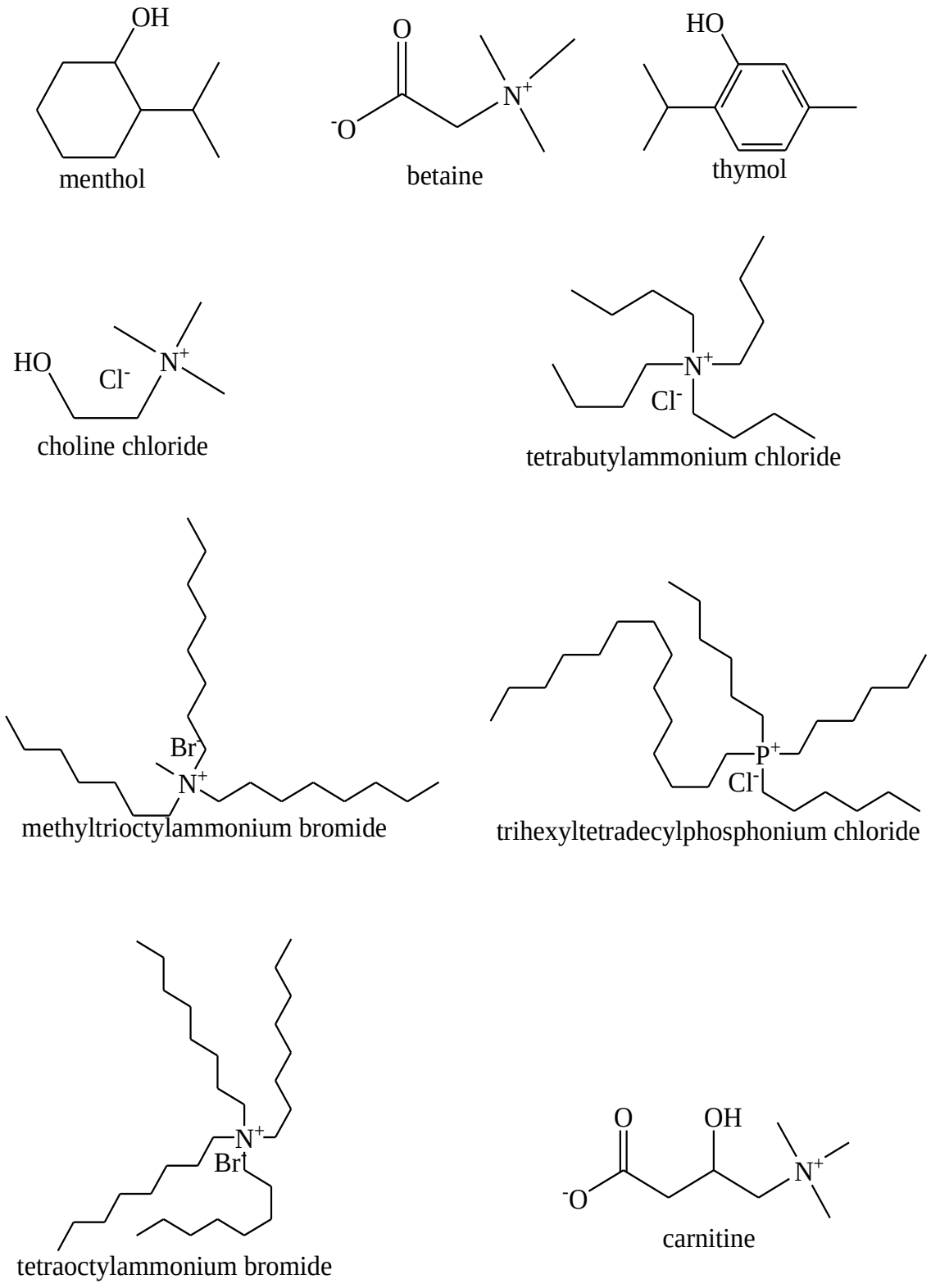

Figure 1.6. Common HBA used for HDES synthesis[101].

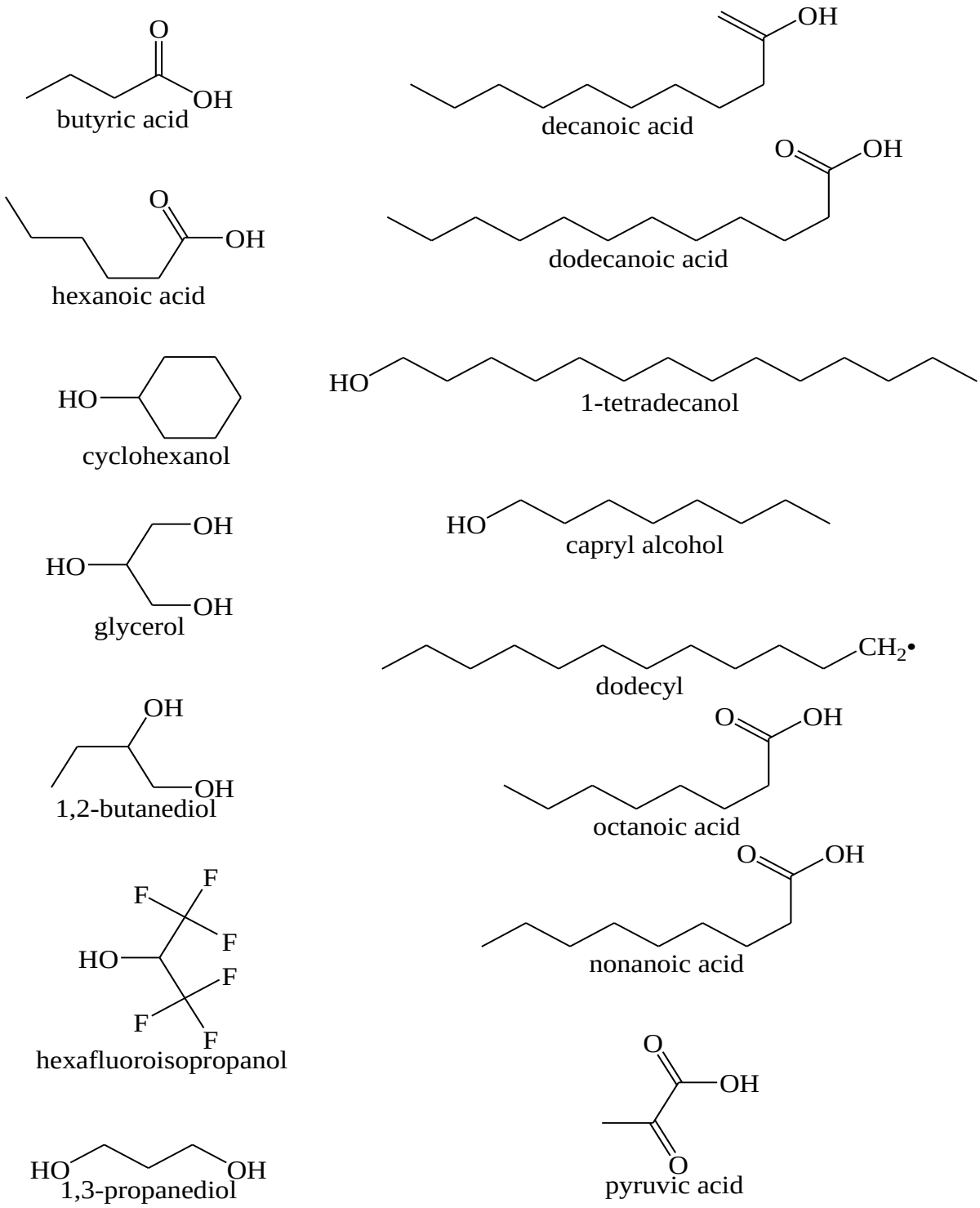

Figure 1.7. Common HBD used for HDES synthesis[101].

CHAPTER TWO

INVESTIGATING ANIONS ROLE IN DEEP EUTECTIC SOLVENTS BY EXPERIMENT AND COSMO-RS

2.1. Introduction

Deep eutectic solvents are formed mostly by mixing hydrogen bond acceptor (HBA) with hydrogen bond donor (HBD) at the correct molar ratio. The melting point depression of DES occurs when the anionic group of the salt weakens in its interaction due to hydrogen bonding with the cationic group of the HBD[35, 102]. Like DES, conventional ionic liquids such as [EMIM][Br], [BMIM][Br], [EMIM][BF_4], [EMIM][Tf_2N], and [EMIM][BF_6] also combine cationic and anionic groups to form liquids with lower melting points. The bulky asymmetric cations coordinate weakly with the anions resulting in improper packing and lowering of the melting point[102].

A variety of HBA and HBD have been reported in literature to form DES but each combination has their unique melting point depending on the strength of interaction. Some of the common used HBA in DES include choline chloride, choline acetate, choline nitrate, ethylammonium chloride, 2-fluoro-N,N,N-trimethylethanaminium, tetrabutylammonium bromide, tetrabutylammonium chloride, lithium bis [(trifluoromethyl)sulfonyl]imide, benzyltriphenylphosphonium chloride, and acetylcholine chloride[38, 103].

Anions in DES and ionic liquids influence some physicochemical and physiothermal properties such as melting point, boiling point, color, vapor pressure, density, surface tension, conductivity, refractive index, and viscosity of the solvent. Recently, Row and Ma[104] reported an anion-dependent extraction of rutin, quercetin, and

scoparone from *Herba artemisiae scopariae* using a variety of ILs as extractive addictive solvents. Their work inferred that the anionic moiety of the IL increased the hydrogen-bond interaction between the IL and the target compound. Anions like NTf_2^- and $N(CN)_2^-$ have been shown to play critical roles in tuning ILs fluidity with concomitant lowering of viscosity[105].

Anions play a critical role in charge transfer, charge distribution, and hydrogen-bond formation in DES. Pioneering work by Abbott et al.[36], showed a decreasing order of anions $F^- > NO_3^- > Cl^- > BF_4^-$ in freezing point of QAS with urea. Despite numerous advantages of anions in DES and ILs, others like BF^{4-} and BF^{6-} pose major concern, especially when used in biocatalysis due to *in-situ* production of hydrofluoric acid.

To date, most literature reports choline chloride as sole source of QAS for DES formation. The low cost, biocompatibility, and availability of the chloride-based salt makes it a good choice for the industry. Although, [Ch]Cl has been extensively studied in the literature to form a strong hydrogen bond in most eutectics, little or no work has been done to thoroughly explain how the anion or replacing the chloride with other halogens may affect physiochemical properties of DES.

In this chapter, an extensive discourse on the impact of [Ch]Cl, [Ch]Br, and [Ch]I with urea, malic acid, and malonic acid were studied at their eutectic molar ratios already established in literature. For example, [Ch]Cl:urea 1:2 and [Ch]Cl:malonic acid 1:1 have been reported to form DES with decreased melting point at 12 °C and 10 °C[35], respectively. The glass transition temperature (T_g) of [Ch]Cl:malic acid 1:1 eutectics is at -56.48 °C[62]. The chloride (Cl^-), bromide (Br^-), and iodide (I^-) anions were selected for this study to broaden our understanding on how size, molecular volume, and electronegativity

difference influences on DES. In all, nine different DES were synthesized and characterized for physical, chemical, and thermal properties. After synthesis, a nondestructive ATR-FTIR was performed to study the nature of the DES formed. Physical characteristics and behavior of the DES based on color, state, viscosity, and flow pattern were observed and recorded. A selection criterion for further characterization of the synthesized DES was based on whether or not the solvent remains liquid at room temperature. The density and refractive index were measured to determine DES purity. To estimate how anions impact DES intermolecular force and thermal stability, thermal gravimetric analysis (TGA and DTA) was measured for the solvent. By using a series of experimental approaches, our results established a correlation on how anions alter polarity, pH, conductivity, and viscosity of DES. Hydrogen-bonding strength of DES was determined by differential scanning calorimetry (DSC) and proton-NMR chemical shift.

To validate the experimental data, quantum computational calculations were performed via COSMO and COSMO-RS approach to demonstrate how the change in anion of the QAS alters activity coefficient at infinite dilution, vapor pressure, and the affinity of water, methanol, ethanol, and acetonitrile for DES. The Conductor-like Screening Model (COSMO) is a quantum mechanics (QM) continuum solvation model[106]. QM continuum solvation models are extension of basic QM (isolated molecules are described at T=0 K in gas phase or in vacuum) to describe liquid phases[107-108]. Before the COSMO theory, parametrization of electrostatic interactions into computational force-field models (molecular dynamics and Monte Carlo simulations) suffered limitations to describe solvation of polarizable molecules[109-110].

The Conductor-like Screening Model for Real Solvents (COSMO-RS)[111] is a quantum mechanical model that integrates quantum theoretical models with dielectric continuum models, local electrostatic interactive surfaces, and statistical thermodynamics to describe unimolecular properties of individual species in a system[107]. In COSMO-RS, the interaction energies of the contact surfaces are calculated due to specific contributions from misfit, hydrogen bonding interaction, and van der Waal interactions[112]. A detailed explanation and calculations involved in COSMO and COSMO-RS is outline in these references[107-109, 113].

2.2. Experimental

2.2.1. Chemicals

Choline chloride, malic acid, malonic acid, and urea were all purchased from Acros Organics and had purity ≥ 99 %. All other chemicals were of analytical grade.

2.2.2. Synthesis of DES

DES were synthesized by mixing choline chloride and HBDs at 1:1 or 1:2 molar ratios and heated at 80 ℃ for 15-30 min under constant stirring at atmospheric pressure until a homogenous liquid was obtained. The prepared DES were cooled to room temperature and stored in a desiccator.

2.2.3. Fourier Transform Infrared (FTIR) Spectroscopy

A Thermo Scientific Nicolet 380 spectrometer with ZnSe attenuated total reflection (ATR) was employed to study the functional groups of three HBD, three HBA, and the nine

synthesized DES at room temperature. In principle, when infrared radiation passes through a sample placed on the ATR crystal, some radiation gets absorbed and others become transmitted. The FTIR then uses an interferometry to record the output spectrum which represents the characteristic fingerprint of the sample. For the experimental procedure, infrared transmittance was collected from 4000 cm^{-1} to 400 cm^{-1} with 128 scans at a resolution of 8 cm^{-1}. Background collection was done before every sample and correction was done for CO_2 and H_2O. Data analysis was done in the OMNIC software.

2.2.4. Density

The density of the DES was determined by gravimetric analysis. A 5.00 mL pipet was calibrated to dispense 5.00 g/mL of water. The balance was calibrated following good laboratory practice (GLP) standards. Each measurement was repeated for at least five times and the average value reported. All density measurements were carried out at room temperature.

2.2.5. Refractive index

The refractive indices of DES were determined using the Bausch & Lomb Abbe-3L refractometer with an accuracy of ± 0.0001 using the sodium D line at 589.3 nm. The refractometer was calibrated using deionized water ($1.3328 \pm 2.89 \times 10^{-4}$ n_D) before measurements at room temperature in triplicate.

2.2.6. Electronic transition

The electronic transition of Nile red in DES was measured at room temperature using a Synergy|H1 microplate reader, Biotek, UV-Vis spectrophotometer. The maximum absorption wavelength (λ_{max}) was set between 400 to 650 nm at 1 nm interval. The working concentration of Nile red was kept as low as 0.5×10^{-4} M to minimize solute-solute interaction.

2.2.7. Viscosity

Temperature dependent viscosities (η/mPa.s) were measured using the Brookfield DV-III Ultra Programmable Rheometer connected to the VWR refrigerated circulating temperature controller. Measurement was done using a CPE-40 cone spindle with 0.5-mL sample volume. Instrument calibration was done using the certified Brookfield viscosity standards with an uncertainty of about 1%. Viscosity readings were done using the standalone mode of operation and cP values for all DES were recorded at room temperature with shear rate of 0.75 s^{-1}. [Ch]Cl:urea and [Ch]Br:urea was selected as model solvents to monitor the influence of the anion on viscosity at varying shear rate from 0.75 s^{-1} to 3.75 s^{-1} and temperature from 25℃ to 65 ℃. Arrhenius plot on temperature-viscosity relationship (equation 2.1) was done in Origin.

$$\ln(\eta) = \ln(A_s) - E_a/R\,(1/T) \qquad \text{(Equation 2.1)}$$

where ln(η) is the natural logarithm of viscosity in mPa.s, In A_s is the pre-exponential factor constant in mPa.s, E_a is the activation energy in $Jmol^{-1}$, R is ideal gas constant in $Jmol^{-1}K^{-1}$, and T is temperature in K.

2.2.8. pH and Conductivity

pH measurements of DES were determined using the Accumet® AB150 pH/mV meter, Fischer Scientific, at 23 ± 0.3 ℃. Calibration of the pH probes were done using pH standards of 4, 7, and 10 buffer solutions with an accuracy of ± 0.002 pH. Conductivity κ measurements were determined using the Oakton Cond 6+ conductivity probe which measures κ and temperature in μS cm^{-1}. Calibration was done using 1000 ppm sodium chloride solution with an uncertainty of about 0.5 %.

2.2.9. Differential scanning calorimetry

The melting temperature (T_m) and glass transition temperatures (T_g) of the HBA, HBD and DES were measured using a TA-Q2000 differential scanning calorimeter at a heating rate of 10 ℃/min. An approximate amount between 5 to10 mg of sample was weighed into aluminum hermetic pan and covered with the lid. DSC measurements for HBA and HBD were done from 25 to 200 ℃, and between -80 to 50℃ for DES. The advanced Tzero™ technology and temperature-controlling capability of the DSC ensured effective and accurate heat flow to the sample. To avoid moisture contamination, a continuous nitrogen purge at a rate of 20 mL/min was set. Accuracy and repeatability of DSC measurements were ensured by calibrating with an indium standard.

2.2.10. Thermogravimetric analysis

TG/DTG measurements were done using Seiko instruments TG/TDA 220 which measures percentage weight loss of samples due to a change in temperature or time.

Approximately, 8-9 mg of sample were weighed into aluminum pan for measurements under nitrogen atmosphere. The high-purity nitrogen purging system (flow = 20 mL/min) provided an inert environment to prevent unwanted oxidation. Sampling was done at every 0.5 sec from room temperature to 350 ℃ at a heating rate of 10 ℃/min.

2.2.11. Computational calculations and parameterization

The 3D-molecular structure and geometry of both HBA and HBD were generated in TmoleX 4.2 using the inbuilt 3D molecular builder. Each compound was generated using their simplified molecular input line entry specification (SMILES) for consistency in the bond distance and bond angle. The optimized geometry of the DES was done using DFT with BLYP functional and triple zeta valence polarized basis set (def-TZVP) for all atoms with resolution-of-index (RI) approximation. All quantum mechanical calculations were performed in the TURBOMOLE computational package (TmoleX 4.2 and COSMOtherm)[108]. Simultaneously, the COSMO file (COSMO-BP-TZVP_file name) of DES was generated at same theoretical computational level. COSMO files are used in the COSMOtherm software to calculate the thermodynamic equilibrium properties. Convergence criteria was set to 10^{-6} Hartree and 200 cycles. Convergence was based on the geometry with lowest electronic self-consistency cycle energy. The COSMOtherm program package was used to calculate the sigma profiles and sigma potentials of the DES together with thermodynamic parameters such as vapor pressure, activity coefficient at infinite dilution (IDAC), density, and partition coefficient[106, 114].

2.3. Results and Discussion

2.3.1. Physical behavior and characteristics

A homogenous mixture was obtained by mixing HBA and HBD at their respective molar ratios. The preparation steps for DES synthesis is simple and takes about 30-60 mins to generate the solvent. DES synthesis requires no purification steps and is simple compared to conventional ionic liquids. The [Ch]Cl and [Ch]Br salts form a highly viscous liquid with urea, malonic acid, and malic acid (Table 2.1.). [Ch]Br:urea forms a clear solution after preparation but solidifies after prolonged stay at room temperature. All the DES formed with [Ch]I QAS remained solid after 5 minutes at room temperature. The characteristic nature of the halide (in QAS) and the HBD determines the color of the DES. In terms of flow pattern, DES formed from malic acid and urea appeared to be more viscous than DES formed from malonic acid.

Table 2.1. Physical characterization of synthesized deep eutectic solvents at 25 °C.

DES	Physical characterization
[Ch]Cl:urea	Liquid at RT, clear, very viscous, flows at RT
[Ch]Br:urea	Liquid at RT, very viscous, clear, solidifies at prolonged storage time
[Ch]I:urea	Clear, solid at RT (minutes after preparation)
[Ch]Cl:malonic acid	Liquid at RT, clear, medium viscosity, flows at RT
[Ch]Br:malonic acid	Liquid at RT, little yellowish, flows at RT, medium viscosity
[Ch]I:malonic acid	Solid at RT, yellowish
[Ch]Cl:malic acid	Liquid at RT, highly viscous, flows with difficulty, light yellowish
[Ch]Br:malic acid	Liquid at RT, highly viscous, flows with difficulty, light yellowish
[Ch]I:malic acid	Solid at RT, yellowish-red

2.3.2. Molecular vibrations and structure analysis of DES

From the results, all the DES shows a stretching O-H band in the FTIR spectra between 3200 and 3500 cm^{-1} which is a characteristic of hydrogen bonding (Fig. 2.1, Fig. 2.2, and Fig. 2.3). This is evidenced by a shift in the O-H stretching band in the DES compared to the O-H stretching band in the individual components. The stretching is probably due to the transfer of electron cloud to form hydrogen bonding. The FTIR spectra of most DES looks similar to the HBD spectra except the presence of new peaks and shift of peaks in the DES[115].

The ammonium identity between 943 and 954 cm^{-1} and a strong carbonyl (C=O) group between 1660 and 1726 cm^{-1} confirms the HBA and HBD interaction. As expected, DES formation resulted in reduction of the C=O peak intensity compared to their corresponding peak in the HBD due to the molecular interaction between the HBA and the HBD. Notwithstanding, all the DES showed a C=O shift to higher wavenumbers due to stretching of the carbonyl band. The stretching of bands to higher wavenumbers may be due to a decrease in bond length because of hydrogen bonding. For example, an increased C=O wavenumber was observed at 1723.6 cm^{-1} and 1719.2 cm^{-1} for [Ch]Cl:malic acid and [Ch]Cl:malonic acid DES, respectively.

Changing the anion alters the intensity of the ammonium identity peak (952 cm^{-1}) in the DES, which in future might be used as a probe to verify DES formation. The intensity of this peak in [Ch]Cl:malic acid (54.2 %) > [Ch]Br:malic acid (53.4 %) > [Ch]I:malic acid. Also, [Ch]Cl:malonic acid (55.4 %) > [Ch]Br:malonic acid (52.3%) > [Ch]I:malonic acid (47.2%). The intensity of 952 cm^{-1} peak in chloride-based DES was found to be greater than bromide-based DES and iodide-based DES with [Ch]I:urea as the only exception.

The differences in intensity of peaks may be due to the change in the dipole moments of atoms due to change in electronegativity when the acceptor group interacts with the donor group. Also, changing the anion in the HBA affects the vibrational pattern in the DES with concomitant changes in the O-H stretching pattern, intensity reduction, and the shift of some peaks in the fingerprint and functional group region.

From the FT-IR data, we can predict that altering the anion component of the HBA affects the nature of the DES formed. For example, [Ch]Cl:malonic acid or [Ch]Cl:malic acid and [Ch]Br:malonic acid or [Ch]Br:malic acid shows similar spectral characteristics compared to [Ch]I:malonic acid and [Ch]I:malic acid. The latter shows little or no O-H stretching pattern which may be due to reduced or no hydrogen bonding. The loss of N-H stretching vibrations in [Ch]Cl/Br:urea between 3200 and 3500 cm^{-1} is an evidence of hydrogen bonding.

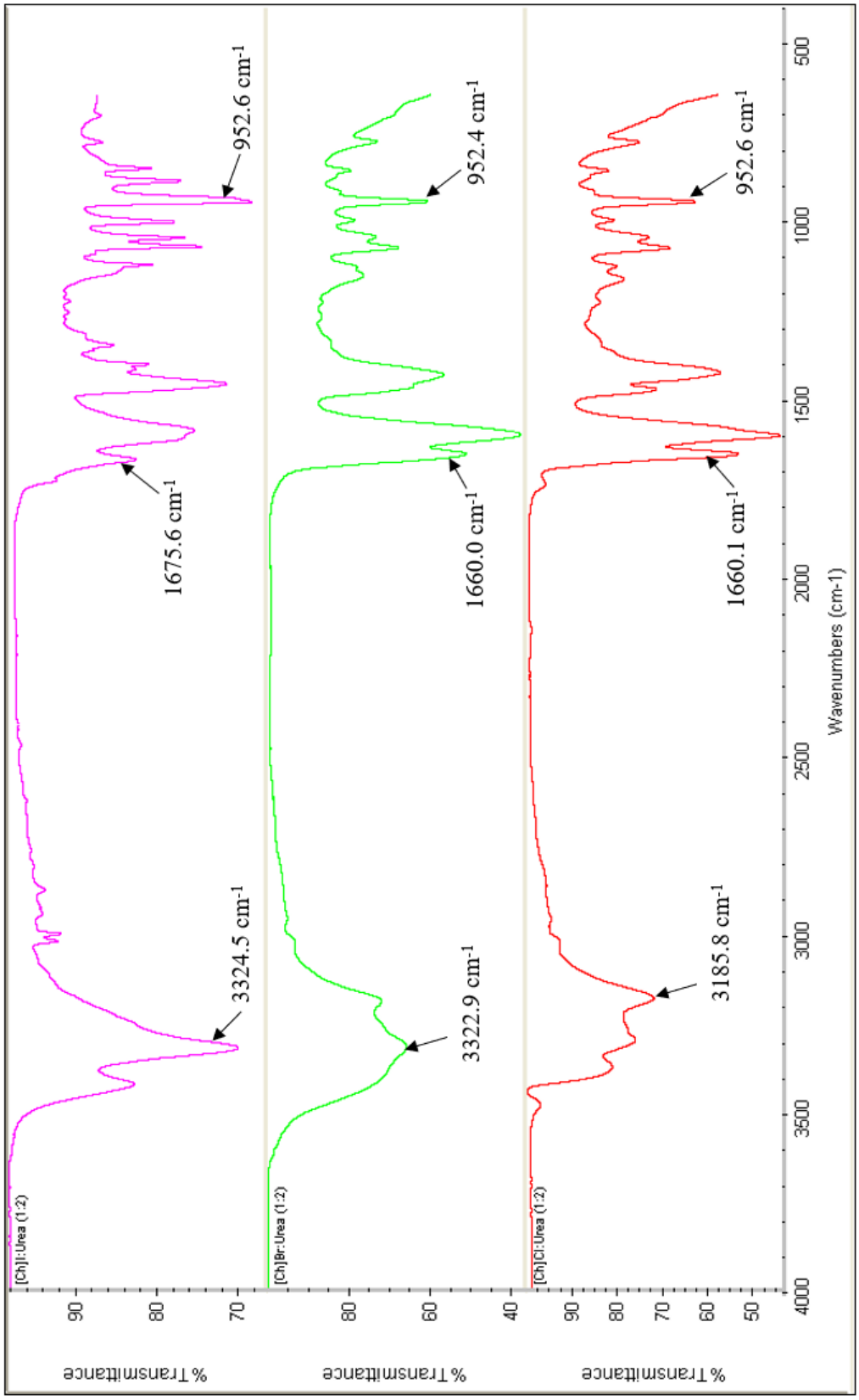

Figure 2.1. FTIR spectra of [Ch]I:urea (magenta), [Ch]Br:urea (green), and [Ch]Cl:urea (red) at 1:2 molar ratio.

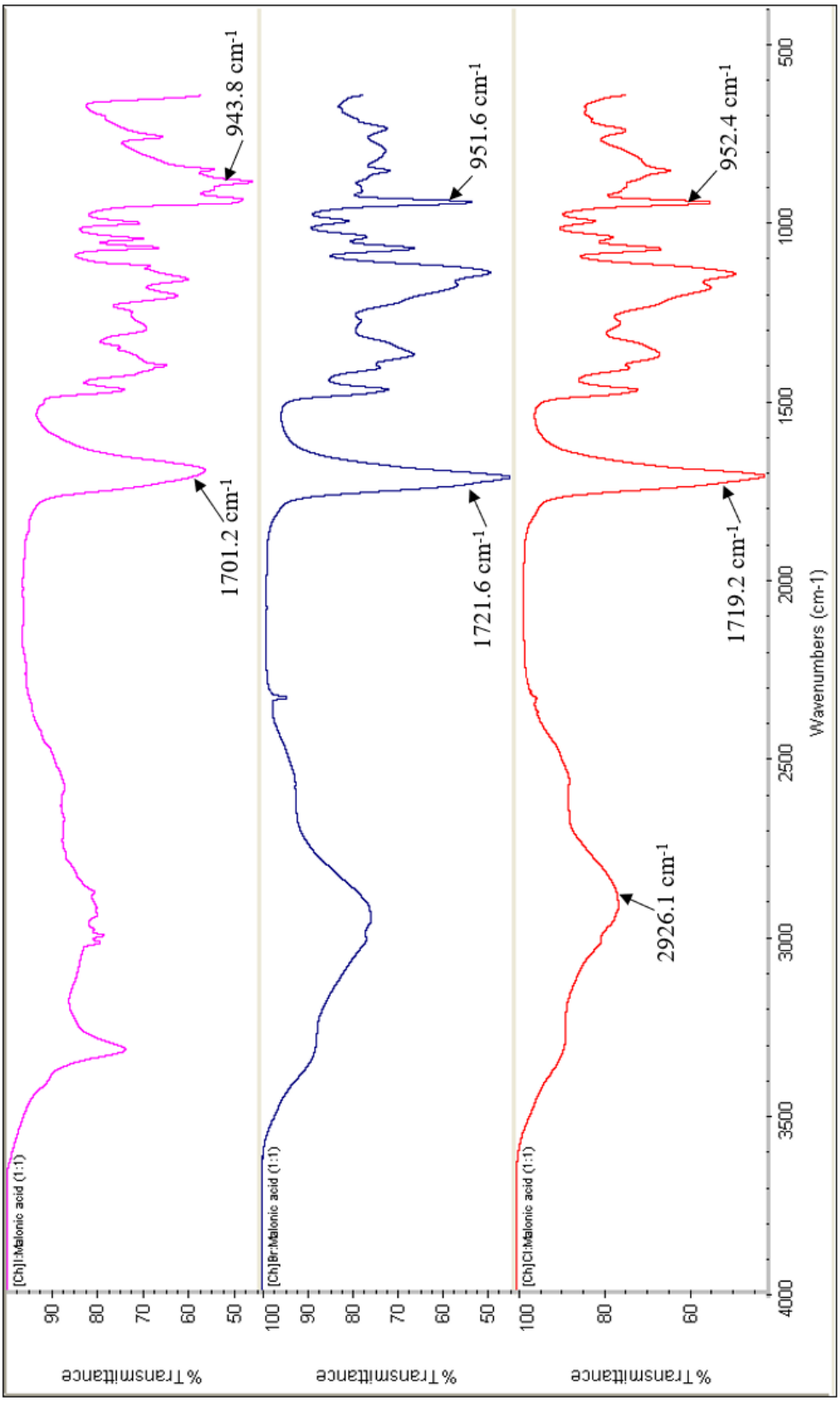

Figure 2.2. FTIR spectra of [Ch]I:malonic acid (magenta), [Ch]Br:malonic acid (blue), and [Ch]Cl:malonic acid (red) at 1:1 molar ratio.

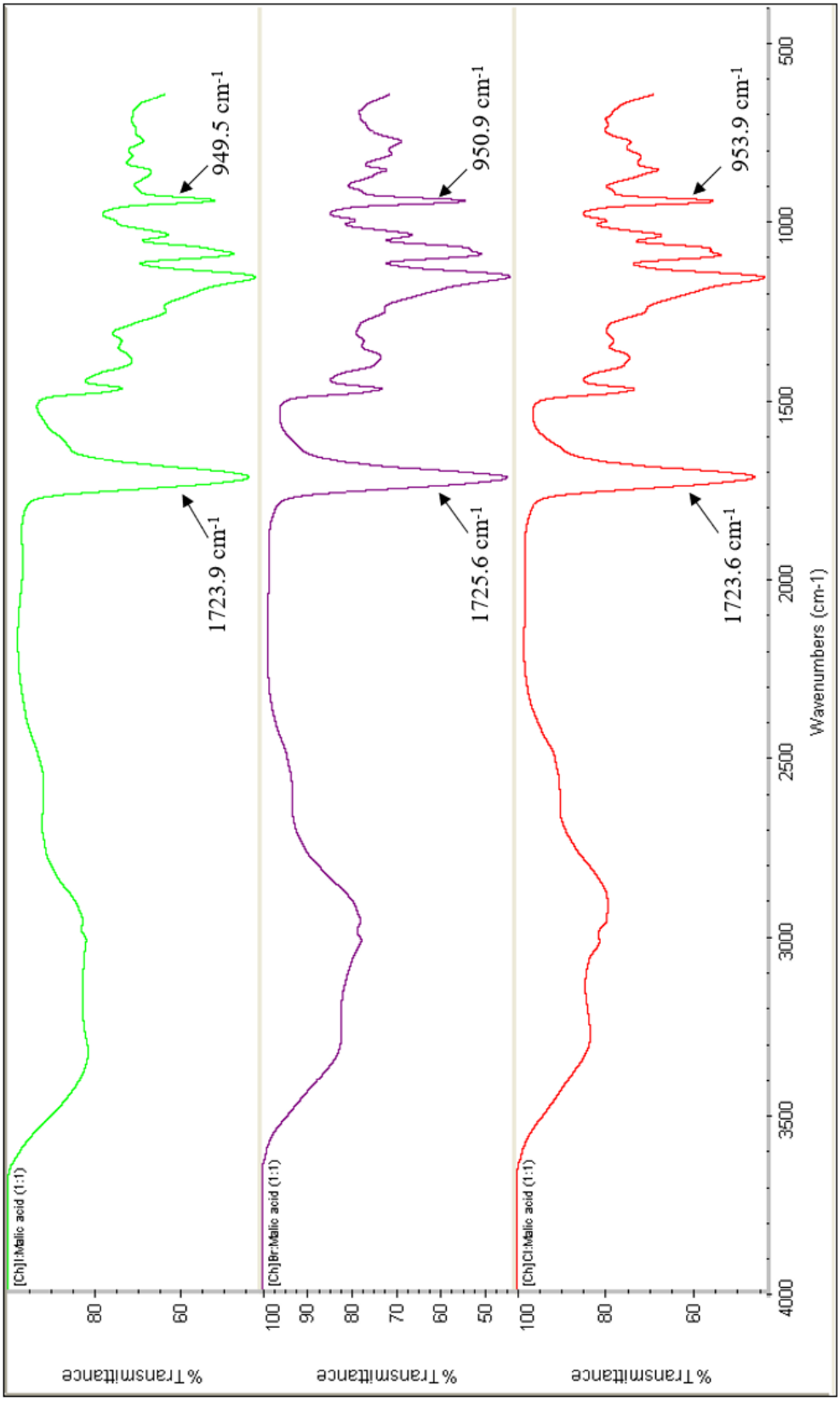

Figure 2.3. FTIR spectra of [Ch]I:malic acid (green), [Ch]Br:malic acid (magenta), and [Ch]Cl:malic acid (red) at 1:1 molar ratio.

2.3.3. Density

Density is an important thermophysical parameter that has been studied extensively for most liquids including ionic liquids and DES[103]. The density of six DES was measured by gravimetric experimental procedures and by simulations. As shown in Table 2.2 and Table 2.3, the experimental and simulated density values are consistent, and the data is comparable to already reported values in literature within the range of 1.1-1.6 g cm^{-3} [47, 103]. The bigger the size of the anion, the higher the value of density and vice versa. DES synthesized from [Ch]Br has density less than or equal to 1.26 g cm^{-3} whereas DES from [Ch]Cl is less than or equal to 1.25 g cm^{-3}. The gravimetric method remains a reliable method for measuring DES, however, comparable data generated by computational simulations makes this method easier and faster. The simulated density values of some DES were compared to experimental data reported in literature[47].

Table 2.2. Experimental density and molecular volume of the synthesized DES.

DES	Density g/cm^3	V_m cm^3/mol
[Ch]Cl:urea (1:2)	1.1876	218.72
[Ch]Br:urea (1:2)	1.3395	255.50
[Ch]Cl:malic acid (1:1)	1.2646	216.45
[Ch]Br:malic acid (1:1)	1.3996	254.51
[Ch]Cl:malonic acid (1:1)	1.2235	199.17
[Ch]Br:malonic acid (1:1)	1.3654	238.89

Table 2.3. Simulated densities of DES at 25 °C.

HBD	[Ch]**Cl**, g/cm^3	[a][Ch]**Cl**, g/cm^3	[Ch]**Br**, g/cm^3	[Ch]**I**, g/cm^3
Urea (1:2)	1.105623	1.1879	1.265318	1.412593
Malic acid (1:1)	1.212491	1.2796	1.374576	1.514014
Malonic acid (1:1)	1.186068	1.2112	1.369014	1.525729
Oxalic acid (1:1)	1.237826	1.2371	1.437371	1.595504
Citric acid (1:1)	1.26678	1.3313	1.396726	1.524873
Acetamide (1:2)	1.079446	1.0852	1.245339	1.39441
Maleic acid (1:1)	1.202076	NA	1.389668	1.545501
Ethylene glycol (1:2)	1.076418	1.1139	1.240394	1.395016
p-toluene sulfonic acid (1:1)	1.222672	1.2074	1.373487	1.507067

[a]Experimental density of DES in literature[47].

The volume occupied by one mole of DES, molar volume (V_m), was calculated by dividing the molar mass of DES by the experimental density (equation 2.2).

$V_m = M/\rho$ (Equation 2.2)

where M corresponds to the molar mass of DES in gmol^{-1}, and ρ is density in g cm^{-3}.

The molar volume of [Ch]Cl:malonic acid is 199.17 cm^3 mol^{-1} and was the smallest, whereas [Ch]Br:urea has the biggest V_m of 255.50 cm^3 mol^{-1}. Abbott et al.[46] reported a molar volume of 210.1 cm^3 mol^{-1} for [Ch]Cl:urea compared to 218.7 cm^3 mol^{-1} obtained in Table 2.2. Though the values are similar, the differences in the density values obtained may be due to temperature fluctuations. In most cases, the higher the molar mass of the DES, the higher the molecular volume. Smaller V_m indicate that the DES is more compact due to hydrogen bonding.

2.3.4. Refractive index

Light passing through a vacuum is faster than in a sample containing particles. Sample particles causes absorption, deflection, and reflectance of light rays. Refractive index is a measure of the speed of light through a sample and acts as a physicochemical indicator used to estimate the purity of samples in a given matrix[116]. Recently, Florindo et. al.,[40] reported a range of DES refractive indices to be between 1.48-1.49 n_D, except [Ch]Cl:levulinic acid which had low index of 1.46 n_D, highlighting the influence of the anionic group. To fully understand this phenomenon, we tested the influence of changing anions of DES mixtures as shown in Table 2.4. From our results, changing the anion in the HBA significantly altered the refractive index of all the eutectic mixtures. This was confirmed by comparing the means of DES using Tukey-Kramer pairwise statistical analysis in JMP. At 95% significance level, all the DES showed a p-value ≤ 0.0163 signifying that the n_D values are different from each other.

Table 2.4. Refractive index of DES.

DES	Refractive index (n_D)
[Ch]Cl:urea	$1.5063 \pm 2.89 \times 10^{-4}$
[Ch]Br:urea	$1.5208 \pm 7.64 \times 10^{-4}$
[Ch]Cl:malic acid	$1.4838 \pm 2.89 \times 10^{-4}$
[Ch]Br:malic acid	$1.4988 \pm 2.89 \times 10^{-4}$
[Ch]Cl:malonic acid	$1.4812 \pm 2.89 \times 10^{-4}$
[Ch]Br:malonic acid	$1.5003 \pm 5.77 \times 10^{-4}$

Increasing the molecular weight of the anion from Cl^- to Br^- in the HBA increases the refractive index between 0.0145 to 0.019 n_D.

The order of increase in refractive index of DES is [Ch]Br:urea > [Ch]Cl:urea > [Ch]Br:malonic acid > [Ch]Br:malic acid > [Ch]Cl:malic acid > [Ch]Cl:malonic acid. A comparable n_D values was reported for [Ch]Cl: malonic acid and [Ch]Cl: urea at 1.5044 and 1.48713 n_D, respectively[40, 103]. In application, refractive indices of DES can be used to measure the electronic polarizability of the solvent or its behavior in solutions by using the Lorentz–Lorenz equation (Equation 2.3)[40, 117].

$$\frac{(n^2-1)}{(n^2+2)\rho m} = \frac{\mathrm{NA}\alpha}{3M} \qquad \text{(Equation 2.3)}$$

where n = refractive index, $\mathcal{P}_m$ = mass density, N_A = universal Avogadro's number, and M = molecular weight of the chemical element of the material.

2.3.5. Polarity

The polarity of the DES was determined by measuring the shift in the maximum wavelength of Nile red dye in a DES microenvironment. The highly acidic nature of some DES makes Nile red an alternative solvatochromic dye compared to Reichardt's betaine dye. The phenolate oxygen of the later becomes protonated in acidic medium and loses its absorption band[118]. Upon protonation, the absorption band of Nile red appears in both acidic and polar solvents[119]. The frequency of light required to excite an electron across the HOMO/LUMO gap determines the absorption maxima. To elucidate the polarity of the prepared DES, most especially concerning the influence of the HBA, the highly polar methanol and medium polarity ethyl acetate was selected as control organic solvents (Fig. 2.4.).

Figure 2.4. Nile red dye in DES and control solvents.

Nile red shows maximum absorption at 553 nm in methanol and 523 nm in ethyl acetate. The bathochromic and hypsochromic shift of Nile red in methanol and ethyl acetate, respectively, is an indicator of the solvent's polarity. Polar solvents and those that form hydrogen bond with Nile red causes increased charge delocalization with resulting shift of the maximum wavelength to red. In fact, polar solvents are able to stabilize the twisted excited state of Nile red and enhances the intramolecular charge transfer leading to bathochromic shift[120]. Experimental wavelength measurements (in nanometers) of both organic solvents and DES in Nile red at 25 ℃ were converted to transition energies in kcal. mol^{-1} by dividing by 28592[118-119]. From Table 2.5., the transition energy of Nile red E_T (NR) in solvents from π to π* transitions show that all the DES synthesized are more polar than either methanol or ethyl acetate. The transition energy of methanol and ethyl acetate are 51.73 and 54.67 kcal. mol^{-1}, respectively, compared to literature values of 52.02 and 54.94 kcal. mol^{-1}[119]. The normalized electron transition (E_T^N) approaches one for nonpolar solvents and zero for polar solvents. The dimensionless E_T^N values for DES ranges from 0.530 to 0.597 whereas methanol and ethyl acetate have 0.649 and 0.740, respectively. The low E_T (NR) values of DES confirms the high polarity of the solvent compared to some traditional solvents.

Table 2.5. Electronic and normalized transition in DES

DES	E_T (NR)/ kcal. mol^{-1}	E_T^N
[Ch]Cl:urea	50.04336	0.597017
[Ch]Br:urea	49.92685	0.593421
[Ch]Cl:malic acid	48.59735	0.552387
[Ch]Br:malic acid	48.29635	0.543097
[Ch]Cl:malonic acid	48.02594	0.534751
[Ch]Br:malonic acid	47.89186	0.530613
Methanol	51.73361	0.649185
Ethyl acetate	54.66815	0.739758

Using this one single parameter as an index of solvent polarity, a proposed increasing order for polarity is ethyl acetate < methanol< [Ch]Cl: urea < [Ch]Br:urea < [Ch]Cl:malic acid < [Ch]Br:malic acid < [Ch]Cl:malonic acid < [Ch]Br:malonic acid. The results show a clear trend that changing the anion of the HBA alters the polarizability of the DES. Since the electronegativity (χ) of Cl^- ion is greater than Br^- ion, it was expected that the polarity of the chloride-based DES should be higher than the bromide counterpart. Regardless of the χ difference between the anions, the bromide-based DES showed higher polarizability than the chloride-based DES studied. This trend indicate that DES polarity may not be attributed solely to the χ difference of the anion, but other factors like dielectric constant may contribute. Based on results, we showed that the bigger size of the Br^- ion makes the anion more polarizable than the Cl^- ion to effect on the polarity.

2.3.6. Behavior of DES viscosity

Viscosity of most available DES has been extensively studied[103, 121]. Nonetheless, data on how Cl^- and Br^- anions affect DES viscosity has not been explored thoroughly. The degree of viscosity increases as the molar ratio of the hydrogen bond donor increases[121].

From our results in Table 2.6., the classical [Ch]Cl:urea has a viscosity of 777.5 ± 23 mPa.s at 25 °C comparable to 750 mPa.s reported in literature[103]. Changing the anion from Cl^- to Br^- approximately doubled the viscosity of the [Ch]Br:urea to 1533 ± 18 mPa.s. The [Ch]Cl:malonic acid and [Ch]Br:malonic acid have viscosity of 836.8 ± 56 and 890.9 ± 28 mPa.s, respectively. A high viscous clear liquid was observed from either [Ch]Cl or [Ch]Br with malic acid. The presence of an extra hydroxyl group in malic acid may account for their high viscosity than its diacid counterpart[40]. This extra hydroxyl group may be involved in hydrogen bond which further increases the viscosity. Unlike [Ch]Cl/Br-based DES, [Ch]I DES with urea, malonic acid, and malic acid solidifies at room temperature and its viscosity could not be determined.

Table 2.6. Viscosity of DES at 25 °C.

DES	Viscosity (cP)
[Ch]Cl:urea	777.5 ± 23
[Ch]Br:urea	1533 ± 18
[Ch]Cl:malonic acid	836.8 ± 56
[Ch]Br:malonic acid	890.9 ± 28
[Ch]Cl:malic acid	1478.3 ± 66
[Ch]Br:malic acid	1216.7 ± 42

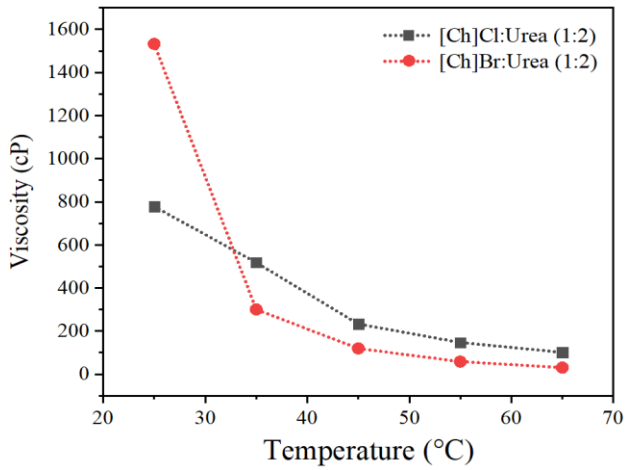

Figure 2.5. Viscosity of DES as a function of temperature.

Using [Ch]Cl:urea and [Ch]Br:urea as model solvents, the temperature effect on viscosity (Fig. 2.5) was investigated by fitting the viscosity-temperature data into the Arrhenius-type equation (equation 2.1). This plot allowed to calculate the activation energy of flow, a measure of intermolecular forces, in the DES[40, 103].

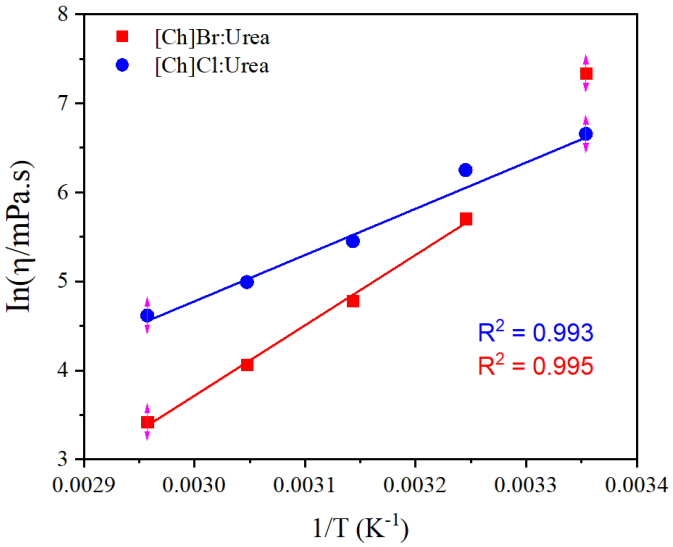

Figure 2.6. Arrhenius plot of DES at 0.75 s^{-1} shear rate.

The E_a of [Ch]Cl:urea was found to be -43.20 ± 0.25 kJ/mol whereas [Ch]Br:urea is 65.71 ± 0.32 kJ/mol (Fig.2.6.). The larger the viscosity, the higher the E_a and the more difficult it is for ions to move past each other due to size or interactions in the DES[40, 103]. Interestingly, the viscosity of both [Ch]Cl:urea and [Ch]Br:urea decreased drastically to 101 mPa.s and 31 mPa.s, respectively, when temperature was increased to 338.15 K (Fig. 2.5.). The low viscosity of [Ch]Cl/Br:urea (≤ 518 mPa.s) even at lower temperature, T=308.15 K, makes it industrially applicable and can compete with conventional organic solvents for synthesis, extraction, and pharmaceuticals.

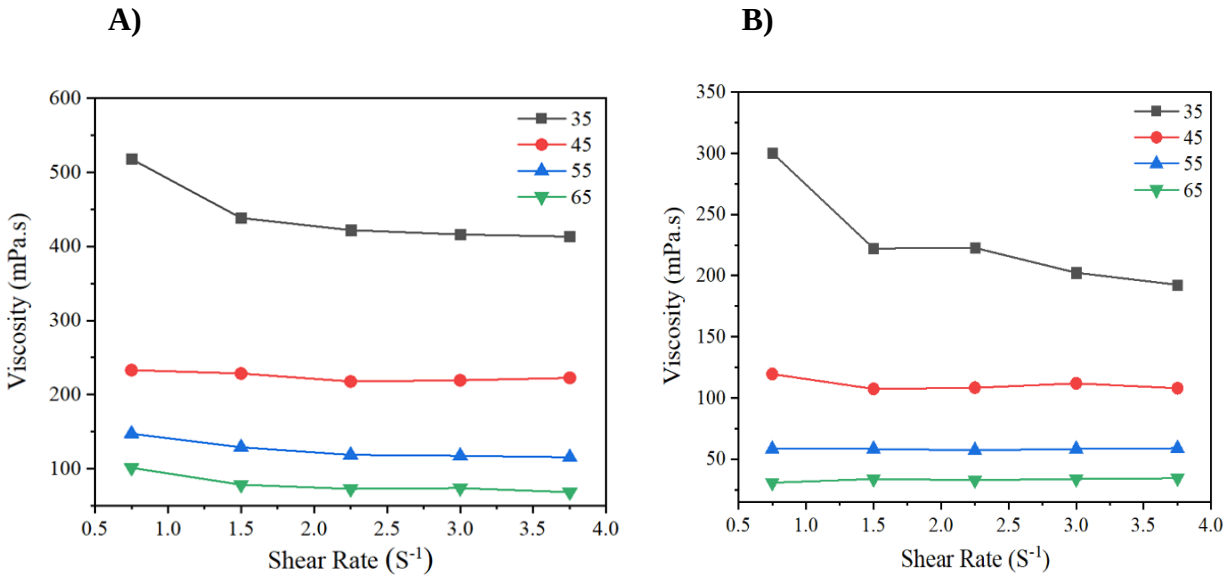

Figure 2.7. Viscosity as a function of shear rate. **A)** [Ch]Cl:urea and **B)** [Ch]Br:urea

The rheological characteristics of [Ch]Cl:urea and [Ch]Br:urea suggest that both solvents behave as Newtonian fluid at temperatures between 35 ℃ to 65 ℃ (Fig.2.7.). Like water, organic solvents, glycerol, and alcohol, a Newtonian fluid exhibits constant viscosity at different shear rates. On the other hand, the DES irrespective of the anion shows a linear relationship between shear stress and shear rate at higher temperatures. Contrary to this, at low temperature less than 35 ℃, and shear rate less than 1.5 s^{-1}, the DES behave as a non-Newtonian liquid due to high viscosity exhibited by hydrogen bonding.

2.3.7. Anions affect pH and conductivity

pH measures the degree of acidity or alkalinity of a solution. The lower the pH values, the higher the availability of free H^+ ions which are not involved in hydrogen bonding. Relatively, choline bromide versus the carboxylic acids DES have lower pH values than DES made with the same acids with choline chloride (Table 2.7.). This is probably due to the relatively stronger hydrogen bond network formed by the Cl^- ion with the protons compared to the Br^- ion. A similar trend was observed when the conductivity (κ) of the DES was measured at increasing temperature. DES with lower pH shows higher conductivity than DES with higher pH. The κ of [Ch]Cl:urea and [Ch]Br:urea at 30 ℃ is 1207.3 ± 4.0 μS cm^{-1} and 1086.7 ± 5.1 μS cm^{-1} (Fig.2.8B.), respectively, compared to 1287 μS cm^{-1} of the former reported in literature[47]. Since [Ch]Br:malic acid had lower pH, its κ from 25 ℃ to 40 ℃ was always higher than [Ch]Cl:malic acid (Fig.2.8A.). The higher the pH, the lower the available free protons, and hydrogen bonding is expected to be high. It should however be mentioned that conductivity of ionic liquids or DES also depends on the availability of charges and their degree of mobility[10].

A comprehensive review by Wasserscheid and Welton (2007) revealed a weak correlation between cation type and size on ILs conductivity[10]. The results point out a strong correlation between anionic size and availability of protons in DES conductivity.

$$\ln(\kappa) = \ln(\kappa_o) - E_a/RT \quad \text{(Equation 2.4)}$$

$$\ln(\kappa) = \ln(\kappa_o) - E_a/R(T-T_o) \quad \text{(Equation 2.5)}$$

Table 2.7. pH of DES measured at room temperature.

DES	pH
[Ch]Cl:urea	9.94
[Ch]Br:urea	10.18
[Ch]Cl:malic acid	0.58
[Ch]Br:malic acid	-0.21
[Ch]Cl:malonic acid	-0.27
[Ch]Br:malonic acid	-1.51

From the plot of the natural logarithm of specific conductivity (ordinate) against the reciprocal of temperature T in K (abscissa), the temperature independent activation energy of conductivity, *E*a, of DES was calculated by multiplying the gas constant R by the slope. The introduction of an extra variable T_o into the fitting process (equation 2.5) makes the temperature dependent Vogel-Fulcher-Tammann (VFT) equation not ideal for calculations[121]. The lower the DES viscosity, the higher the conductivity.

This inverse relationship is explained by the Walden rule which shows a strong relationship between fluidity (inverse of viscosity) and ionic conductivity[121-123]. The activation energy of conductivity of [Ch]Br:malic acid is 47.06 ± 0.30 kJ mol^{-1}, [Ch]Br:urea is 42.11 ± 2.6 kJ mol^{-1}, [Ch]Br:malonic acid is 37.55 ± 0.44 kJ mol^{-1} , [Ch]Cl:malic acid is 40.89 ± 0.35 kJ mol^{-1}, [Ch]Cl:urea is 37.52 ± 0.68 kJ mol^{-1}, and [Ch]Cl:malonic acid is 29.93 ± 0.19 kJ mol^{-1} (Fig. 2.8.).

The results indicate that increasing the anion size of the HBA increases the E_a of conductivity. A recent report shows that increasing the anionic size of ionic liquids increase their conductivity, however, no clear correlation has been established[10, 123]. Although, size may impede DES mobility, nonetheless, the bromide anion may weakly interact with the available protons, making them (proton charges) available to conduct.

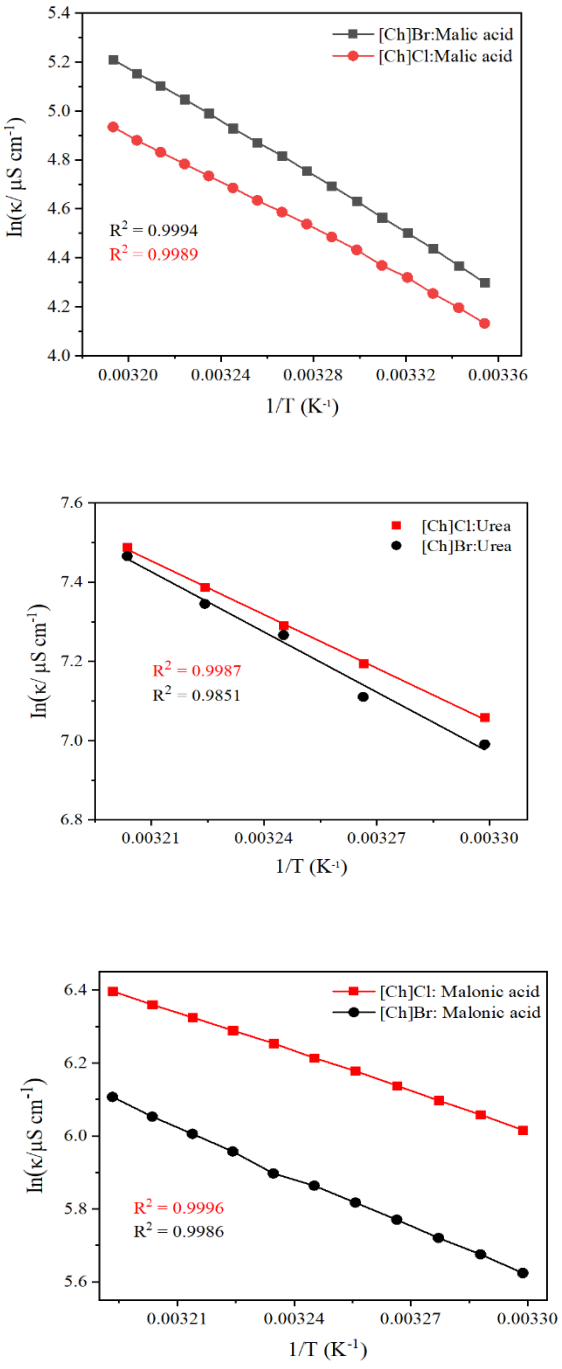

Figure 2.8. Arrhenius plot of the natural logarithm of conductivity versus the inverse of temperature.

2.3.8. Influence of anions on DES melting point

Differential scanning calorimetry (DSC) measures temperature and heat flow associated with the thermal transition of the sample. The thermal phases of urea, malonic acid, malic acid, [Ch]Cl, and [Ch]Br were analyzed using the TA universal analysis software. Melting point is an endothermic process and first-order phase transition in crystalline polymers. Conversely, glass transition is a second-order transition with no heat transfer as temperature rise causes amorphous glassy material to be in a rubbery form. The T_g of [Ch]Cl:malic acid is -56.48 °C[124], and T_m for [Ch]Cl:urea and [Ch]Cl:malonic acid are 12 °C[36] and 10 °C[35], respectively. Comparably, the T_g of [Ch]Cl:malic acid and [Ch]Br:malic acid were found to be -55.61 °C and -53.89 °C, respectively (Table 2.8.). An increase in melting temperature occurs when [Ch]Cl:maleic acid (mp = 36.21 °C) is changed to [Ch]Br:maleic acid (mp = 71.24 °C) due to changing the anion in the salt. From Table 2.8., as the size of halides increase, DES melting point increases and consequently affects the physical characteristics of the liquid. From the aforementioned, most HBA containing iodide halides solidifies within the first 10 min after preparation at room temperature.

Table 2.8. Melting and glass transition temperature of DES

HBD	[Ch]Cl	[Ch]Br	[Ch]I
Urea	19.21	35.53	70.27
Malic acid	-55.61*	-53.89*	31.24
Malonic acid	8.52	-2.68*	52.25

*T_g = glass transition temperature

2.3.9. Thermogravimetric analysis (TGA)

2.3.9.1. Effect of anions on DES stability

A TGA analysis measures the mass loss of a sample placed in a furnace as it undergoes a series of thermal events. By this, the thermal stability of the DES can be estimated by analyzing the behavior of their thermal cycling. Unlike choline iodide, [Ch]Cl and [Ch]Br DES stays liquid at room temperature and was of interest to determine their thermal stability. Keeping in mind, atomic radii of Cl^- and Br^- increase with increasing atomic number, and electronegativity of Cl^- is greater than Br^-, the tendency of forming hydrogen bonding between the two halides will differ. Hydrogen bond in most DES occurs through charge delocalization between the halide and the HBD[34]. Due to the difference in size and electronegativity of the anions, it is expected that the hydrogen bond profile would be different. It is not surprising the melting point of chloride-based DES are relatively lower than bromide-based DES and iodide -based DES. Simulation results by COSMO-RS shows that Cl^- ions form relatively stronger hydrogen bond with HBD and has advantage to form eutectic solvents compared to Br^- and I^-.

Table 2.9. Decomposition temperatures of DES by thermogravimetric analysis.

DES	T_{onset}/°C	T_{endset}/°C	$T_{1/2}$/°C
[Ch]Cl:urea	173.53	273.43	259.71
[Ch]Br:urea	194.73	286.22	272.46
[Ch]Cl:malic acid	173.20	277.23	250.60
[Ch]Br:malic acid	179.43	279.22	260.51
[Ch]Cl:malonic acid	124.37	155.48	150.0
[Ch]Br:malonic acid	131.11	163.93	158.38

The results demonstrate that varying the anion alter the acceptor's ability to interact with the donor. The inability for the I^- to form stronger hydrogen bond makes [Ch]I and HBD mixtures solid at room temperature. The impact of DES anions on thermal stability remains untapped and such data are missing in the literature. By using the thermal degradation or mass loss as an index for stability, we analyzed the degradation profile of all six DES mixtures by TGA and DTG (Table 2.9.). T_{onset} is defined as the temperature at which the DES begin to loss approximately 3 % of its percent weight, T_{endset} is the temperature at which DES degradation stops, and $T_{1/2}$ is the temperature at half weight percent. From the results, the T_{onset} values for the DES depict the strength of the intermolecular force between the HBA and the HBD (Fig. 2.9.). The stronger the intermolecular forces, the higher the thermal stability of the DES (high T_{onset} value). From Table 2.9., the T_{onset} of [Ch]Br:urea > [Ch]Cl:urea, [Ch]Br:malic acid > [Ch]Cl:malic acid, and [Ch]Br:malonic acid > [Ch]Cl:malonic acid. The stronger intermolecular force between [Ch]Br and urea or malonic acid confirms the high viscosity values obtained for those DES. The high $T_{1/2}$ values for most DES explains the possibility of applying the solvent industrially even at elevated temperatures. The DTG thermogram of [Ch]Cl:malonic acid (Fig. 2.9E) and [Ch]Br:malonic acid (Fig. 2.9F) shows major peaks at 155 ℃ and 164 ℃, respectively, representing malonic acid degradation. The detachment of malonic acid from the HBA at such low temperature relative to the other HBD is an indication of the weaker intermolecular force between malonic acid and the acceptor.

Regarding how different HBDs effect on the intensity of hydrogen bonding, the T_{onset} of [Ch]Cl:urea > [Ch]Cl:malic acid > [Ch]Cl:malonic acid and [Ch]Br:urea > [Ch]Br:malic acid > [Ch]Br:malonic acid. Although, malonic acid and malic acid are

dicarboxylic acids, malic acid interacts strongly with the HBA with $T_{1/2} > 250$ ℃. Due to the extra hydroxyl group in malic acid, it is possible for the acid to form a more or stronger hydrogen bonds. The ΔT_{onset} between the [Ch]Cl/Br with malic acid DES is approximately 48 ℃ different compared to [Ch]Cl/Br with malonic acid. The results indicate that different HBD can significantly alter the intermolecular interactions and the nature of the DES. The thermal stability data corroborate with other structural characterization studies to establish the necessity of both HBA and HBD as integral agents during DES formation.

A) [Ch]Cl:urea

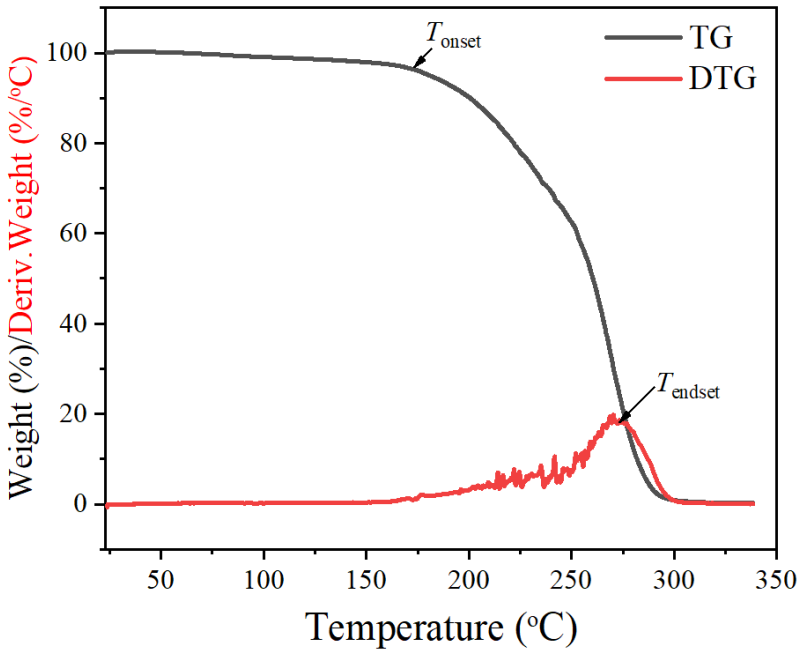

B) [Ch]Br:urea

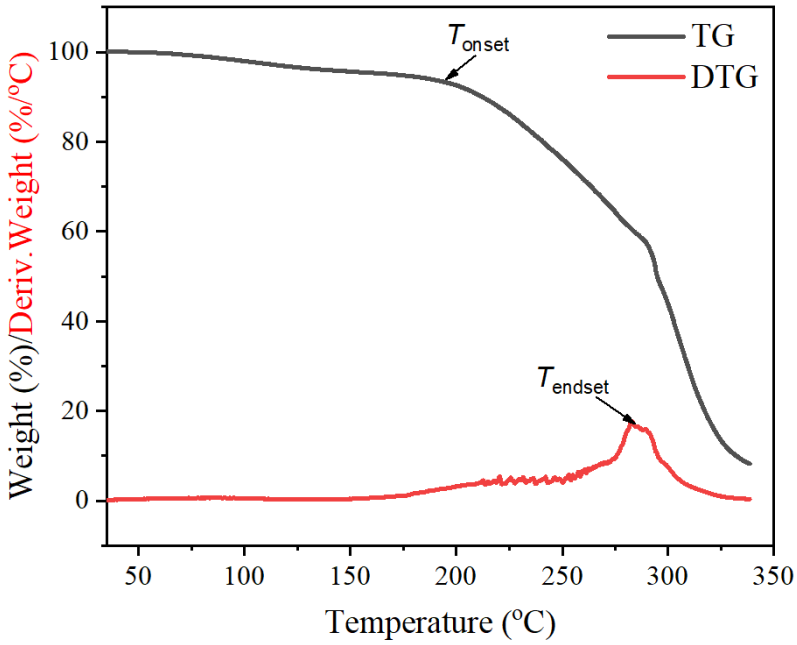

C) [Ch]Cl:malic acid

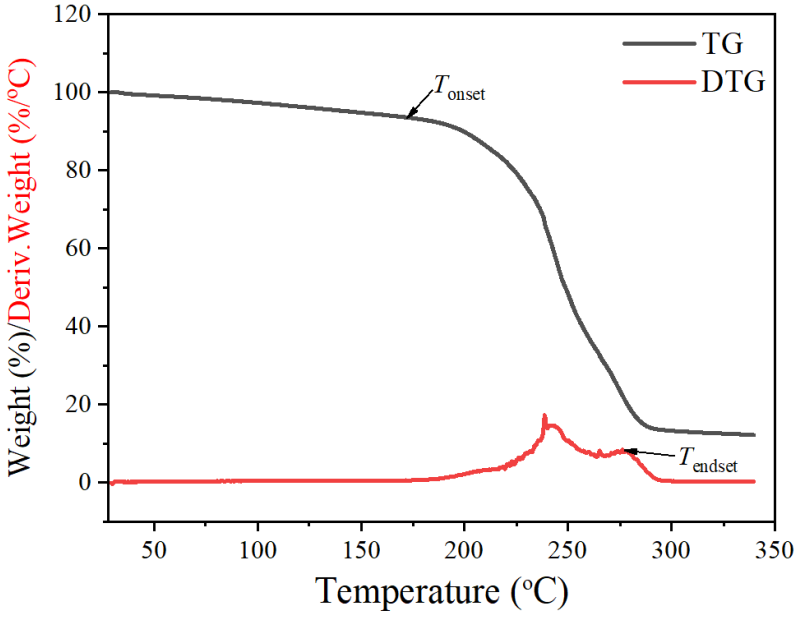

D) [Ch]Br:malic acid

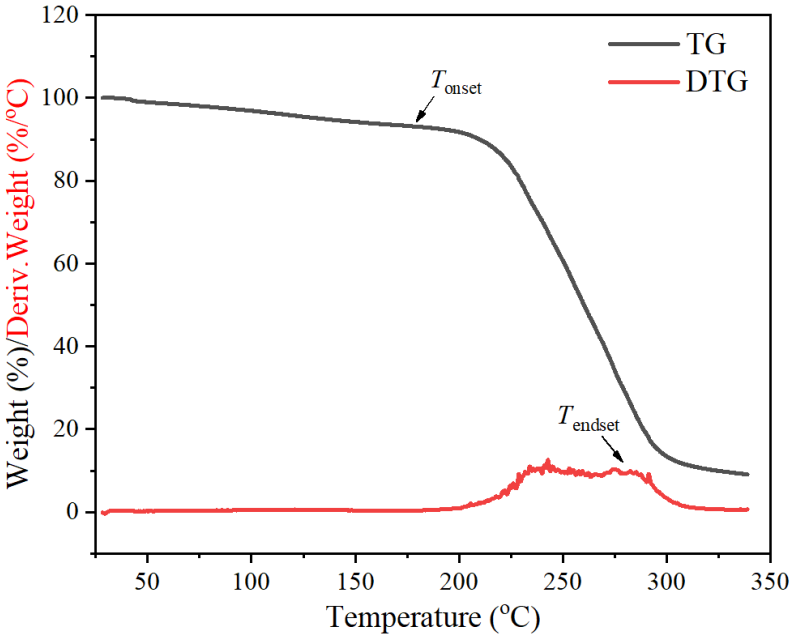

E) [Ch]Cl:malonic acid

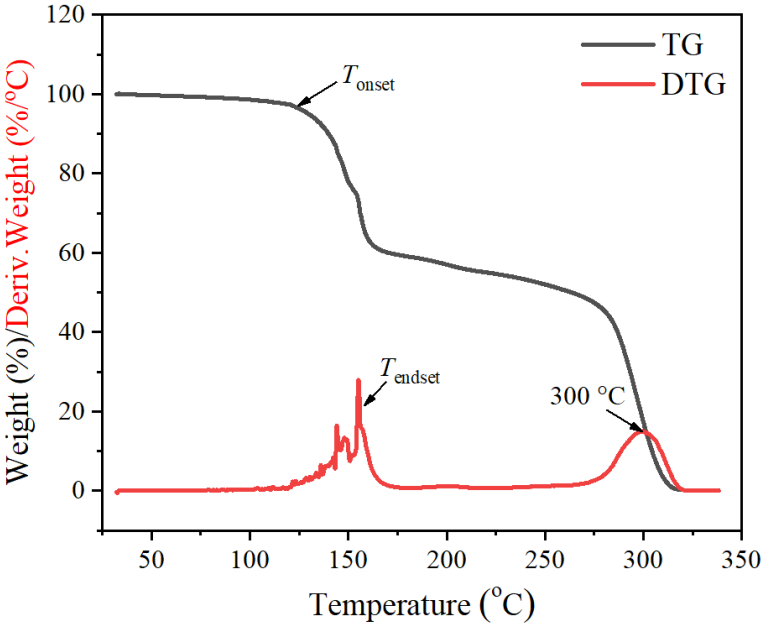

F) [Ch]Br:malonic acid

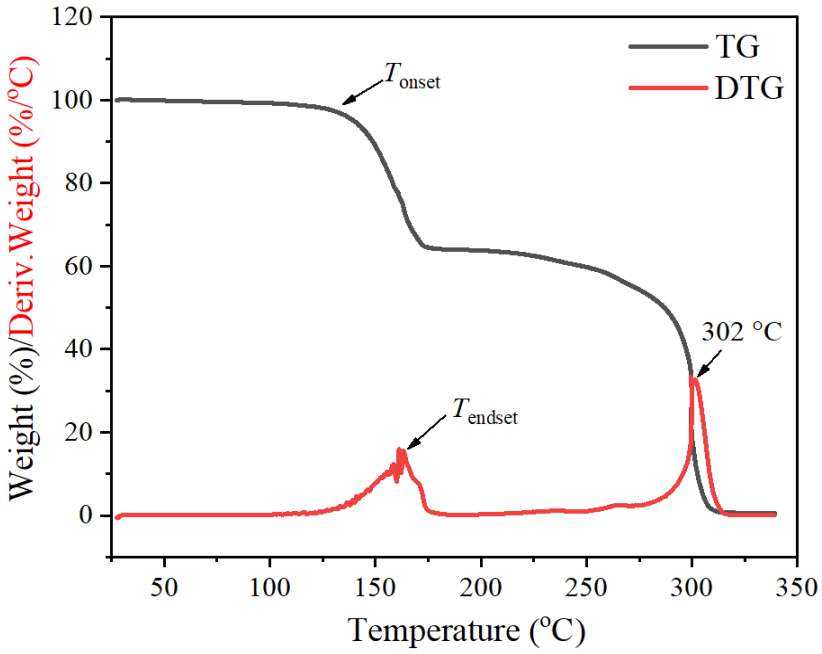

Figure 2.9. Thermogravimetric analysis of DES. **A)** [Ch]Cl: urea, **B)** [Ch]Br: urea, **C)** [Ch]Cl: malic acid, **D)** [Ch]Br: malic acid, **E)** [Ch]Cl: malonic acid, and **F)** [Ch]Br: malonic acid.

2.3.10. COSMO and COSMO-RS Theory

2.3.10.1. COSMO Surfaces

In COSMO, the solute forms a cavity and are calculated in a virtual conductor environment. The atom-specific charges on the solute induces a polarization charge density (σ) on the interface between the cavity and the conductor to cancel the resulting electric field within the conductor and its surrounding[110, 112]. In doing this, the solute molecule is then converged to its energetically optimal state in a conductor with respect to electron

density. From Fig. 2.10., the COSMO surface of the acceptor compound combines with the donor at the correct molar ratio to form DES. The polarizable charge density at the molecules surface is then calculated and termed as the screening charge density (SCD, σ), a good local descriptor for a molecules polarity. Electrostatic interaction arises from the contact of two different SCDs since in reality, no conductor exists between two molecules surface[107].

From the sigma profiles generated (Fig. 2.11.), the graph can be divided into three parts depending on the screening charge density. HBD have negative SCD ($-0.0084\ e/Å^2 \leq \sigma$) and HBA have positive SCD ($\sigma \geq +0.0084\ e/Å^2$)[125-126]. Between this region is the non-polar region. SCD at $-0.0084 \leq \sigma \geq +0.0084\ e/Å^2$ is considered sufficiently polar to induce hydrogen bonding. The screening charge density of molecules make COSMO-RS an efficient tool to qualitatively and quantitatively predict the polarity of molecular surfaces. In terms of polarity, positive SCD represent negative polarity whiles the negative SCD describes positive polarity. The σ-profile describes the thermodynamic behavior of individual components, whereas σ-potential describes the affinity or interactions of compounds with other components[126]. At the acceptor region of the QAS sigma profile, the charge density of the anions decreases in the order $Cl^- > Br^- > I^-$ (Fig. 2.11A). Although, the sigma profile of the QAS has a donor region, no significant change occurred in their charge density. The difference in size and electronegativity of the QAS impacted on their charge density. Plotting the charge density ($e/Å^2$) against the chemical potential ($\mu(\sigma)$/kcal/mol$Å^2$) shows that [Ch]Cl has the highest affinity for HBD (more negative $\mu(\sigma)$ value) and [Ch]I have the lowest affinity (less negative $\mu(\sigma)$ value) for HBD.

Conversely, [Ch]I have the highest affinity for HBA whiles [Ch]Cl has the lowest. The results give a clear indication that the Cl^- ion can interact strongly with induced H^+ ion to form hydrogen bonds than the Br^- and I^- counterparts.

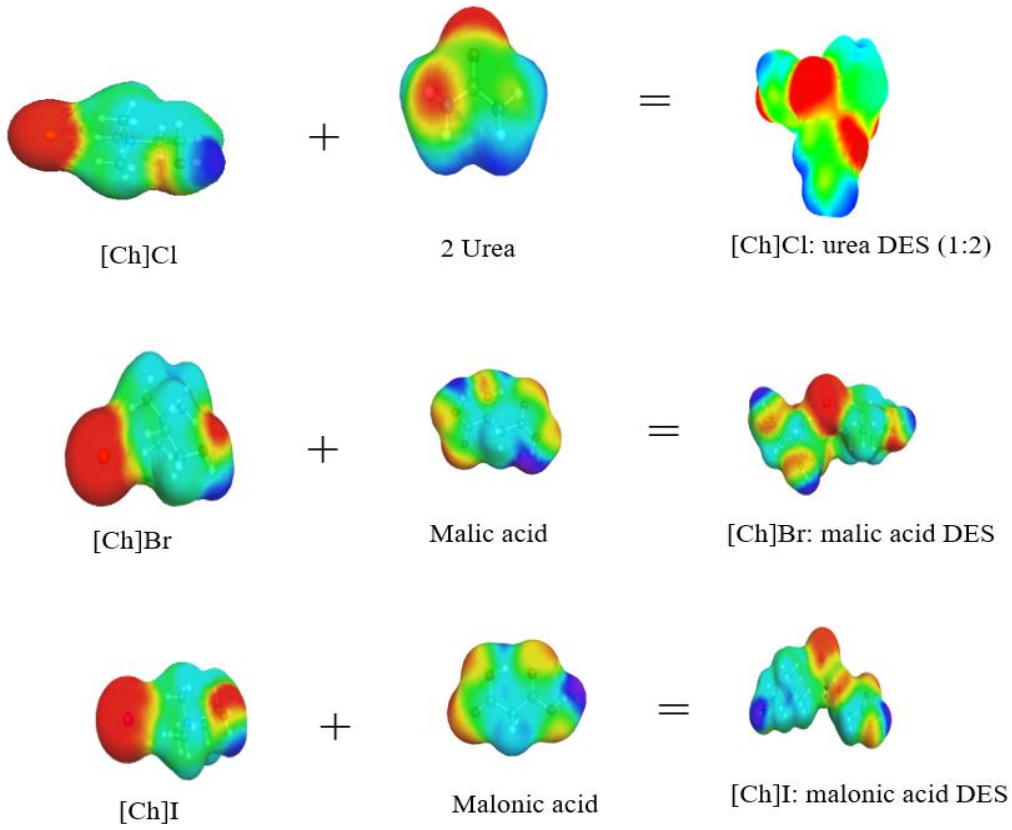

Figure 2.10. Schematic representation of DES formed by mixing hydrogen bond acceptor with hydrogen bond donor. Red = HBA region, and Blue = HBD region.

A)

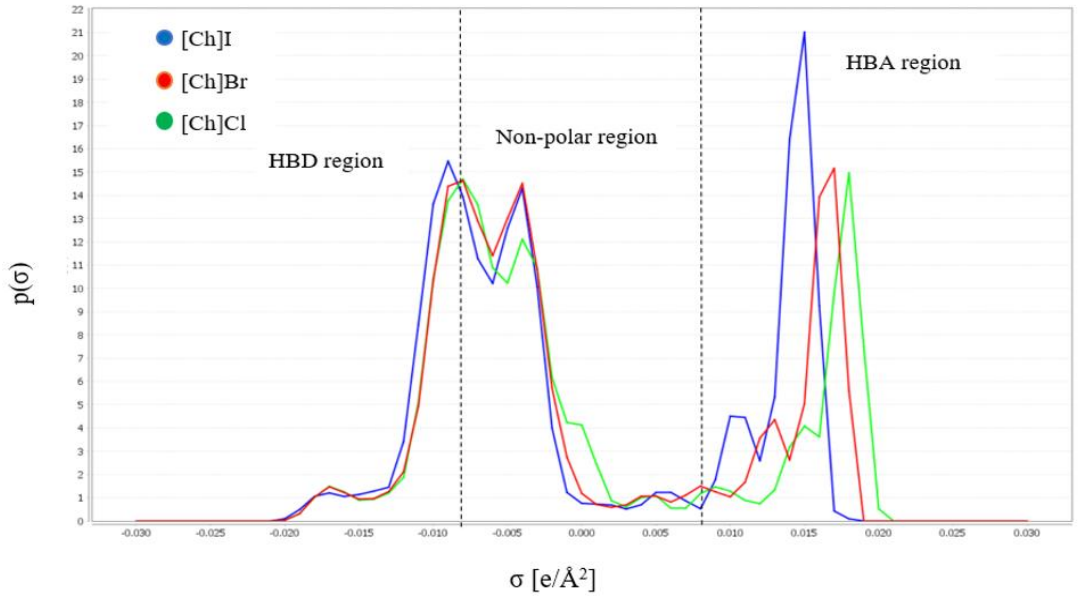

B)

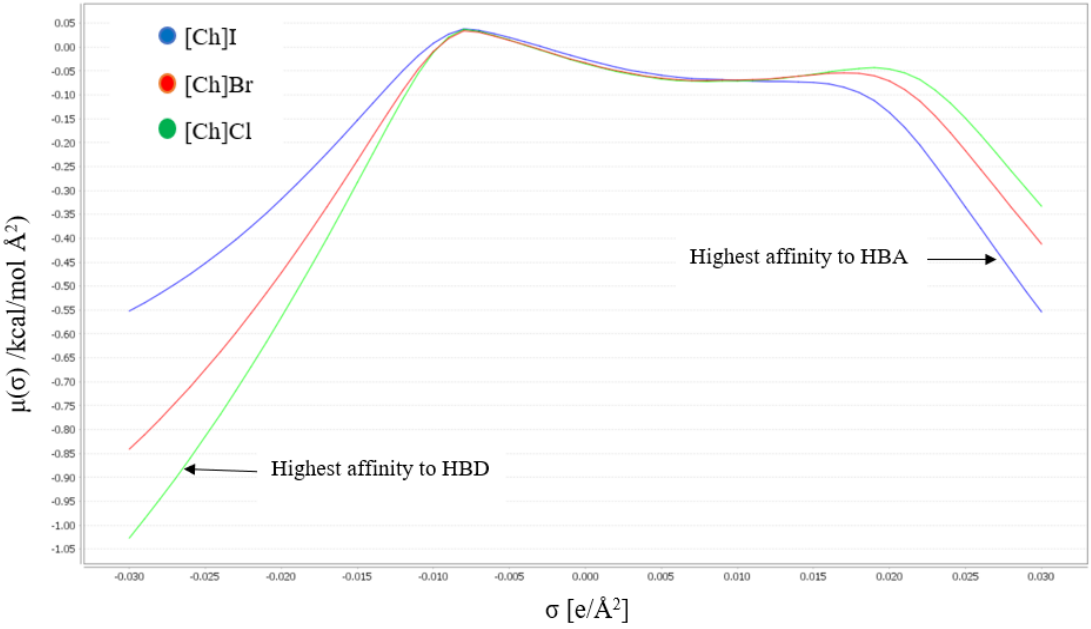

Figure 2.11. Effect of anions on the hydrogen bond acceptor. **A) =** Sigma plot and **B**) = sigma potential of the QAS.

2.3.10.2. Effect of HBD in DES formation

HBD affect charge surface polarity of DES mixtures. In this study, we selected nine known HBD from the literature and categorized them into two groups based on their acidity. The acidic group consist of malic acid, malonic acid, pTSA, oxalic acid, and citric acid whereas the non-acidic group comprised of urea, xylitol, acetamide, and ethylene glycol. Among the acidic HBD, [Ch]Cl: malic acid had the most negative μ (σ) value of -0.74 kcal/mol $Å^2$ whereas [Ch]Cl: citric acid has the lowest value of -0.36 kcal/mol $Å^2$. Since surface charge density affects polarity and hydrogen bonding interaction, we can predict the strength of hydrogen bonding of DES in increasing order [Ch]Cl:citric acid < [Ch]Cl:pTSA < [Ch]Cl:oxalic acid < [Ch]Cl:malonic acid < [Ch]Cl:malic acid (Fig. 2.12. and Fig. 2.13.). The opposite is true for the DES with highest potential to accept other molecules. The high σ distribution of citric acid-based DES is due to the seven oxygen atoms from the tricarboxylic acid (Fig.2.12A). Also, it is not surprising that pTSA has the highest distribution at the non-polar region of the sigma profile because of the aromaticity of the benzene group. The peaks located between -0.008 and -0.023 $eÅ^{-2}$ represent H atoms used in hydrogen bonding. For the 'non-acid' HBD, [Ch]Cl:ethylene glycol 1:2 had the most nonpolar character. In terms of hydrogen bonding interaction, the decreasing order follows as [Ch]Cl:urea > [Ch]Cl:xylitol > [Ch]Cl:ethylene glycol > [Ch]Cl:acetamide with μ (σ) values of -0.86, -0.82, -0.78, and -0.63 kcal/mol $Å^2$, respectively. As discussed previously, the TG/DTG plot showed a stronger intermolecular interaction (higher onset decomposition temperature, T_{onset}) of [Ch]Cl: urea greater than [Ch]Cl:malic acid and [Ch]Cl:malonic acid. Simulations by COSMO-RS supports the experimental data due to the hydrogen bonding pattern established.

COSMO-RS simulations can be used to estimate the strength of hydrogen-bonding in DES and further classify the solvent based on their polarity in a time efficient manner.

A)

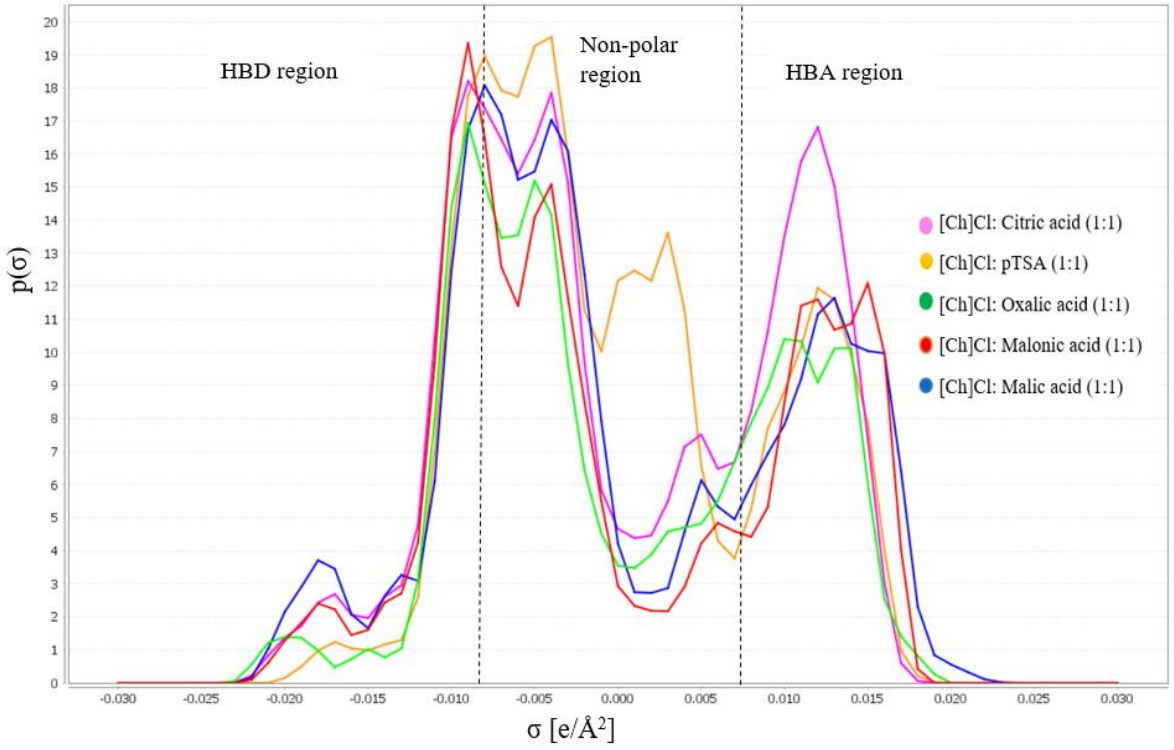

B)

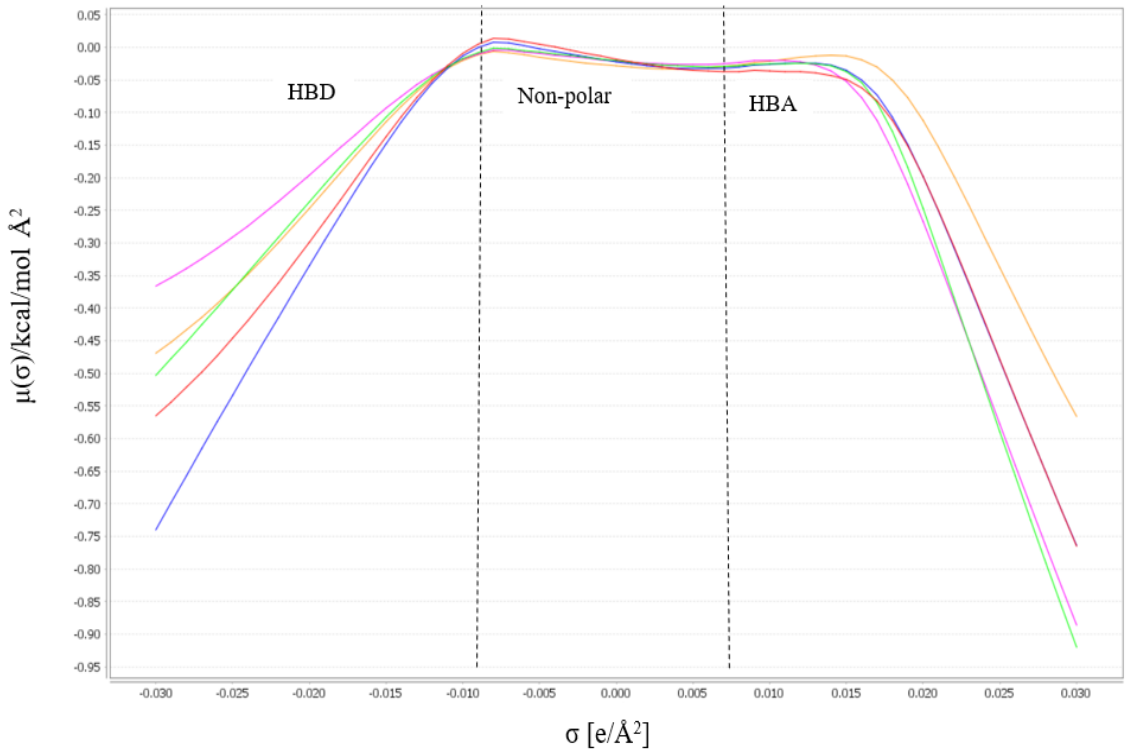

Figure 2.12. Effect of acidic HBD on DES formation. **A) =** Sigma plot of DES with acidic HBD and **B**) = sigma potential of DES with acidic HBD.

A)

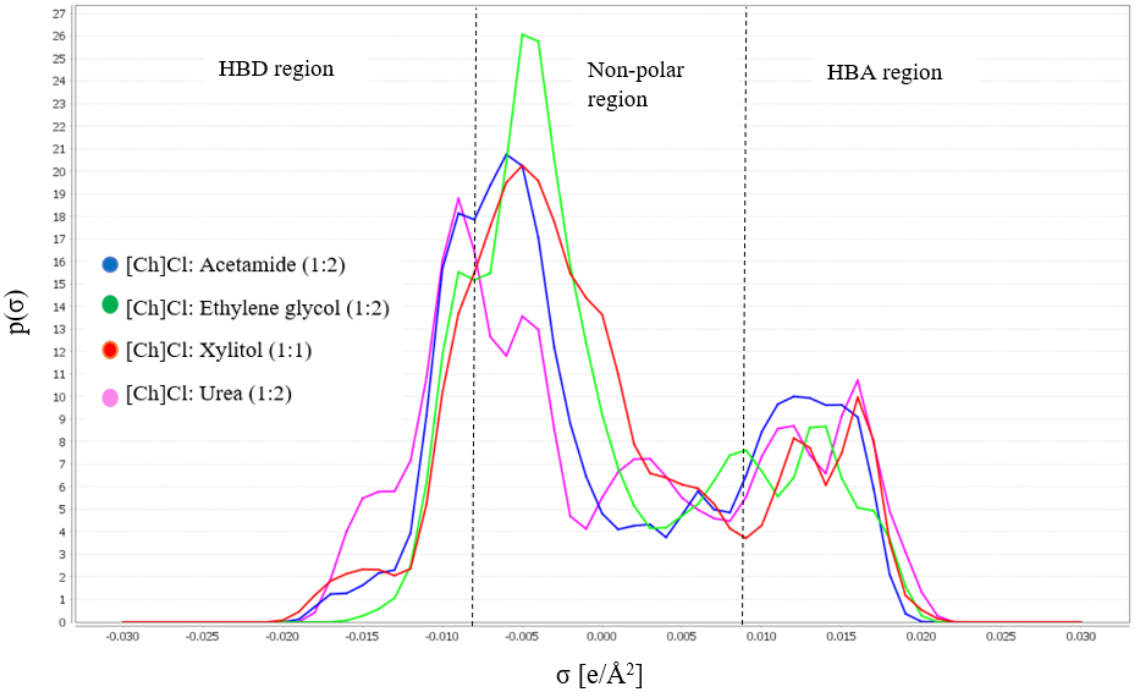

B)

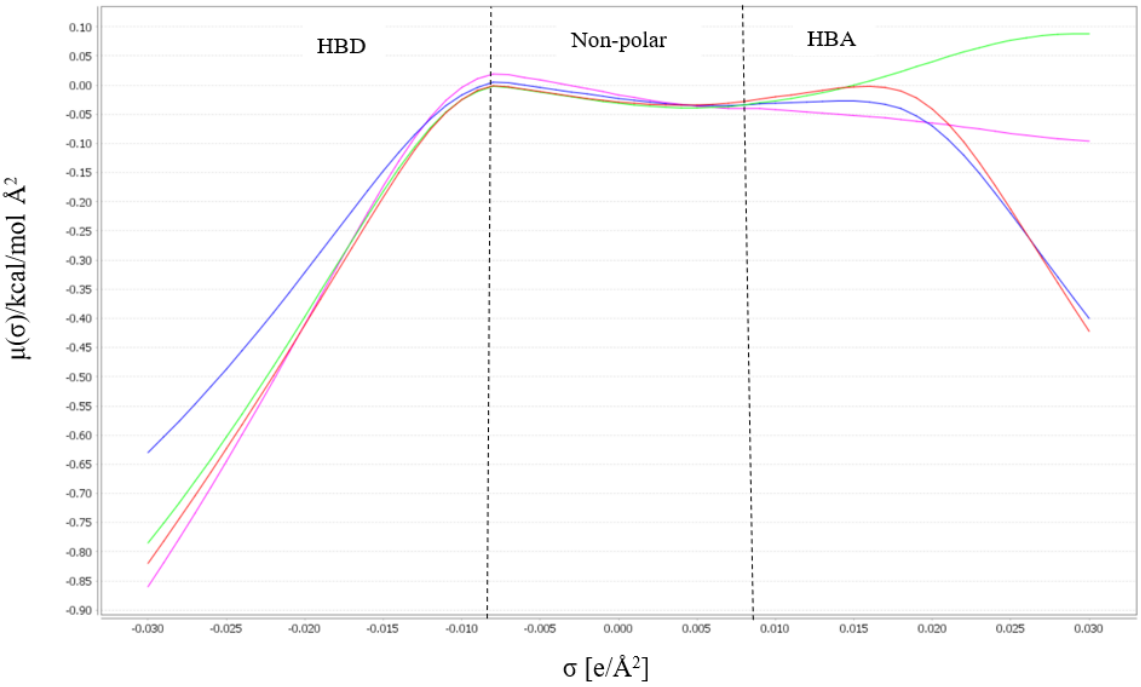

Figure 2.13. Effect of non-acidic HBD on DES formation. **A) =** Sigma plot of DES with non-acidic HBD and **B)** = sigma potential of DES with non-acidic HBD.

2.3.10.3. Effect of anions in DES

To further understand how anions impact DES formation, we selected and simulated [Ch]Cl, [Ch]Br, and [Ch]I with urea and malic acid as hydrogen bond donors. Malic acid and urea were selected because of their high donating strength to form hydrogen bonds. From Fig. 2.14A and Fig. 2.15A, the H atoms of the sigma profile between -0.008 and -0.023 $eÅ^{-2}$ had the same charge distribution p (σ) but variations occurred at the acceptor region (> σ + 0.008). Variations at the acceptor region is due to electronegativity difference and size of the QAS. In terms of hydrogen bonding interactions, the chloride-based DES shows higher affinity for HBD and less affinity for HBA.

The μ (σ) of [Ch]Cl:malic acid, [Ch]Br:malic acid, and [Ch]I:malic acid is -0.74, -0.67, and -0.46 kcal/mol $Å^2$, respectively, whereas [Ch]Cl:urea, [Ch]Br:urea, and [Ch]I:urea gave -0.86, -0.82, and -0.77 kcal/mol $Å^2$ (Fig. 2.14B. and Fig. 2.15B.). From the results, increasing the size and/or decreasing the electronegativity of the anion decreases the chemical potential of the DES. Interestingly, [Ch]Cl and [Ch]Br show similar distribution pattern across all DES formed demonstrating the possibility of using replacing the most used [Ch]Cl, with [Ch]Br.

A) Sigma profile DES formed with malic acid and different anions.

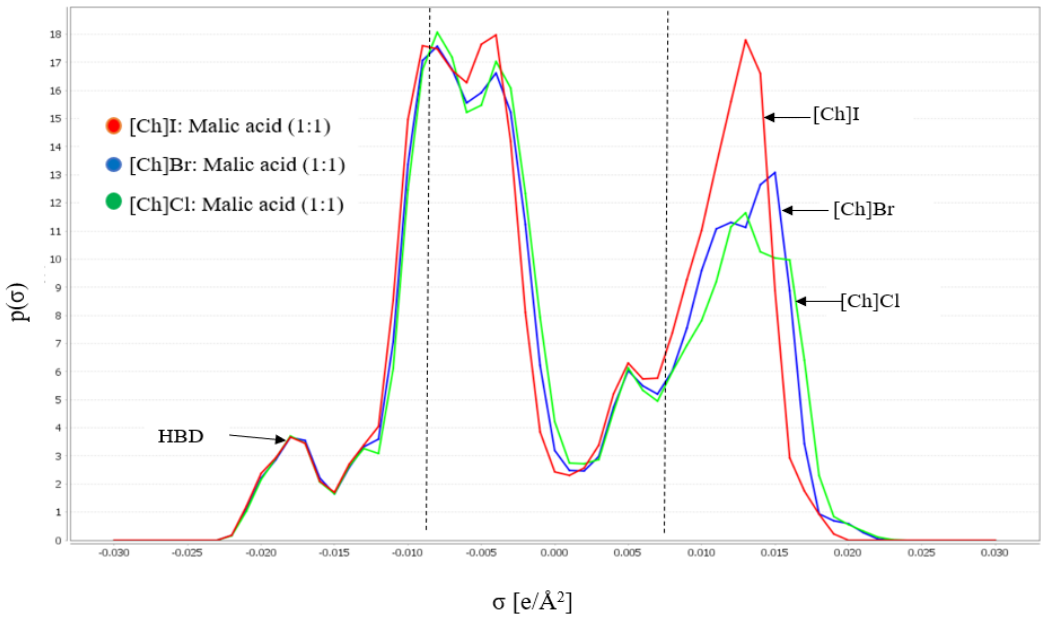

B) Sigma potential DES formed with malic acid and different anions.

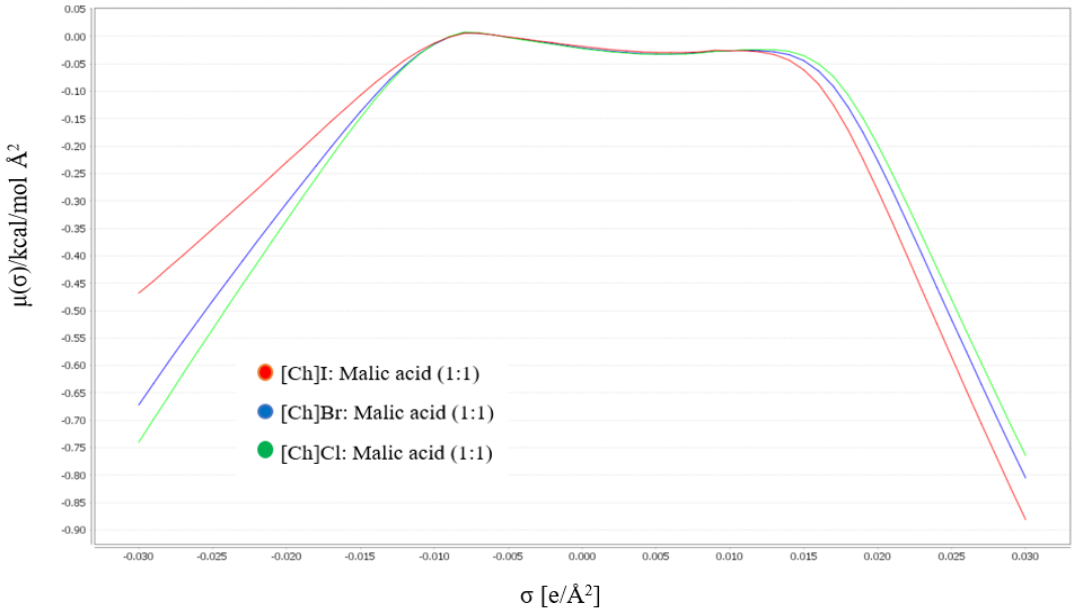

Figure 2.14. Effect of different HBA on DES formation. **A) =** Sigma plot of DES with malic acid and **B**) = sigma potential of DES with malic acid.

A) Sigma profile DES formed with malic acid and different anions

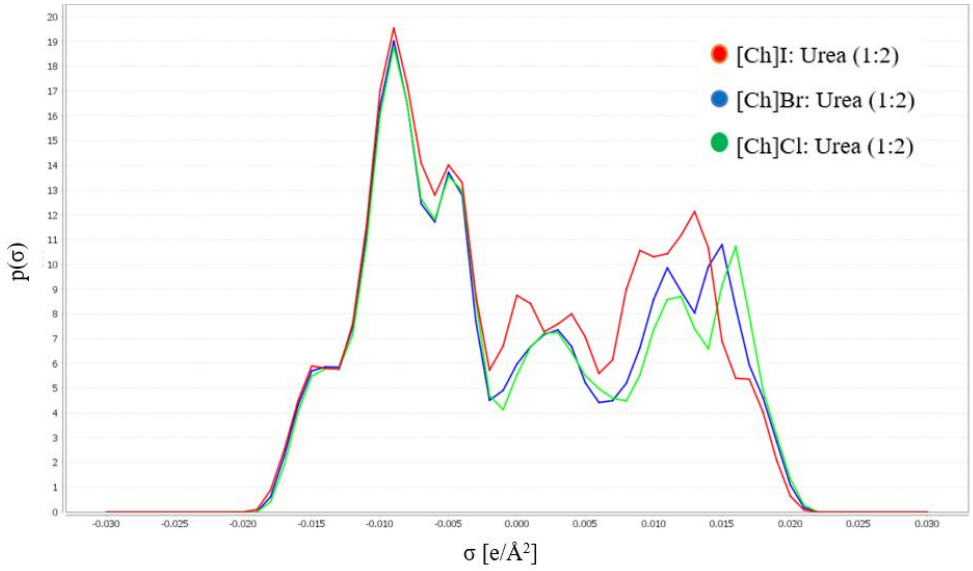

B) Sigma potential DES formed with malic acid and different anions

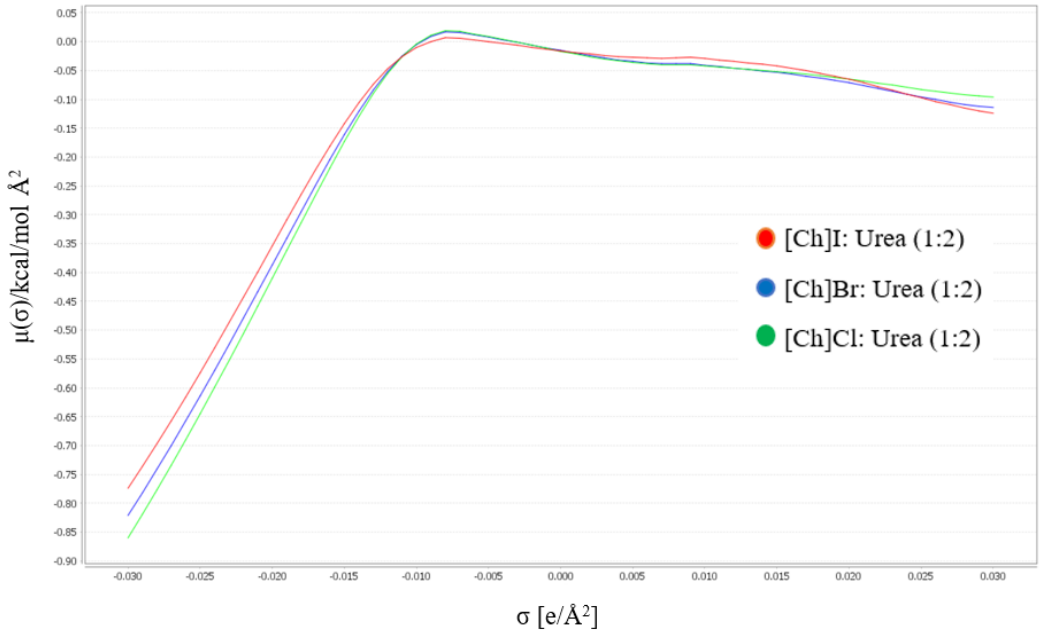

Figure 2.15. Effect of different HBA on DES formation. **A) =** Sigma plot of DES with malic acid and **B**) = sigma potential of DES with malic acid.

2.3.10.4. Vapor pressure

For environmental applications such as cleaning surfaces, coating, and dehydration, vapor pressure becomes an inevitable parameter to avoid for environmental sustainability. Total vapor pressure (PV_{tot}) is a thermodynamic parameter that describe the tendency of a molecule to escape into the atmosphere and therefore measures the attractive force holding solvent particles together. Aissaoui et al.[115], showed that combining [Ch]Cl with glycols reduces the volatility of the glycols[115]. In view of this, it was hypothesized that altering anions will significantly change the vapor pressure of the resulting DES. In this study, we tested our hypothesis by studying the volatility of [Ch]Cl, [Ch]Br, and [Ch]I with a variety of hydrogen bond donors. As the van der Waal forces increases, QAS volatility decreases with increasing size of the anion. The PV_{tot} of [Ch]Cl and [Ch]Br are similar and could explain why the two acceptors share in common some physicochemical properties (Fig. 2.16.).

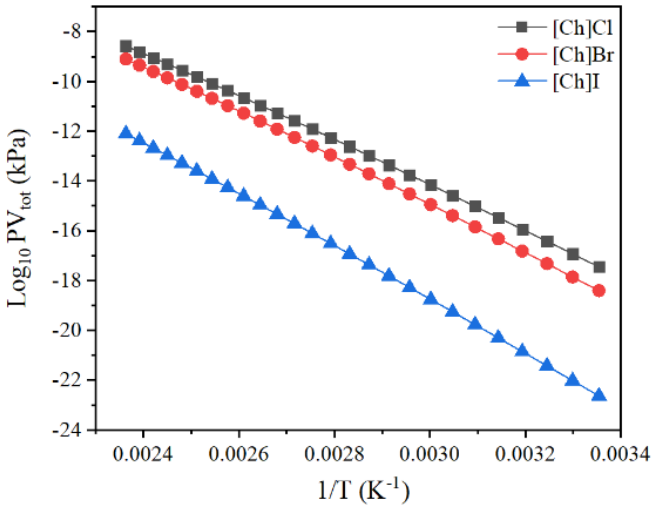

Figure 2.16. Simulated vapor pressure of hydrogen bond acceptors at 25 °C.

From the simulated results at room temperature (Fig. 2.17.), [Ch]Cl:malic acid had the lowest vapor pressure of 1.4936×10^{-26} kPa compared to 2.35×10^{-26} kPa of [Ch]Br:malic acid. Between 25 ℃ to 150 ℃, [Ch]Cl:citric acid has PV_{tot} values between 2.6818×10^{-26} kPa to 1.1328×10^{-13} kPa whereas [Ch]Br:citric acid DES is from 1.51×10^{-21} kPa to 1.88×10^{-10} kPa. The low volatility of chloride-based DES is due to the strong intermolecular interaction between the donor and the acceptor.

A) Vapor pressure of [Ch]Cl with different HBD

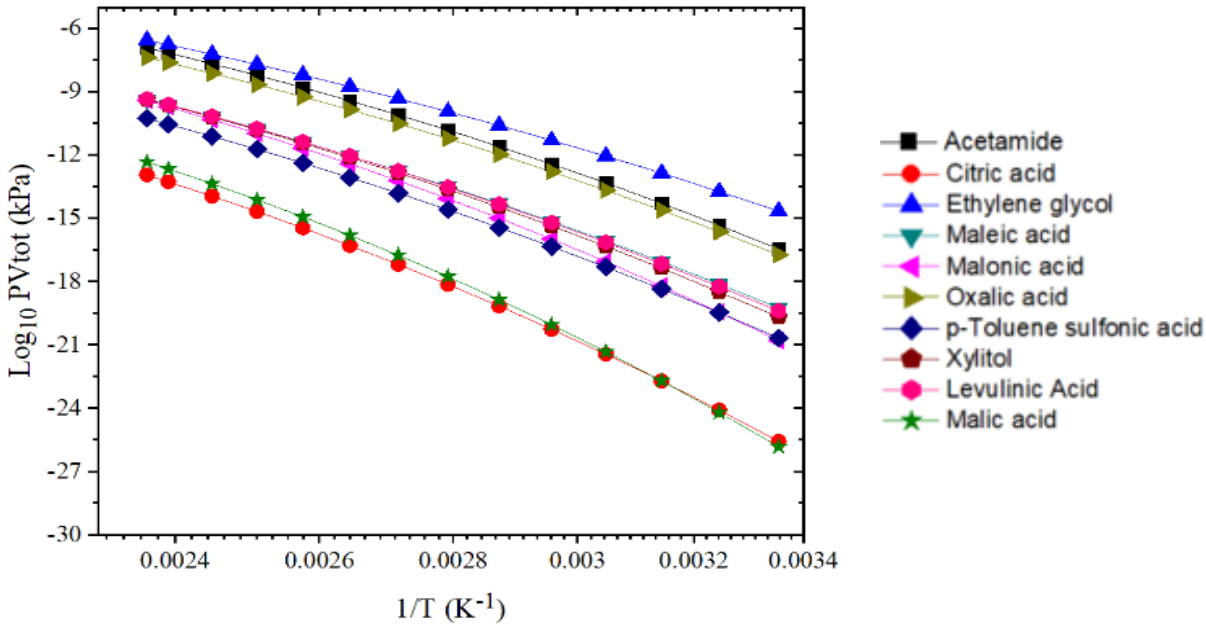

B) Vapor pressure of [Ch]Br with different HBD

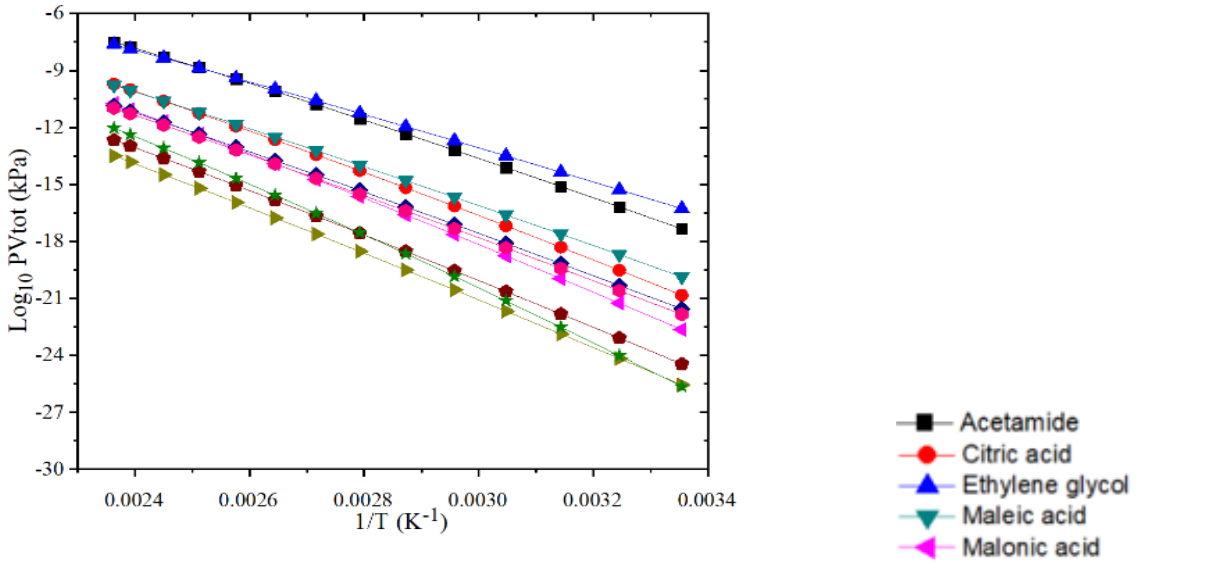

C) Vapor pressure of [Ch]I with different HBD

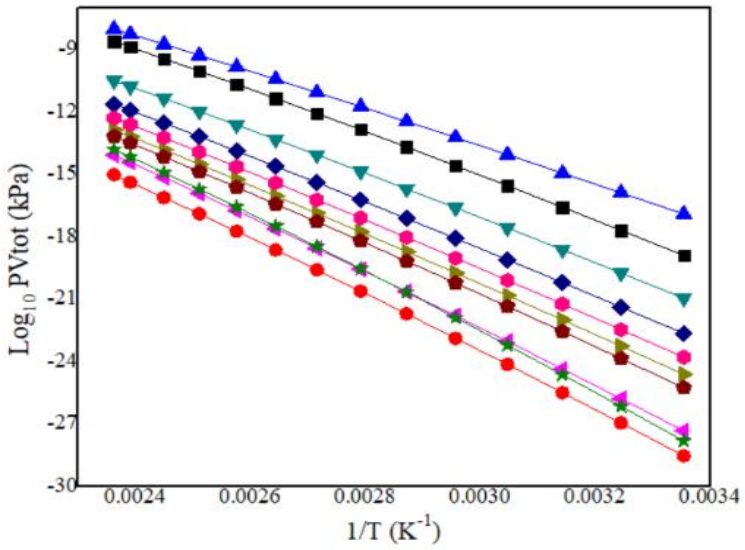

Figure 2.17. Vapor pressure of DES by varying both HBA and HBD. **A**) Vapor pressure of [Ch]Cl with different HBD, **B**) Vapor pressure of [Ch]Br with different HBD, and **C**) Vapor pressure of [Ch]I with different HBD. All DES is 1:1 molar ratio except choline halide with acetamide or ethylene glycol which is 1:2.

Surprisingly, [Ch]Br:oxalic acid had the lowest PV_{tot} of 2.78×10^{-26} kPa among all the bromide-based DES and is about 1.506×10^{-9} kPa lower than [Ch]Cl: oxalic acid. Choline chloride and bromide DES with ethylene glycol had the highest vapor pressure among all the DES studied. The PV_{tot} of [Ch]Cl:ethylene glycol is 2.1555×10^{-15} kPa which is relatively lower than the 8.5×10^{-14} kPa of [Ch]Cl:ethylene glycol 1:3 predicted by Aissaoui et al.[115] The difference may be due to the nature of the eutectic mixture formed. The significantly lower vapor pressure of DES compared to glycols (< 0.01 kPa), make DES a suitable solvent to implement in the industry, especially for the dehydration of natural gases. From the results (Fig. 2.17.), a difference in the anion of the QAS significantly impact on the vapor pressure of DES. The results can corroborate with other physiochemical parameters to help select the appropriate DES mixture for industrial applications and for environmental sustainability.

2.3.10.5. Activity coefficient

Activity coefficient at infinite dilution (IDAC), γ^{∞}, is a useful measure of nonideality of liquid mixtures and is essential for predicting solvents for extractive distillations. A detailed comparison of the original and modified UNIFAC Group Contributions Methods (GCMs) and the COSMO-RS thermodynamic models for determining activity coefficient has been described[127]. The chemical potentials derived from COSMO-RS simulations were run in COSMO*therm* to determine activity coefficient by the expression:

$$\gamma^{i}_{s} = \exp(\mu^{i}_{s} - \mu^{i}_{i}/RT) \qquad \text{(Equation 2.6)}$$

where μ^{i}_{s} is the chemical potential of the solvent *s*, and μ^{i}_{i} is the chemical potential of the pure compound *i*.

For calculating γ^{i}_{s} at infinite dilution (γ^{∞}), the molar fraction of the solutes (water, methanol, acetonitrile and ethanol) and DES (solvent) was set to zero and one, respectively, in the COSMO*therm* activity coefficient panel. In this thermodynamic calculation, the behavior of the limiting pure compound (solute) is fully surrounded by the solvent molecules. To fully understand the behavior of the choline halides in DES, γ^{∞} of water and methanol in DES were studied. COSMO-RS can account for polarity and hydrogen bonding in aqueous systems making it a better alternative compared to UNIFAC methods for predicting activity coefficient[127]. In view of this, methanol and water were selected as solutes for studying the behavior of choline halides on activity coefficient. From the results, the γ^{∞} of water in [Ch]Cl:acetamide, [Ch]Br:acetamide, and [Ch]I:acetamide, all at 1:2 molar ratio, increased as temperature increases (Fig. 2.18A.). Due to the differences in the anions, all the DES behave differently with unique γ^{∞} values.

A) **B)**

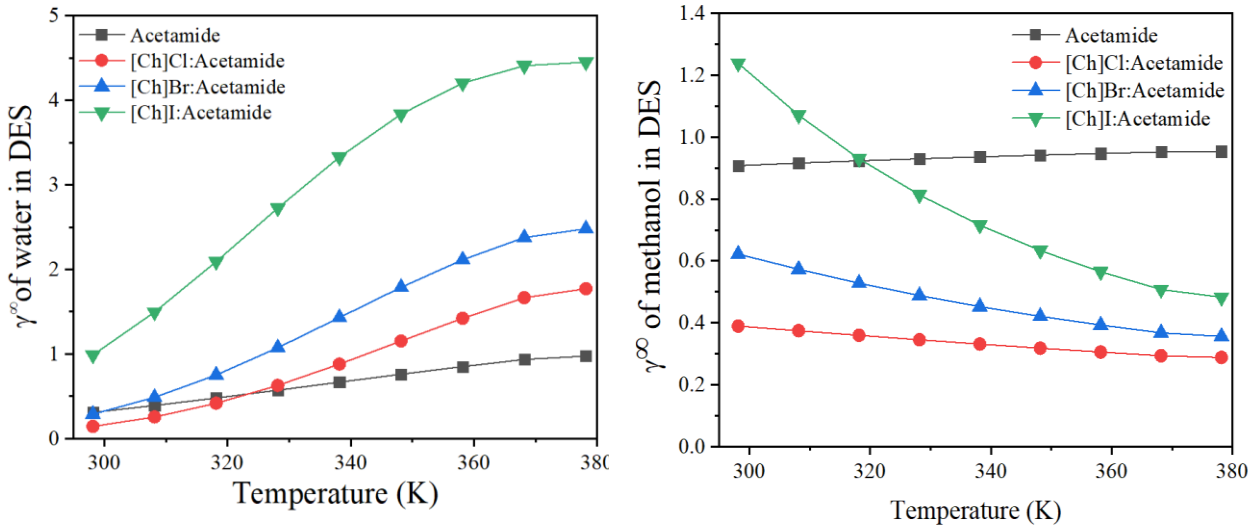

C)

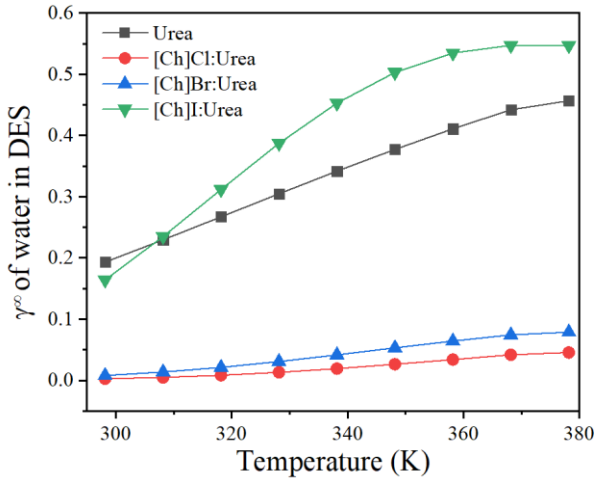
Urea
[Ch]Cl:Urea
[Ch]Br:Urea
[Ch]I:Urea
γ∞ of water in DES
Temperature (K)

D)

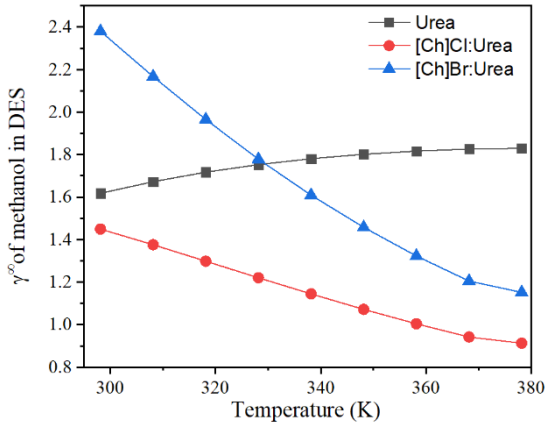
Urea
[Ch]Cl:Urea
[Ch]Br:Urea
γ∞ of methanol in DES
Temperature (K)

E)

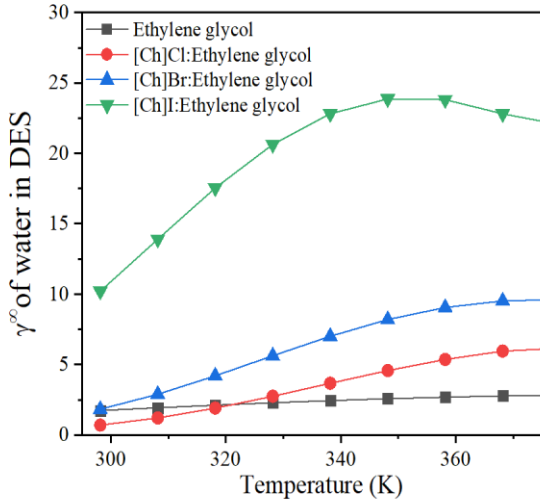
Ethylene glycol
[Ch]Cl:Ethylene glycol
[Ch]Br:Ethylene glycol
[Ch]I:Ethylene glycol
γ∞ of water in DES
Temperature (K)

F)

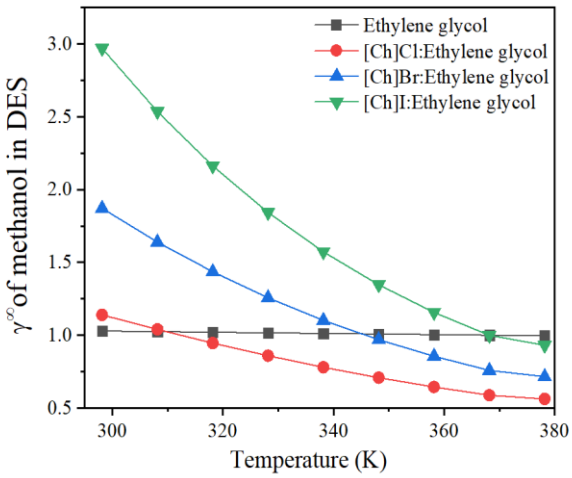
Ethylene glycol
[Ch]Cl:Ethylene glycol
[Ch]Br:Ethylene glycol
[Ch]I:Ethylene glycol
γ∞ of methanol in DES
Temperature (K)

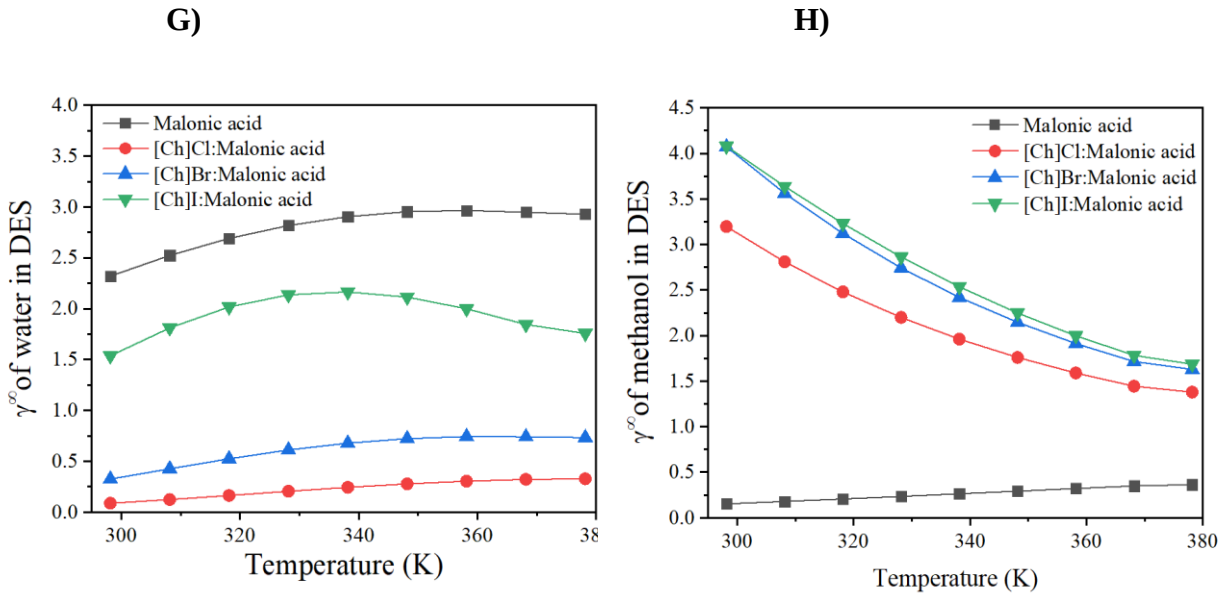

Figure 2.18. Effect of anions on the infinite activity coefficient of solvents in DES. **A)** infinite activity coefficient of water in DES using acetamide as HBD; **B)** infinite activity coefficient of methanol in DES using acetamide as HBD; **C)** infinite activity coefficient of water in DES using urea as HBD; **D)** infinite activity coefficient of methanol in DES using urea as HBD; **E)** infinite activity coefficient of water in DES using ethylene glycol as HBD; **F)** infinite activity coefficient of methanol in DES using ethylene glycol as HBD; **G)** infinite activity coefficient of water in DES using malonic acid as HBD; **H)** infinite activity coefficient of methanol in DES using malonic acid as HBD.

Considering the γ^{∞} of water in [Ch]Cl/Br/I:acetamide between 25 °C to 105 °C (Fig. 2.18.), the γ^{∞} values of [Ch]Cl, [Ch]Br, and the [Ch]I are between 0.142565-1.771202, 0.288727-2.479585, and 0.987586-4.451059, respectively, signifying a higher affinity of [Ch]Cl:acetamide for water. On the contrary, in methanol, all the DES showed a decrease

in γ^{∞} as temperature increases 25 ℃ to 105 ℃. Changing the choline halide in DES affects the activity coefficient of water and methanol at infinite dilutions. As expected, water has γ^{∞} values less than unity in [Ch]I: urea, [Ch]Br:urea, and [Ch]Cl:urea, whereas γ^{∞} values of methanol in [Ch]Cl:urea and [Ch]Br:urea is greater than 1 at temperatures ≤ 85 ℃ (Fig. 2.18C and Fig. 2.18D). A similar result was obtained by using [Ch]Cl/Br/I:malonic acid and [Ch]Cl/Br/I:ethylene glycol. The results indicate that anions significantly alter the thermodynamic activity coefficient at infinite dilution for both water and methanol in DES. The differences may be due to the differences in the molecular interaction between the HBD and the halide acceptor which is attributed to dipoles and hydrogen bonding.

In summary, this chapter shows that changing anions alter the physicochemical properties of DES due the differences in size and electronegativity. In view of this, the strength of hydrogen bonding differs resulting to the differences in the melting point depression. It can be seen that choline bromide can sometimes be used to replace choline chloride for making DES, however, this is mostly application specific. The combined experimental methods with COSMO-RS computational simulation shows that anions are influences the chemical potential and activity coefficient of the DES.

CHAPTER THREE

SYNTHESIS, CHARACTERIZATION, AND POTENTIAL APPLICATIONS OF HYDROPHOBIC DES FOR PIPERINE EXTRACTION

3.1. Introduction

Natural products, such as bioactive compounds, from medicinal plants provide unlimited opportunities for new drugs due to the unmatched availability of chemical diversity in their extract[128]. Extraction of the analyte of interest is a critical step in analytical chemistry before a separation and characterization step is performed. Due to the diverse polarity range of bioactive compounds, the selection of appropriate solvent system to extract nonpolar compounds remain a challenge. Most frequently, organic solvents such as chloroform, dichloromethane, hexane, ethanol, and methanol are used to extract bioactive compounds from plant materials[128]. The classical and routine liquid-liquid extraction (LLE)[129] used by most chemists employ organic solvents for separation. Some of the most used organic solvents are toxic and environmentally unfriendly. The concept of green chemistry and green solvents is gaining popularity due to the resulting low toxicity and sustainable nature of the solvent. Deep eutectic solvents are no exception to these new designer solvents with exceptional tunability and properties. The application of deep eutectic solvents for LLE and bioactive compounds extraction from diverse matrices have been reviewed[56, 130]. To date, nearly all DES synthesized are hydrophilic, and are limited to the extraction of only polar molecules or metabolites[81]. The concept of hydrophobic DES (HDES) evolved recently by van Osch et al.[55] in 2015 when they combined quaternary ammonium salts (QAS) with decanoic acid. The water-immiscible HDES was applied to

extract water insoluble volatile organic compounds (VOCs) with high yield and efficiency[55]. Since then, active research is ongoing to investigate how HDES are synthesized and their application in diverse fields. Some recent applications of HDES include, but are not limited, to carbon dioxide capture[131] and analytical extraction of pesticides[89], bisphenol A[88], artemisinin from *Artmisia annua* leaves[84], polyaromatic hydrocarbons[87], synthetic pigments in beverages[93], phytocannabinoids[97], and polyprenyl acetates from *Ginkgo biloba* leaves[98]. Extraction of bioactive compounds with HDES has become popular due to the 'greenness' of the extraction process, high solvent recovery rate, and ease approach of tuning the solvents polarity. Some common HBDs used for HDES synthesis include decanoic acid, hexanoic acid, capric acid, lauric acid, palmitic acid, stearic acid, dl-menthol, and thymol whereas some common HDAs include N8881-Cl, N8881-Br, N8888-Br, N8888-Cl, and N4444-Cl[88-90, 98]. One of the major drawbacks of HDES is the cost and energy involved in derivatizing the HBA moiety with longer alkyl groups (C4-C8). Industrially, this make the QAS expensive to buy compared to its organic solvent competitors.

The objective of this chapter is to design a cost-effective solvent system with similar chemical and physical properties compared to the already established HDES with efficiency in extracting bioactive compounds. The newly synthesized HDES consist of butyric acid (BA), valeric acid (VA), hexanoic acid (HA), and caprylic acid (CA) as hydrogen bond donors, and choline chloride as hydrogen bond acceptor at 1:2, 1:3, and 1:4 molar ratios. The solvent was further characterized for functional groups using FTIR, chemical shift by NMR, melting by DSC, viscosity by rheometer, and water activity by using AquaLab water-activity meter. The resulting HDES was used as an extractive media

to isolate piperine, a bioactive compound responsible for pungency in black paper, by using subcritical conditions and microwave-assisted extraction.

Over the past years, piperine has proven to be a potent, naturally occurring alkaloid with undisputable therapeutic and health benefits[132]. A comprehensive review on piperine's traditional use in digestion, diabetes, flu, blood purifier, enhancing enzymatic activity, anti-ulcer, anti-oxidant, diuretic, antimicrobial, and anticarcinogenicity has been reviewed[133-136]. As the most abundant bioactive alkaloid in black pepper, the limited solubility of piperine makes it important to develop a solvent system with tunable solubility to maximize its extraction. Ionic liquids coupled with ultrasonic-assisted extraction has been used previously to extract piperine from white pepper[137]. The challenge is the use of high power at 500 W and longer extraction time of 30 minutes to attain optimum yield[137]. An ultrasonic-assisted extraction (UAE) extraction at 40 °C, ultrasonic power of 175 W, and frequency at 25 kHz for 20 min was found efficient to extract piperine from *Piper longum* in acetone (4.53 mg/g), ethanol (4.32 mg/g), and hexane (4.08 mg/g) compared to 1.01 mg/g, 0.98 mg/g and 0.84 mg/g yield obtained in conventional batch system, respectively[138].

Recently, a DES-based pretreatment method was used to enhance microwave extraction of essential oils from *Piper nigrum* and white pepper[139]. The selectivity of microwave extraction makes it a robust analytical technique which targets analytes based on their dielectric constant[133]. Raman et al.[140] showed that microwave-assisted extraction (MAE) of piperine has higher yield in nonpolar solvents than in slightly polar solvents and has higher purity in petroleum ether (95%) than in dichloromethane (72%) and ethanol (60%). Due to the significant absorption of microwave radiation by polar solvents, their

penetration depth becomes smaller to extract piperine compared to nonpolar solvents that have no interaction with microwave radiations[140]. Despite the higher yield of piperine in petroleum ether and toluene, the negative impact on using such environmentally hostile solvents for extraction is problematic. Other extraction technologies used for piperine extraction include subcritical fluid extraction (SFE). SFE uses solvents above their subcritical temperatures and pressures with concurrent enhancement in the fluid penetration power and mass transfer. For the first time, HDES was applied as an extractive media for the extraction of piperine from *Piper nigrum* using MAE and a variant of SFE. To evaluate the effectiveness of our method, we compared the piperine content from both peppercorns and ground black pepper.

3.2. Experimental

3.2.1. Chemicals

Choline chloride ([Ch]Cl), butyric acid (BA), hexanoic acid (HA), and caprylic acid (CA) were all purchased from Acros Organics, and valeric acid (VA) (Alfa Aesar) all had purity ≥ 99 %. All other chemicals were of analytical grade. Peppercorns and ground pepper were purchased from Walmart Supercenter, Brookings, SD.

3.2.2. Synthesis of HDES

DES were synthesized by mixing choline chloride and HBDs at 1:2, 1:3, or 1:4 molar ratios and heated at 80 ℃ for 15-30 min under constant stirring at an atmospheric pressure until a homogenous liquid is obtained. In some cases, HDES was synthesized by vortexing. The prepared DES were cooled to room temperature and stored in a desiccator to prevent it from absorbing atmospheric moisture. As shown in Fig. 3.1., the graphical

representation of the compounds represents their respective surface polarity. For example, all the HBD (BA, VA, HA, and CA) shows blue color for the hydrogen bonding proton, red color for the carbonyl (C=O) functional group (this can act as a proton acceptor), and the green color is the nonpolar region. Similarly, the chloride ion in the choline chloride (HBA), which act as proton acceptor, is red, whereas the hydroxyl proton is blue. The longer the alkyl chain length of the HBD, the longer the nonpolar green surface. The difference in the carbon chain length of the donor molecule is expected to influence the physical and the chemical nature of the DES synthesized. These HBD were selected for HDES synthesis because little or no work has been done in literature involving BA, VA, HA, and CA with [Ch]Cl.

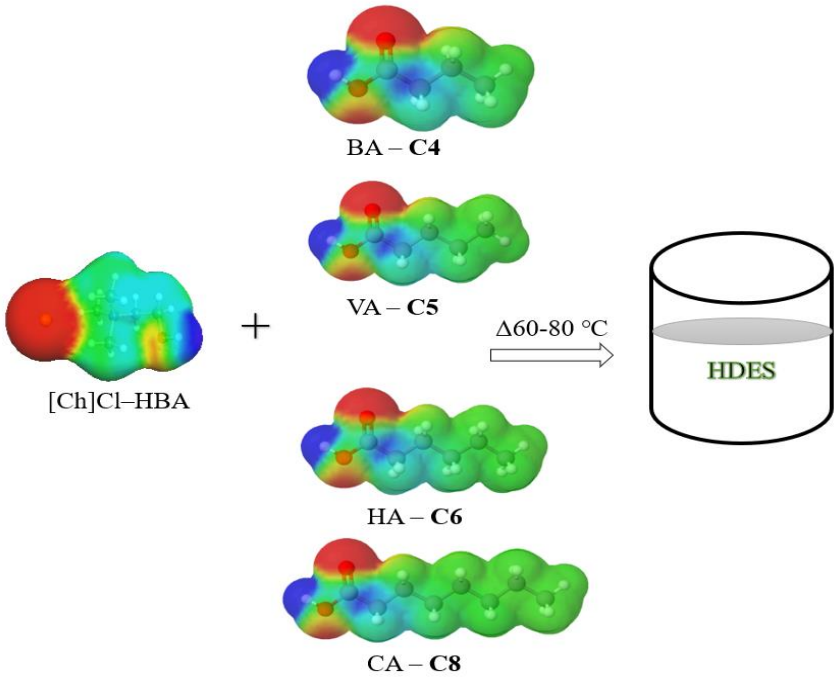

Figure 3.1. Synthesis of HDES by using [Ch]Cl as HBA and butyric, valeric, hexanoic, and octanoic acid as HBD. HBD graphical representation by Molview and the HBA graphics was generated by using Cosmotherm.

3.2.3. Physicochemical properties of HDES

Differential scanning calorimetry (DSC), thermogravimetric analysis (TGA), Fourier transform infrared (FTIR) spectroscopy, nuclear magnetic resonance (NMR), and viscosity measurements were done using experimental procedures described in previous chapters. The octanol-water partition coefficient (K_{ow}) of HDES was measured using the traditional shake flask method coupled with gravimetric procedures. In this method, the tested solvent (HDES) is mixed with equal volumes of octanol and water mixture and shaken until an equilibrium is attained between the two phases[141]. After phase separation, the concentration of HDES in each phase was calculated by gravimetric analysis. The water activity (a_w) of HDES and its constituents (HBA and HDB) were measured using the benchtop 4TE water activity meter (AquaLab. Pullman, WA). The 4TEV meter uses the chilled-mirror dewpoint technique to measure a_w by equilibrating the liquid phase water in the sample with the vapor phase water in the head-space and measuring the relative humidity of the head-space (Aqualab 4TE Manual). The meter has thermoelectric components that help regulate the temperature of the measuring chamber. Unless stated otherwise, all measurements were done at room temperature. The meter was calibrated with deionized water (a_w = 0.99935) with a coefficient of variation of 0.50%. To prevent linear offsets and assure data reliability, deionized water calibration was used for periodic verification. The physicochemical properties measured in this work are listed in Figure 3.2.

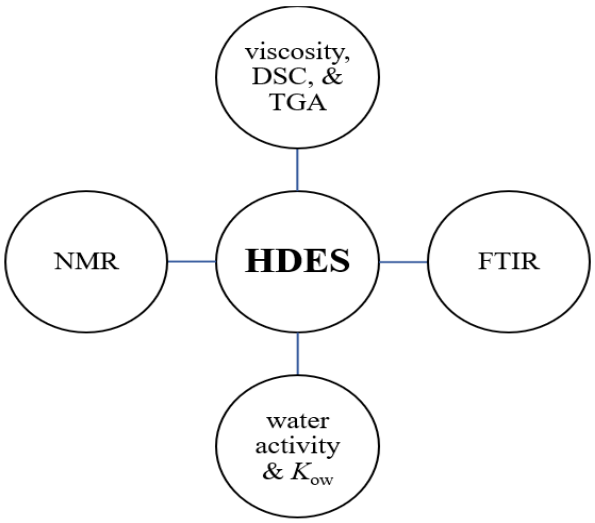

Figure 3.2. HDES physicochemical properties measured.

3.2.4. Extraction of piperine from black pepper

3.2.4.1. Microwave-assisted extraction and Subcritical extraction

HDES-based microwave-assisted extraction (MAE) was performed in a commercial microwave oven (Advantium 120). Samples (0.1 g) of ground, fresh peppercorn or ground pepper (0.250 mm mesh size) was added to 20 mL of HDES in the glass vessel (Fig. 3.3). The mixture was vortexed for 60 sec for mixing. After microwave irradiation for 3 minutes at 10 MPa, the samples were allowed to cool before liquid-liquid extraction with ethyl acetate. Under subcritical condition extraction (SCE), same experimental conditions were used except for performing the reaction in a bioreactor with the vessel temperature set at 200 ℃ for 20 minutes. Before analysis in HPLC, the ethyl acetate extract was concentrated through a nitrogen purge. The sample was filtered with a 0.25-μm nylon membrane and spiking with o-terphenol as internal standard. Analysis was

done in UHPLC (Ultimate 3000 Thermo Fischer UHPLC system) equipped with C_{18} column and UV/VIS detector at 340 nm. For quantification, all samples and standards were spiked with 100 µL of 1,000 ppm of o-terphenol internal standard. A gradient elution (acetonitrile and water mixture for 15 mins) was used as mobile phase. The five different spiked-standards (1000 ppm, 500 ppm, 250 ppm, 125 ppm, and 62.5 ppm) were injected (N=3) and the calibration plot of signal ratio verse concentration was plotted. Chromatogram integration was done in Thermo Scientific Chromeleon software, whereas data analysis was performed in Origin Pro 18 (OriginLab Massachusetts, USA.) to generate the regression equation and the coefficient of regression (R^2).

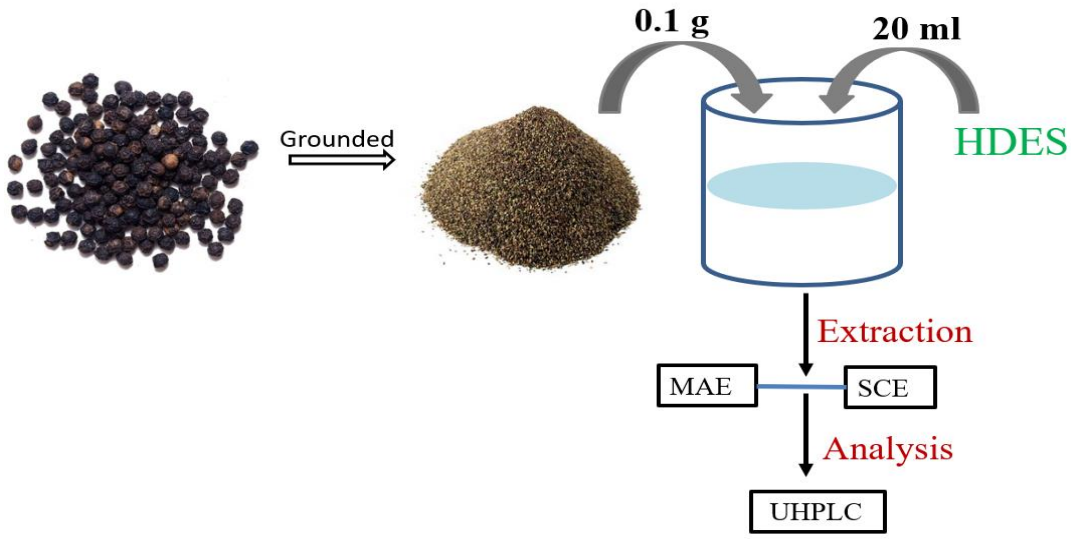

Figure 3.3. A step-by-step procedure for the extraction of piperine from *Piper nigrum.*

3.3. Results

3.3.1. Physical properties of HDES

The synthesis of HDES, like DES is very simple and has advantage over ILs since no purification steps are required. The HDES are mostly clear liquids except the 1:2 molar ratios which are cloudy and turbid. As indicated in Fig. 3.4A, [Ch]Cl and hexanoic acid form HDES by heating and stirring. HDES can also be prepared without heating by mixing and vortexing the constituents (Fig. 3.4B).

A) **B)**

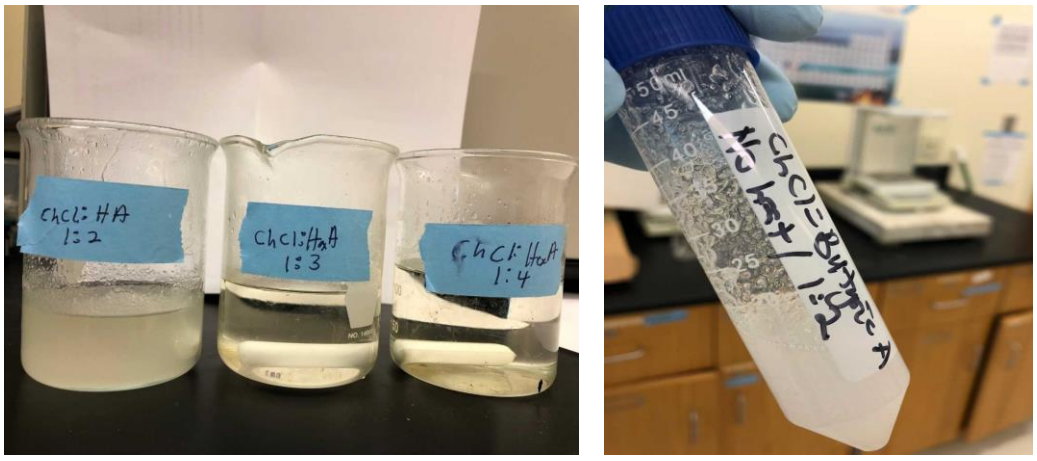

Figure 3.4. A) HDES synthesized by heating and stirring by using [Ch]Cl:HA at 1:2, 1:3, and 1:4 molar ratios. **B**) HDES synthesized without heating from [Ch]Cl:BA at 1:2 molar ratio.

3.3.2.Water activity of HDES

Most DES are hygroscopic. If choline chloride forms hydrophobic DES with BA, VA, HA and CA, it is expected that the free water in the solvent should be minimal. The

amount of water in every sample can be categorized into two groups, namely, water content and water activity. Water content, or moisture, is a quantitative measure of the total amount of water in a sample, whereas water activity (a_w) measures the thermodynamic energy status or free water available in the solvent. The latter is a reliable physiochemical indicator for predicting the feasibility of using DES for chemical, enzymatic, and microbial studies[142]. Thus, an increased lipase activity was observed in [Ch]Cl:urea when the a_w increased from less than 0.02 to 0.15[143]. The a_w of the newly synthesized HDES was measured and compared to the a_w of the individual components in the eutectic mixture. As shown in Fig 3.5., the a_w of butyric acid is less than 0.02, whereas VA, HA, and CA have a_w of 0.1564 ± 0.0036, 0.170233 ± 0.0020, and 0.374333 ± 0.0078, respectively.

As the alkyl chain length of the HBD increases, the a_w increases because water does not mix nor interact with the HBD making it available for detection. The HBA, choline chloride, has a water activity of 0.2275 ± 0.00042. From the results, HDES formed from HBA and HBD does not make the resulting solvents water activity additive. The involvement of some water molecules in hydrogen bonding may account for the nonadditive behavior of the HDES water activity. In theory, the hydrogen-bonded water molecules cannot evaporate and thus make head-space measurements impossible. The [Ch]Cl:BA HDES had the lowest a_w whereas [Ch]Cl:CA HDES had the highest a_w. The results depict that water activity increases as the hydrophobicity of the HDES increases because the available free water does not interact with the hydrophobic alkyl chain length. In general, the synthesized HDES has low water activity. As recently reported[73], thirteen different DES studied at 40 ℃ showed water activity values between 0.116 to 0.662. The newly synthesized DES have water activity values less than 0.26, which is desirable for

diverse applications in enzyme catalysis and other biochemical applications at low acidic environments.

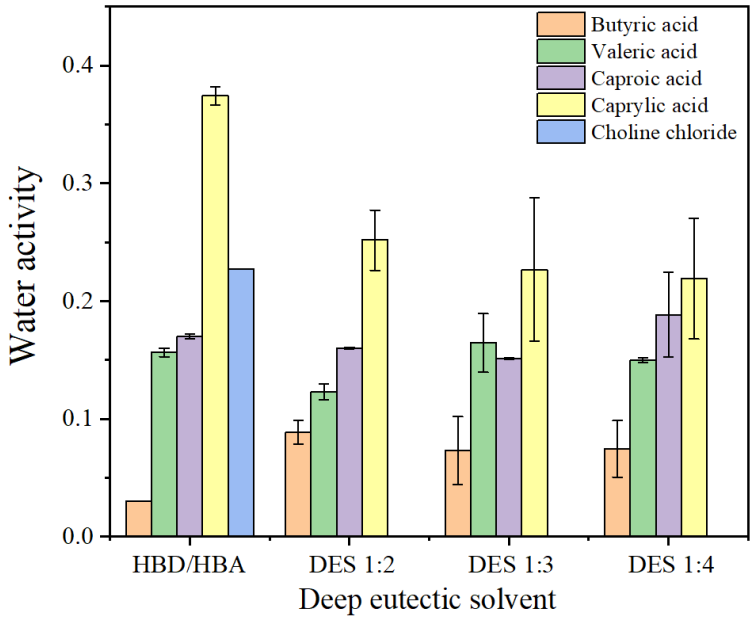

Figure 3.5. Thermodynamic water activity of carboxylic acid-based DES.

3.3.3. Thermal stability and water content

Fig. 3.8A-D and Fig. 3.9A-D represent the TGA and differential thermogravimetric (DTG) analysis for HDES and its constituents. Table 3.1. summarizes the temperature at which 50% of the HDES weight is lost ($T_{1/2}$). The $T_{1/2}$ for all the HBD is lower than their corresponding eutectic mixtures. The $T_{1/2}$ for [Ch]Cl:BA 1:2, [Ch]Cl:VA 1:2, and [Ch]Cl:HA 1:2 are 160.1 ℃, 210.2 ℃, and 238.6 ℃, respectively, thus higher than 115.3 ℃ of butyric acid, 135.7 ℃ of valeric acid, and 148.5 ℃ of hexanoic acid. The only exception is [Ch]Cl:CA 1:2 HDES which has lower $T_{1/2}$ (172.9 ℃) compared to caprylic acid, with $T_{1/2}$ of 193.9 ℃. The increased $T_{1/2}$ of most HDES is a qualitative indicator of the strong intermolecular interactions occurring with concomitant increase in thermal

stability. Hydrogen bonding is a major intermolecular force which contributes to DES thermal stability. Fig. 3.6. shows the DTA plot of [Ch]Cl with two peaks between 67 ℃ to 103 ℃ and 292 ℃ to 339 ℃ with the former representing water loss and the later as [Ch]Cl decomposition temperature. The decomposition temperature of solvents is a significant thermal parameter used to determine the temperature ranges at which the solvent remains liquid for various applications[40].

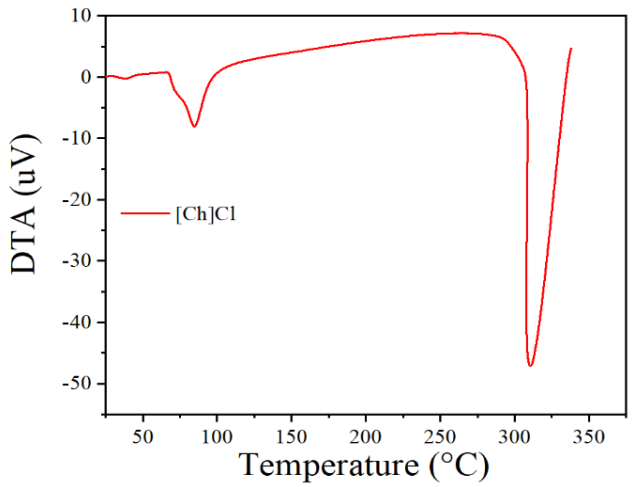

Figure 3.6. Differential thermal analysis of choline chloride.

The decomposition temperature of the HBD increases as the alkyl chain length increases. As shown on the DTG thermograph (Fig. 3.7.), the presence of water in the HBD makes the water decompose simultaneously with the acid resulting in the broad decomposition profile observed. The onset decomposition temperature of most HDES lies between the constituents, except for [Ch]Cl:CA 1:2. From the TGA and DTG thermograms (Fig. 3.8 and Fig. 3.9), almost all HDES show three mass-loss steps; (1) loss of water and weakly interacted HBD, (2) the HDES, and (3) [Ch]Cl.

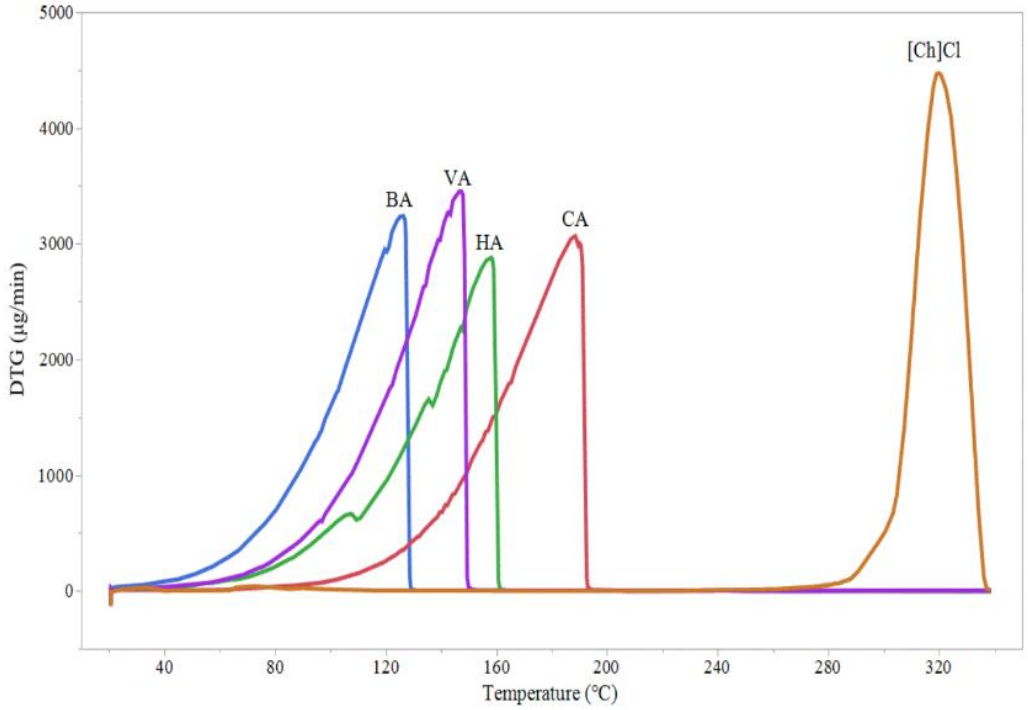

Figure 3.7. DTG analysis of hydrogen-bond donors used for HDES synthesis.

The DTG plot of [Ch]Cl:HA 1:2 shows water loss of from 65 ℃ to 118 ℃ followed by decomposition of the HDES at an onset temperature of 183 ℃ to an endset temperature of 240 ℃. At the first decomposition cycle, the [Ch]Cl:HA 1:3 loses 46% of the solvent at 165 ℃ whereas the [Ch]Cl:HA 1:4 loses 82% at 175 ℃. The high weight loss can be attributed to the loss of hexanoic acid and water. At 247 ℃, [Ch]Cl:HA 1:2 still had about 43 w.% of the solvent remaining. The high thermal properties of [Ch]Cl:HA 1:2 can be attributed to the strong intermolecular forces occurring within the solvent and confirms its eutectic nature compared to similar HDES with 1:3 and 1:4 molar ratios. After the loss of water from the [Ch]Cl:BA 1:2 HDES, the decomposition endset is approximately 190 ℃. Likewise, the [Ch]Cl:VA 1:2 shows water loss between 60-122 ℃ and decompose from 150 ℃ to 208 ℃.

Table 3.1. Temperature of HDES at half decomposition

HDES	Mole ratio	$T_{1/2}$ (°C)	Constituents	$T_{1/2}$ (°C)
[Ch]Cl:BA	1:2	160.1	BA	115.3
[Ch]Cl:BA	1:3	168.2	VA	135.7
[Ch]Cl:BA	1:4	147.2	HA	148.5
[Ch]Cl:VA	1:2	210.2	CA	193.9
[Ch]Cl:VA	1:3	181.7	[Ch]Cl	326.7
[Ch]Cl:VA	1:4	168.2		
[Ch]Cl:HA	1:2	238.6		
[Ch]Cl:HA	1:3	184.4		
[Ch]Cl:HA	1:4	156.7		
[Ch]Cl:CA	1:2	172.9		
[Ch]Cl:CA	1:3	193.9		
[Ch]Cl:CA	1:4	193.9		

The thermal properties of [Ch]Cl:BA like any other eutectic mixture is a result of the contributing effects from the individual constituents. Choline chloride does not associate strongly with caprylic acid (1:2) leading to its lowered thermal stability. The high thermal stability of [Ch]Cl with BA, VA, and HA at 1:2 molar ratio (as evidenced in the TGA and DTG plots), is due to hydrogen bonding occurring between the donor and the acceptor. The high decomposition rate (high peak) associated HDES with 1:3 and 1:4 molar ratio even at low temperatures might be due to the excess donor molecules present which do not interact with limiting acceptor molecules.

Thus, the HBD interacts weakly with [Ch]Cl at 1:3 and 1:4 molar ratios and supports earlier assertions that DES formation and properties are strictly affected by the molar ratio of the constituent materials.

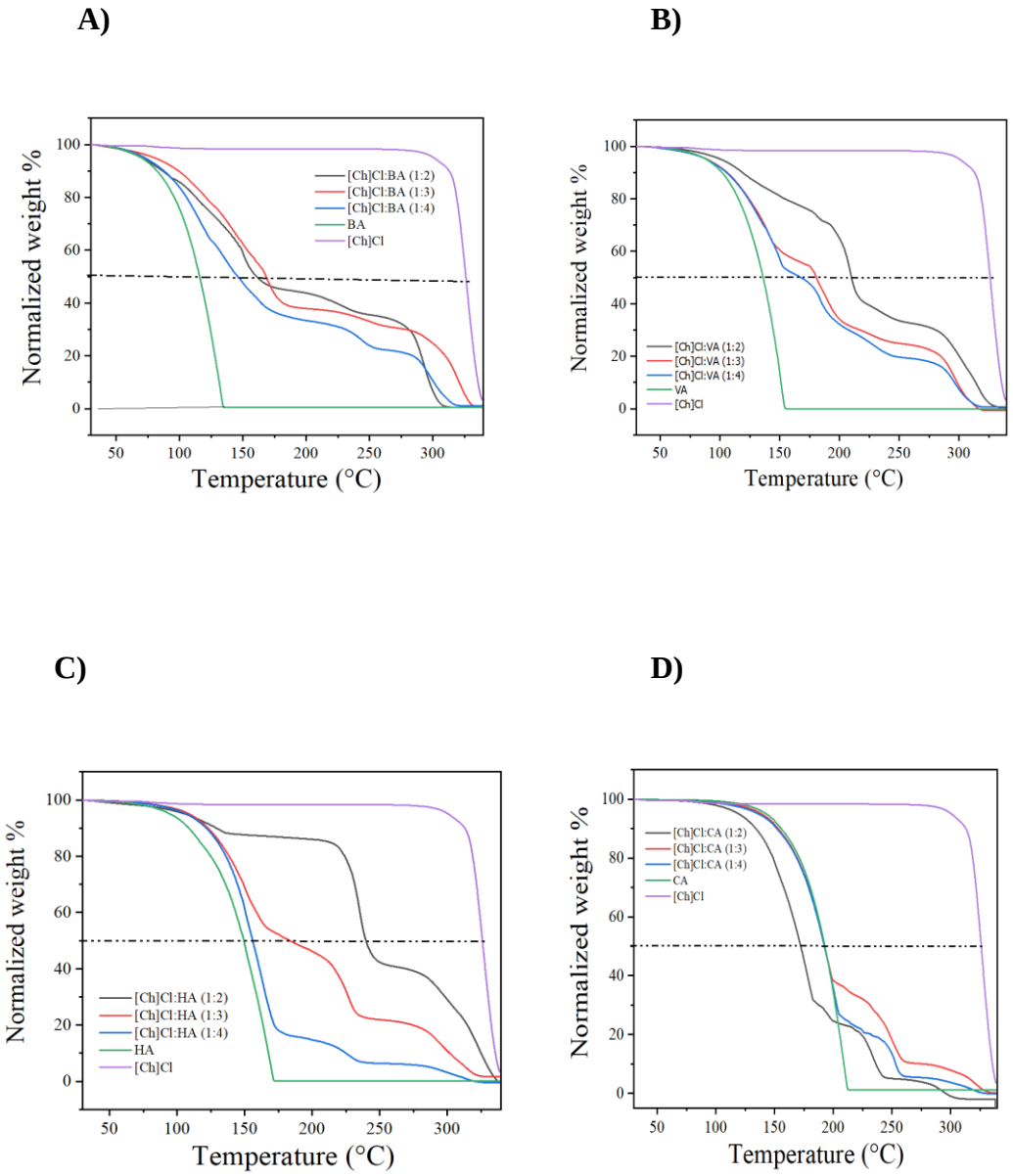

Figure 3.8. Thermogravimetric plots of different HDES. **A)** [Ch]Cl:BA, **B)** [Ch]Cl:VA, **C)** [Ch]Cl:HA, and **D)** [Ch]Cl:CA.

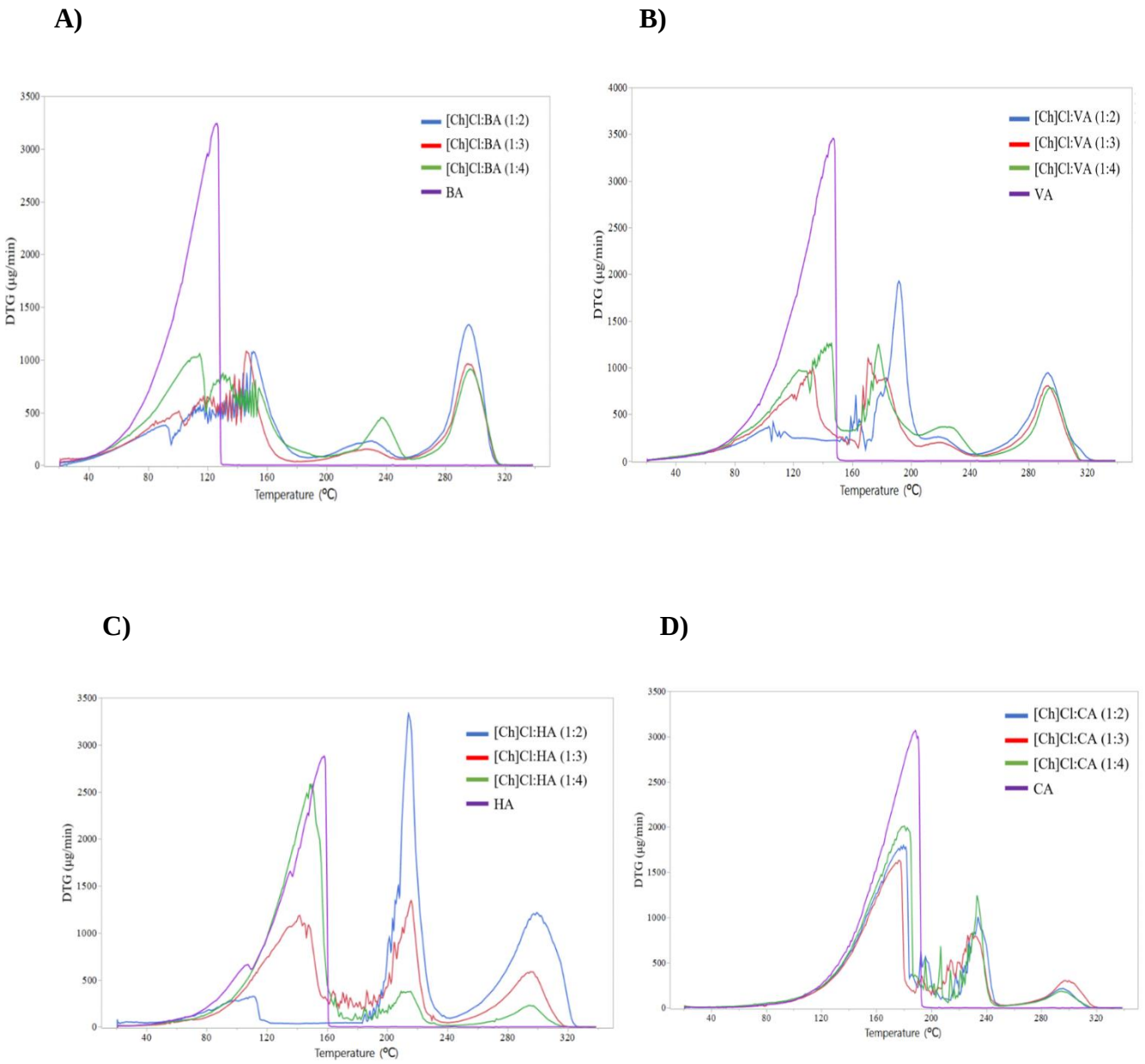

Figure 3.9. Differential thermogravimetric plots of HDES. **A)** [Ch]Cl:BA, **B)** [Ch]Cl:VA, **C)** [Ch]Cl:HA, and **D)** [Ch]Cl:CA

3.3.4. Melting point

Like ionic liquids, the depression of DES melting point is as a result of the interaction between the quaternary ammonium salt and the HBD. This interaction changes the lattice energy and entropy of both the donor and the acceptor molecules[47]. Specifically, the halide anion of choline chloride interacts with protons of the donor molecule through hydrogen bonding. Table 3.2 shows the melting point of the HBD as -8.13℃, -35.24℃, -6.13 ℃, and 16.53℃, respectively, for BA, VA, HA, and CA. The melting point of the HBD correspond to values provided on the safety data sheet by the vendors and validates the reliability of our DSC machine. The [Ch]Cl:BA HDES has a melting point of -17.96 ℃, -20.21 ℃, and -13.15 ℃ at 1:2, 1:3, and 1:4 molar ratios, respectively. The depression in the melting point is an indication of the mixture's eutectic nature.

Table 3.2. Melting point and latent heat of fusion of HDES.

HBD and DES	Mole ratio	T_m (℃)	Latent heat of fusion (J/g)	T_g/T_c
Butyric Acid		**-8.13**	112.9	T_g= -48.16
[Ch]Cl:BA	1:2	-17.96	71.72	-
[Ch]Cl:BA	1:3	-20.21	40.06	T_c= -65.92
[Ch]Cl:BA	1:4	-13.15	74.79	T_g= -48.30
Valeric Acid		**-35.24**	103.7	-
[Ch]Cl:VA	1:2	-35.31	50.51	-
[Ch]Cl:VA	1:3	-34.96	72.41	T_c= -72.09
[Ch]Cl:VA	1:4	-34.89	63.08	T_c= -67.12
Hexanoic acid		**-6.13**	126.5	-
[Ch]Cl:HA	1:2	-5.45	117.95	-
[Ch]Cl:HA	1:3	-5.36	124.5	-
[Ch]Cl:HA	1:4	-5.71	118.9	-
Octanoic Acid		**16.53**	93.06	-
[Ch]Cl:CA	1:2	14.39	80.30	T_g= 2.72
[Ch]Cl:CA	1:3	16.96	101.3	T_g= 5.84
[Ch]Cl:CA	1:4	17.91	104.5	T_g= 6.05

Hydrogen bonding and charge transfer between the donor and the acceptor might be the contributing factor for this melting depression. The difference in melting temperature at different molar ratios make DES an ideal solvent whose physical and chemical property can be easily tuned to suit diverse applications. Although, [Ch]Cl:VA 1:2 and [Ch]Cl:HA 1:2 did not change significantly in melting temperature from the donor, however, the mixture forms a eutectic solvent. The formation of a eutectic mixture lowers the heat of fusion of the HDES. The heat of fusion decreased from 112.9 J/g in butyric acid to 71.7 J/g in [Ch]Cl:BA 1:2. Conversely, [Ch]Cl:CA 1:3 and [Ch]Cl:CA 1:4 neither decreased its melting point nor lowered in latent heat of fusion. This is a good indication that caprylic acid at higher molar ratios with [Ch]Cl do not form a eutectic mixture.

3.3.5. Viscosity

One of the key attributes of DES is their high viscosity at lower temperatures which drops as temperature increases. The viscosity of the HDES was measured first at ambient temperature, presented in Table 3.3. Mostly, 1:2 molar ratio of HDES has high viscosity due to hydrogen bonding and van der Waal interactions. The differences in the alkyl chain length of the HBD might also account for the viscosity differences. The viscosity at 25 ℃ of [Ch]Cl:BA 1:2 is 1757 ± 14 cP, [Ch]Cl:BA 1:3 is 54.1 ± 3.5 cP and [Ch]Cl:BA 1:4 is 13.3 ± 1.8 cP. The drastic change in viscosity shows that selecting the appropriate molar ratio is critical to DES formation and affects the physiochemical properties of the resulting solvent. Pertinent to HDES industrial applicability, it is inevitable to study how shear rate and temperature affects characteristics of the solvent.

The effect of shear rate and temperature was measured by following the Arrhenius-type equation to calculate the activation energy, preexponential factor and the correlation regression of selected HDES (Fig.3.10.).

Irrespective of shear rate increase from 1.50 to 3.75 sec, the activation energy and the preexponential factor of [Ch]Cl:BA 1:3 averaged at -30.5 ± 0.23 kJ/mol and -8.62 ± 0.08 mPa.s, respectively (Table 3.4.). The activation energy in [Ch]Cl:BA (1:3) is lower than [Ch]Cl:VA (1:3) which might be due to the alkyl chain length and increased interactions in the HBD (valeric acid). As the activation energy of the DES increases, the preexponential factor also increases. The highest E_a (-75.5 kJ/mol) value was attained at a shear rate of 0.75 s for [Ch]Cl:VA (1:3) with preexponential value of -26.7 mPa.s and R^2 = 0.936.

Table 3.3. Viscosity of HDES at 25 ℃.

DES	Mole ratio	Viscosity (cP)
[Ch]Cl:BA	1:2	1757 ± 14
[Ch]Cl:BA	1:3	54.1±3.5
[Ch]Cl:BA	1:4	13.3 ± 1.8
[Ch]Cl:VA	1:2	1497 ± 41
[Ch]Cl:VA	1:3	44.5 ± 11
[Ch]Cl:VA	1:4	36.8 ± 5.3
[Ch]Cl:HA	1:2	1778.7 ± 84
[Ch]Cl:HA	1:3	1563 ± 79
[Ch]Cl:HA	1:4	1808.5 ± 18
[Ch]Cl:CA	1:2	1594.7 ± 31
[Ch]Cl:CA	1:3	1561.3 ± 70
[Ch]Cl:CA	1:4	1723.7 ± 89

Table 3.4. Activation energy and preexponential factor of HDES at different shear rates.

Shear rate	E_{ab}(kJ/mol)	InAs(mPa.s)	R^2
[Ch]Cl:BA (1:3)			
0.75 SR	-33.611	-9.777	0.9634
1.50 SR	-30.443	-8.655	0.9934
2.25 SR	-30.829	-8.698	0.9849
3.00 SR	-30.559	-8.620	0.9961
3.75 SR	-30.293	-8.503	0.9981
[Ch]Cl:BA (1:4)			
0.75 SR	-41.405	-13.830	0.9506
1.50 SR	-48.302	-16.659	0.9698
2.25 SR	-35.815	-11.495	0.9436
3.00 SR	-29.771	-9.0603	0.9994
3.75 SR	-30.323	-9.2827	0.9883
[Ch]Cl:VA (1:3)			
0.75 SR	-56.931	-18.968	0.9442
1.50 SR	-51.939	-16.975	0.9449
2.25 SR	-67.941	-22.871	0.7750
3.00 SR	-60.228	-19.826	0.7720
3.75 SR	-33.378	-9.7392	0.9858
[Ch]Cl:VA (1:4)			
0.75 SR	-39.155	-12.408	0.9295
1.50 SR	-38.666	-12.232	0.9100
2.25 SR	-34.494	-10.531	0.9301
3.00 SR	-33.130	-9.9884	0.9556
3.75 SR	-32.094	-9.5586	0.9751

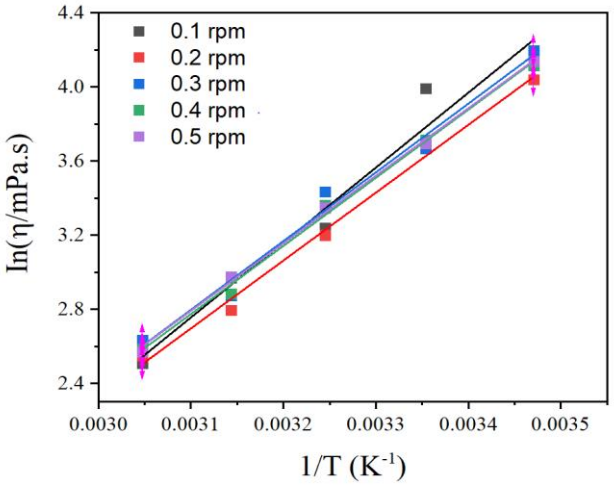

A) [Ch]Cl:BA 1:3

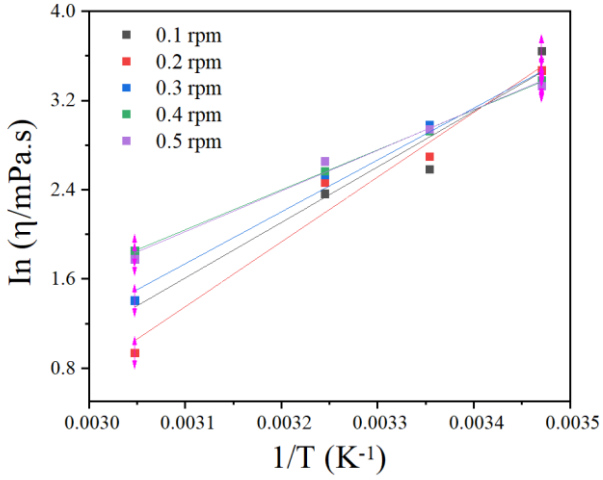

B) [Ch]Cl:BA 1:4

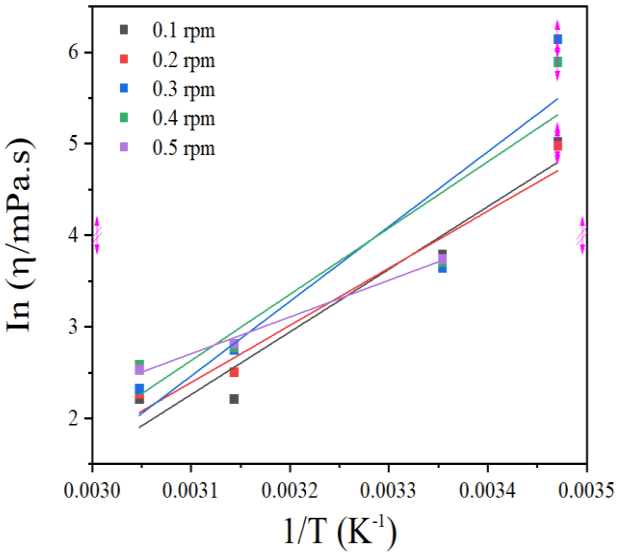

C) [Ch]Cl:VA 1:3

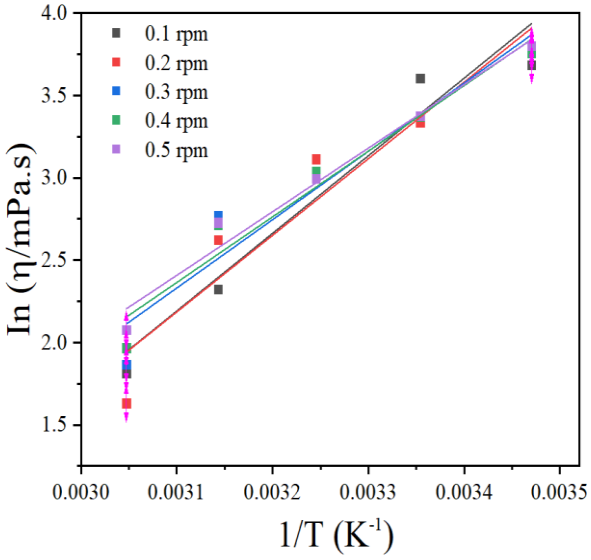

D) [Ch]Cl:VA 1:4

Figure 3.10. Arrhenius-type plot of HDES from 288.15 K to 328.15 K.

3.3.6. FTIR and Chemometrics

As a newly synthesized solvent, the composition mechanism and chemical structures of HDES are still unknown and hence investigated in this study. From the results, HDES contain peaks from both the donor and the acceptor. A characteristic carbonyl (C=O) peak can be seen at 1707 cm^{-1} to 1716 cm^{-1} from the donor and an ammonium peak between 951 cm^{-1} to 953 cm^{-1} from the acceptor. From Fig. 3.11. to Fig. 3.14., all the HDES show a C-H stretching band between 3000 and 2800 cm^{-1} for CH_3 and CH_2 alkane groups. Most of the HDES at a 1:2 molar ratio show increased O-H stretching between 3200 and 3500 cm^{-1} than their corresponding 1:3 and 1:4 molar ratios. A new peak at 1176 cm^{-1} to 1187 cm^{-1} can be attributed to C-O stretching possibly due to ester impurities. The C-N stretching band in [Ch]Cl might be a possible cause for the vibration at 1083 cm^{-1}.

The fingerprint region and the O-H stretching band of HDES at 1:4 molar ratio appears similar to the corresponding HBD. Thus, it becomes a challenge to pinpoint the dissimilarities on the spectra, especially at the fingerprint region. Also, whenever a new solvent is synthesized, FTIR has become a robust technique to quickly assay structural composition prior to using other expensive analytical instrumentations like NMR, x-ray crystallography, and atomic spectroscopy for structural analysis. Some of these analytical testing involves skilled personnel to operate the instrument. It however becomes imperative to devise a simple way to interpret the closely related fingerprint region of the FTIR spectra. To investigate whether butyric acid, valeric acid, hexanoic acid, and caprylic acid indeed formed HDES with choline chloride, and to fully interpret the fingerprint and O-H region of the spectra, we employed computational statistical methods to our chemical data by a process called chemometrics.

Chemometrics is the science of extracting data obtained from analytical chemical systems by using mathematical and statistical algorithms. Through multivariate unsupervised principle component analysis (PCA), we performed a chemometric analysis of FTIR data obtained from different HDES systems to study patterns and relationships with already known DES in literature. PCA reduces the dimensionality of a complex original data set and allows investigation into the relationship of the new variables known as Principal Components (PC's)[144]. PCAs find patterns in a complex data set without prior knowledge about the sample history. Mathematically, PC's are calculated by the linear combination of variables that maximize variance[145]. The first, second, and subsequent PC's minimize the perpendicular distance between the original data and are uncorrelated[144]. Due to this, PC's are geometrically orthogonal with the first two PC's explaining the variance of the majority of the original data. The graphical output called the score plot group similar items in a cluster whereas dissimilar items are positioned in some distance away.

In order to explore how HDES relate to already known DES, we performed PCA analysis of FTIR data obtained by different eutectic systems using the fingerprint wavelength region between 650 cm^{-1} to 1000 cm^{-1} and the hydrogen bonding region from 3100 cm^{-1} to 3600 cm^{-1}. These regions were selected for chemometrics because it captures several DES characteristic peaks and has the unique ammonium identity peak and the hydroxyl peak around 950-953 cm^{-1} and 3200-3500 cm^{-1}, respectively. The first derivative normalization data pretreatment was used to correct baseline shifts prior to importing the values into JMP 14 (SAS Institute Inc.) for analysis (Fig. 3.15.).

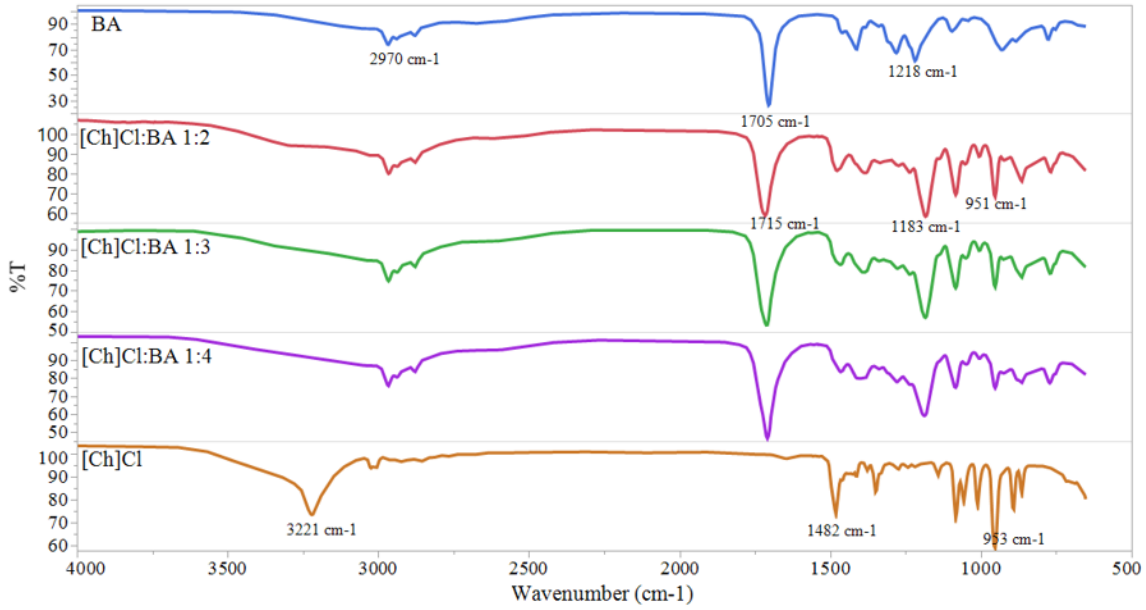

Figure 3.11. FTIR spectra of [Ch]Cl and butyric acid HDES at different molar ratios.

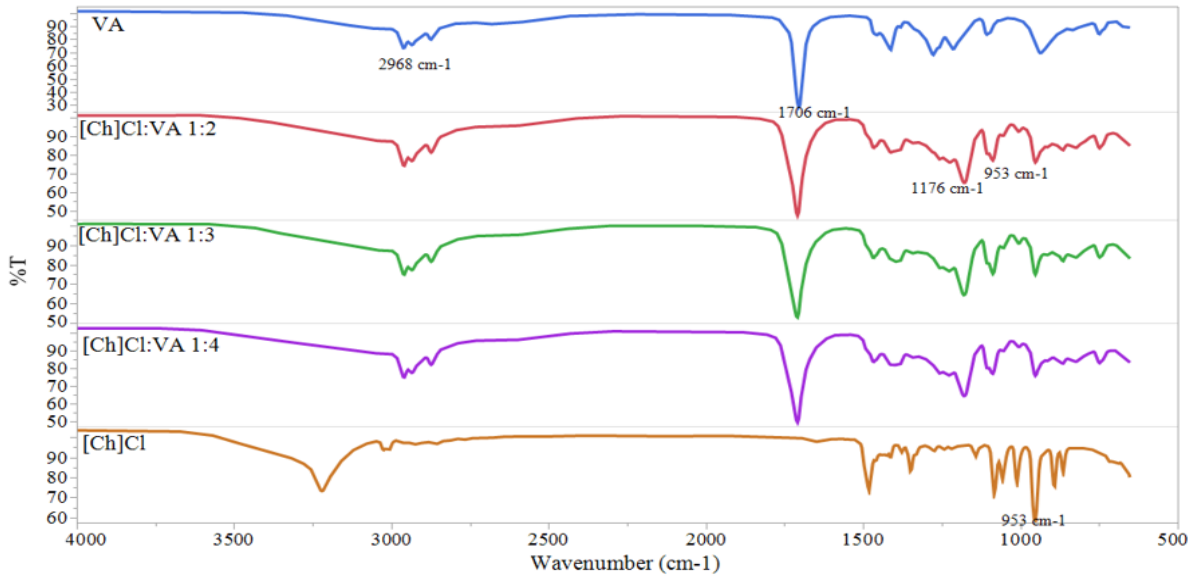

Figure 3.12. FTIR spectra of [Ch]Cl and valeric acid HDES at different molar ratios.

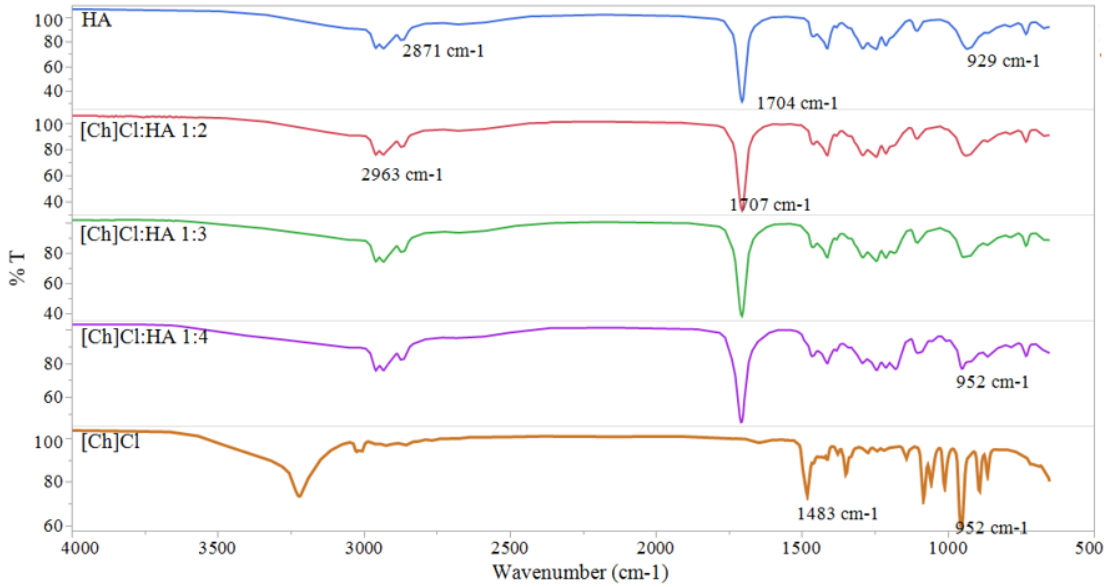

Figure 3.13. FTIR spectra of [Ch]Cl and hexanoic acid HDES at different molar ratios.

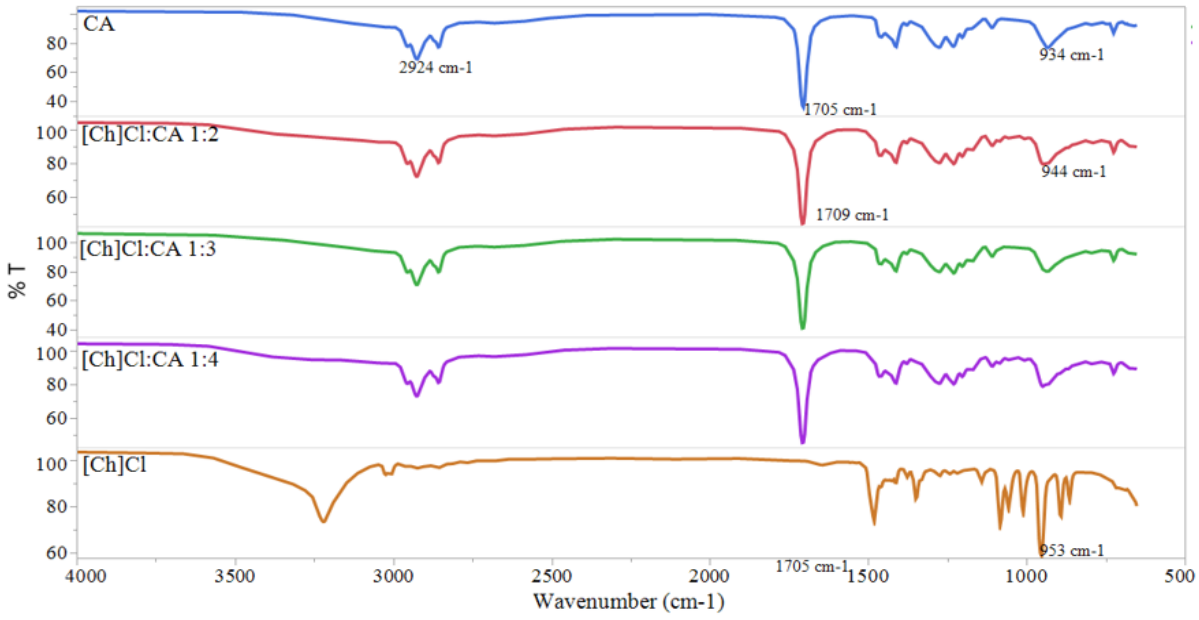

Figure 3.14. FTIR spectra of [Ch]Cl and caprylic acid HDES at different molar ratios.

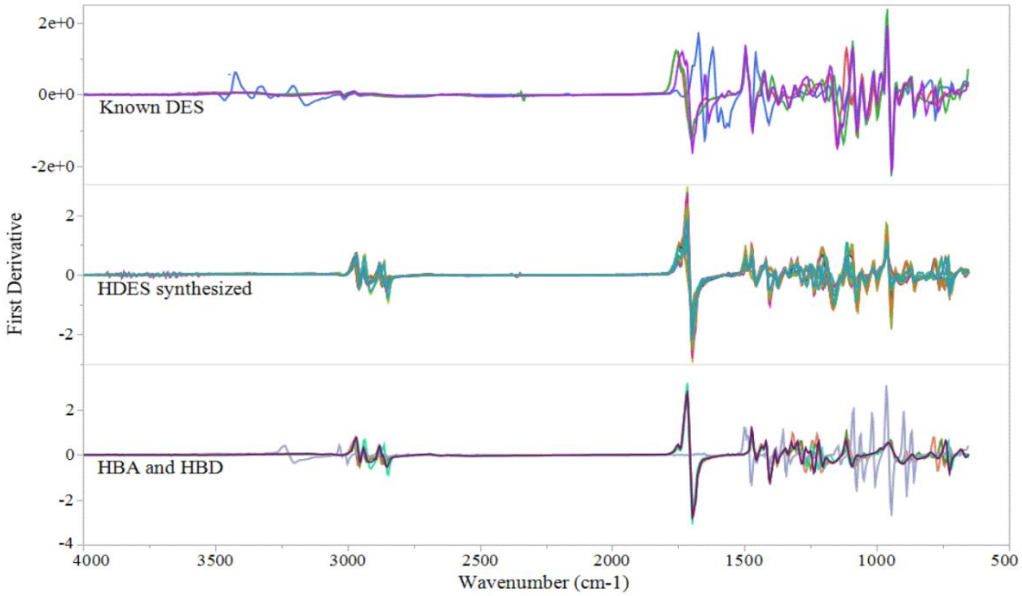

Figure 3.15. Pretreatment of HDES FTIR spectra by first derivative.

3.3.6.1. Fingerprint region of the DES

From Fig. 3.16., PC1 and PC2 accounts for 68.5 % of the total variation in the original data set. All the variables correlate positively with the first principal component (PC1) except urea. As shown on the score plot, the hydrogen-bond donors (blue dot) cluster together in the positive quadrant (except urea) of the PC2 together with some HDES (encircled in green). Conversely, choline chloride (red dot), [Ch]Cl:urea, [Ch]Cl:malic acid, and [Ch]Cl:malonic acid cluster with some HDES (encircled in blue) in the positive quadrant of PC1. Interestingly, both PC1 and PC2 showed negative correlation with urea. The close location of some HDES to the acidic HBD and some together with the HBA introduced the question as to which wavelengths the PCA uses to maximize variability or discriminate between variables. This was answered by plotting the first and second principal components against wavelength as shown in Fig. 3.17.

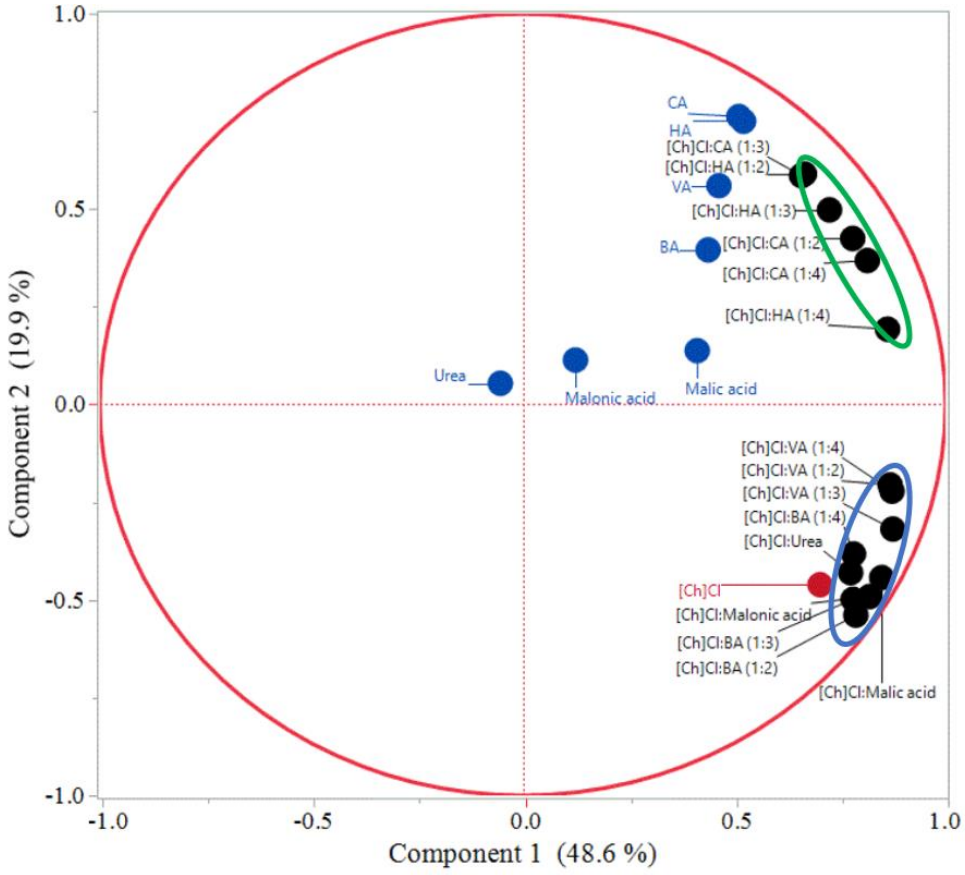

Figure 3.16. PCA plot of HDES and its constituents

From the results, the ammonium identity peak at 952 cm^{-1} and the carboxylic peak at 728 cm^{-1} was used by PC1 and PC2, respectively, to determine variability in the fingerprint region. This explains why urea correlates negatively with both PC1 and PC2 due to the absence of both wavelengths in pure urea. Also, the prepared HDES share similar ammonium characteristics with known DES such as [Ch]Cl:malic acid, [Ch]Cl:malonic acid, and [Ch]Cl:urea. The HDES encircled in green have more of the carboxylic identity peak than the ammonium identity peak signifying their high acidic content. In a broader perspective, chemometrics can be extended to characterize and group similar solvents and other materials. Most at times, FTIR spectra of DES appear similar to the spectra of the

HBD, however, these results give further insight about the contribution of the HBA to the fingerprint region. The BA and VA-based HDES synthesized have ammonium identity peak similar to those in [Ch]Cl:malic acid, [Ch]Cl:malonic acid, and [Ch]Cl:urea. On the contrary, the chemometric analysis showed that hexanoic acid and caprylic acid acid-based HDES cluster away from the ammonium identity peak and behave more like an acid or a donor. Although, the FTIR data and PCA analysis indicate high acidity of some HDES, hence, the need for other techniques to confirm the results.

3.3.6.2. Hydrogen bonding

To validate our FTIR chemometric results, we expanded our study to the hydrogen-bonding region of the spectra. Since DES is defined on the basis of intermolecular interactions via hydrogen bonding between the donor and the acceptor molecules, our expectation is that solvents with similar hydrogen bonds between 3500 cm^{-1} and 3100 cm^{-1} will cluster. Interestingly, in Fig. 3.18., all the HBD (colored in blue) clustered in one quadrant with the exception of malic acid and urea.

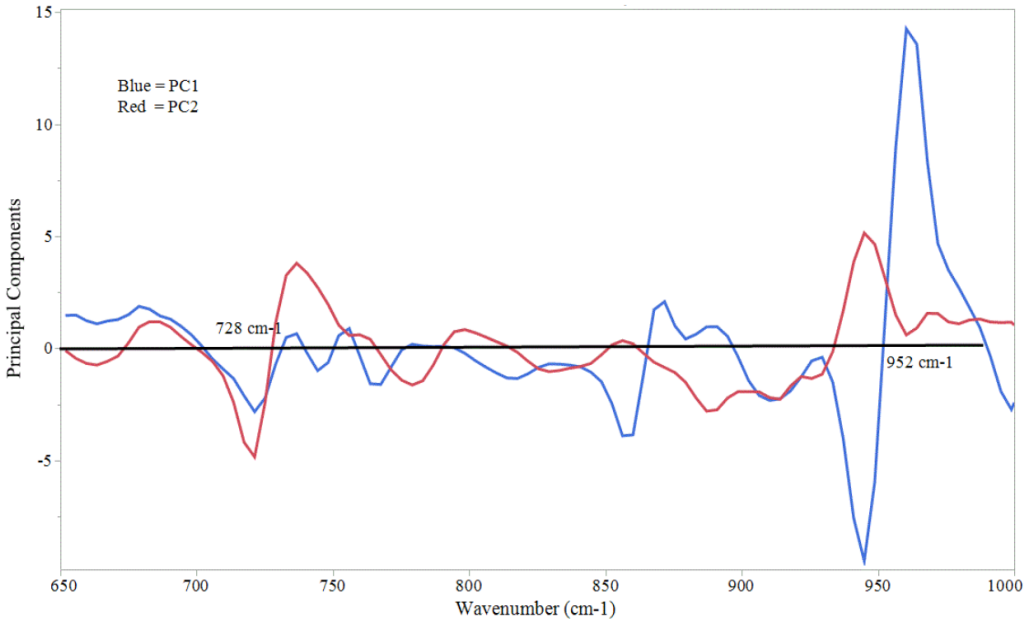

Figure 3.17. Plot of first and second principal components against wavelength.

The extra hydroxyl (-OH) group of malic acid make it more susceptible to form hydrogen bond compared to other acids studied. The [Ch]Cl:VA 1:2 although possessing high ammonium identity peak, clusters close to the acids which might be attributed to minimal hydroxyl stretching bands. [Ch]Cl:malic acid and [Ch]Cl:malonic acid cluster in the same quadrat; nonetheless, the different locations of these DES on the score plot confirms the difference in the hydrogen-bonding behavior in the O-H stretching region. Apart from [Ch]Cl:BA and [Ch]Cl:HA 1:4 that appeared at the same location on the score plot, all the other HDES shows different O-H stretching profile. Our results indicate that a simple, robust, and cost effective FTIR chemometrics is a faster approach to study new solvent systems and evaluate their relationships based on hydrogen-bonding.

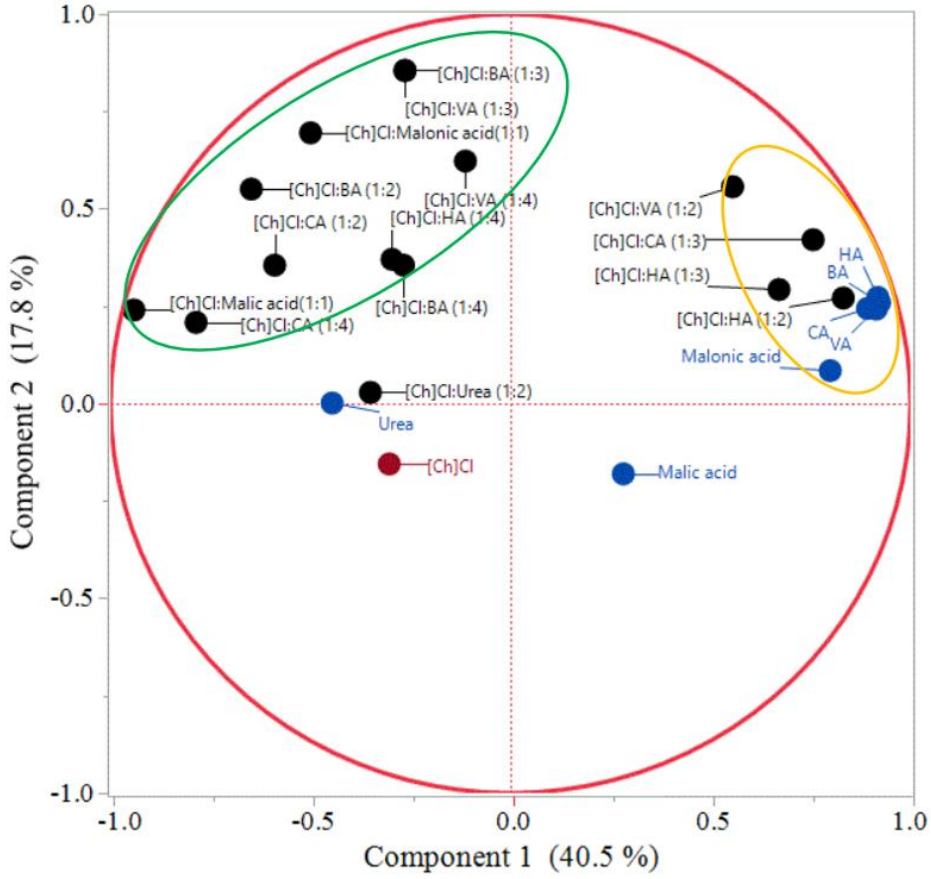

Figure 3.18. PCA plot of DES and HDES by using the hydrogen bonding region (3500 cm^{-1} and 3100 cm^{-1}) of the FTIR spectra.

3.3.7. ^{1}H NMR characterization

The interaction between choline chloride and butyric acid, valeric acid, hexanoic acid, and caprylic acid were characterized using ^{1}H NMR. The HDES shows a reduction in water content (chemical shift at 2.5 ppm) compared to the individual constituents confirming our water activity and TGA results. From Fig. 3.19., it can be seen that the DES experience chemical shift when the donor and the acceptor groups interact. Table 3.5 gives the chemical shift of HDES. A shift in ^{1}H NMR signal to the lower field as observed in 1:2

and 1:3 molar ratios of most HDES is an evidence of the presence of hydrogen bonding[38]. Although the chemical shift in HDES do not change significantly from the constituents, however, the interaction between the donor and the acceptor molecules caused a reduction in the intensity of the methylene protons on choline chloride. Moreover, the loss of the hydroxyl proton (-OH) on both the donor and the acceptor molecules in the HDES confirms interaction between the two. The question as to whether an ester bond is formed by mixing carboxylic acids with [Ch]Cl resurface here.

Recently, Florindo et al.[40] showed the formation of ester impurities by mixing and heating cholinium cation and glutaric acid. Although our FTIR analysis showed a unique C-O stretching between 1176 cm^{-1} to 1187 cm^{-1} , we confirmed ester impurities formation by mixing raw materials with heating. A choline chloride and butyric acid HDES (1:2) was prepared without heating the components. An NMR spectrum of the resulting HDES shows a proton at 12 ppm, a characteristic carboxylic proton which is absent in the heated HDES samples. The results corroborate ester formation during the heating process, hence a controlled system should be instituted when synthesizing DES from an acid and QAS. Florindo et al.[40] showed that an absolute deviation of 6.25% and 0.15% in viscosity and density values, respectively, between the heated and nonheated DES. The minimal ester impurity does not undermine the applicability of the eutectic mixture for its intended application for extracting bioactive compounds from *Piper nigrum*.

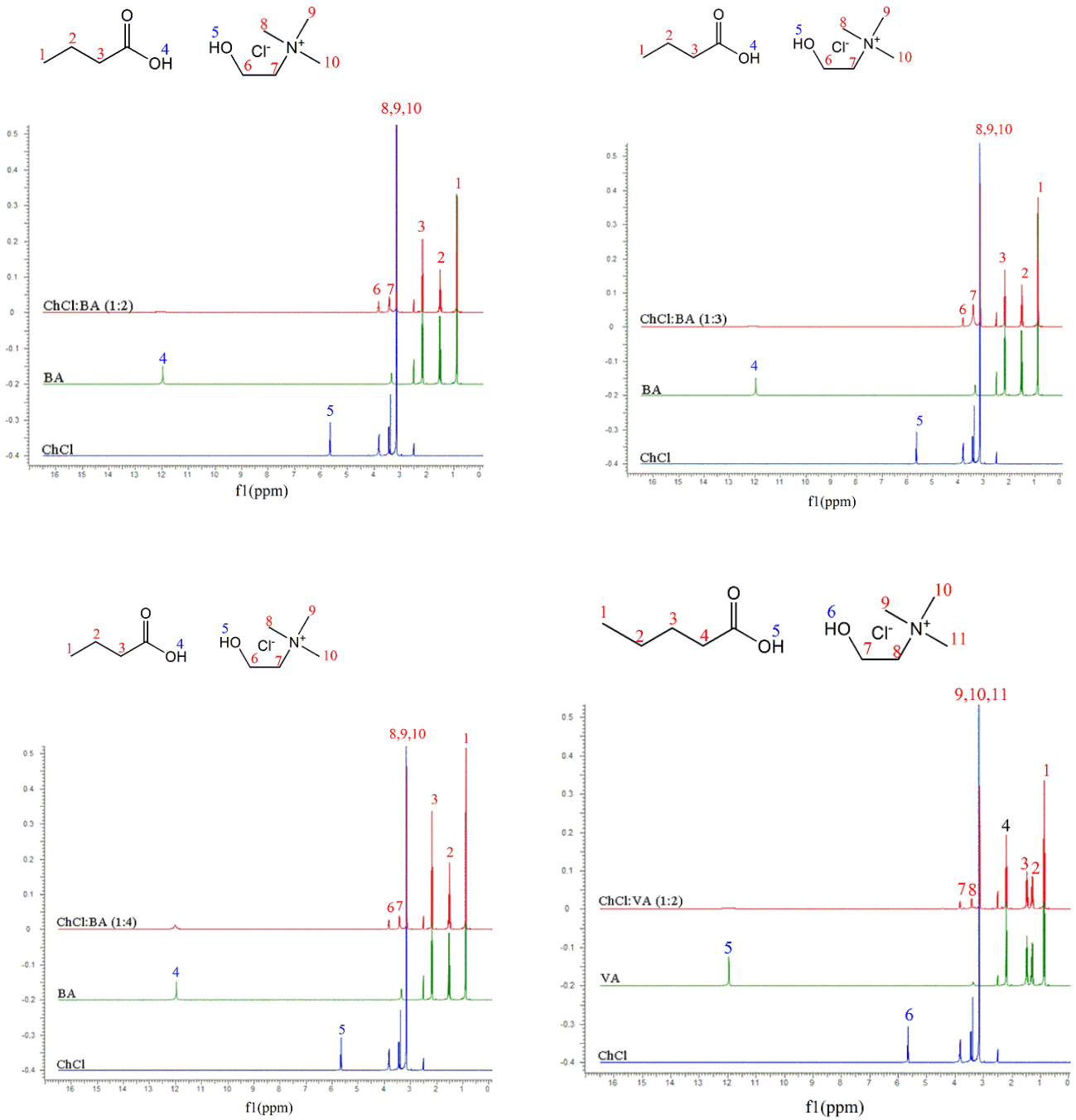

Figure 3.19. Stacked ^{1}H NMR of HDES and their constituents.

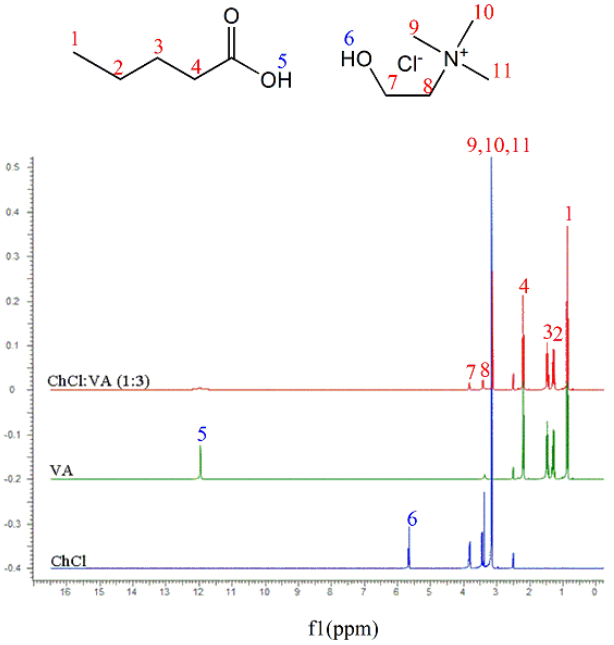

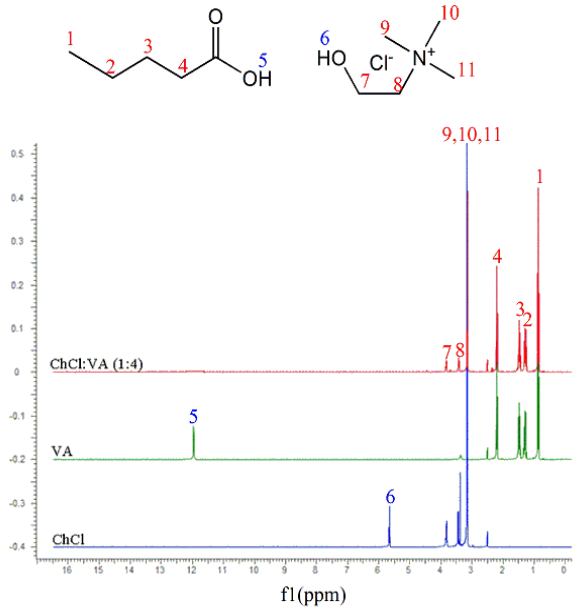

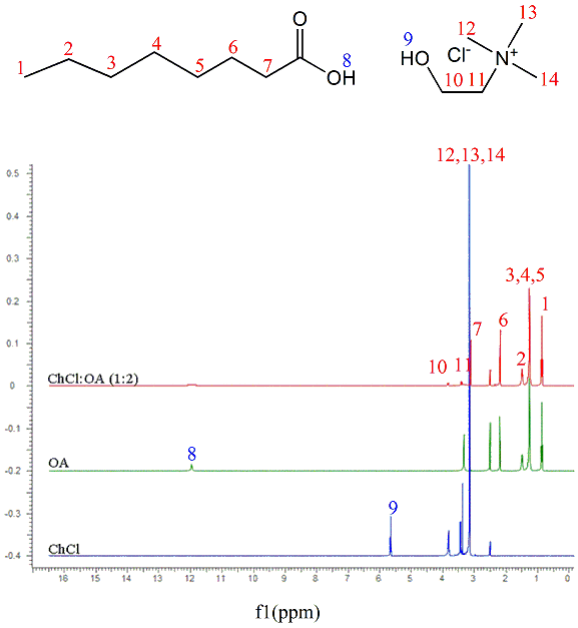

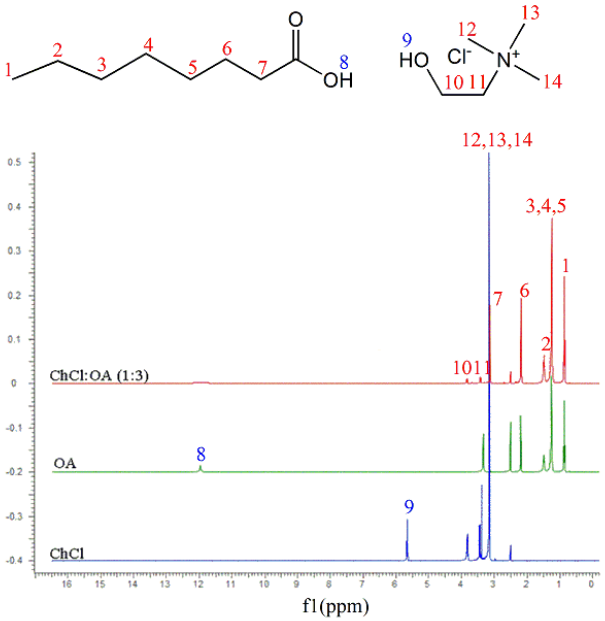

Stacked H NMR of HDES with its constituents *cont'd.*

Table 3.5. ^{1}H NMR chemical shift of HDES and its constituents.

Proton	**BA and [Ch]Cl**	1:2 **[Ch]Cl:2BA**	1:3 **[Ch]Cl:BA**	1:4 **[Ch]Cl:BA**
1	0.88	0.88	0.87	0.87
2	1.51	1.51	1.50	1.51
3	2.18	2.18	2.18	2.18
4	11.97	-	-	-
5	5.66	-	-	-
6	3.82	3.83	3.83	3.83
7	3.44	3.43	3.41	3.42
8,9,10	3.15	3.14	3.13	3.14
Proton	**VA and [Ch]Cl**	**[Ch]Cl:VA**	**[Ch]Cl:VA**	**[Ch]Cl:VA**
1	0.87	0.85	0.86	0.86
2	1.29	1.29	1.31	1.31
3	1.48	1.45	1.49	1.49
4	2.19	2.22	2.22	2.19
5	11.96	-	-	-
6	5.66	-	-	-
7	3.82	3.82	3.84	3.83
8	3.44	3.43	3.43	3.44
9,10,11	3.15	3.14	3.13	3.14
Proton	**HA and [Ch]Cl**	**[Ch]Cl:HA**	**[Ch]Cl:HA**	**[Ch]Cl:HA**
1	-	0.862	0.861	-
2, 3	-	1.259	1.260	-
4	-	1.493	1.497	-
5	-	2.199	2.190	-
6	-	-	-	-
7	-	-	-	-
8	-	3.837	3.831	-
9	-	3.444	3.457	-
10,11,12	-	3.160	3.163	-
Proton	**CA and [Ch]Cl**	**[Ch]Cl:CA**	**[Ch]Cl:CA**	**[Ch]Cl:CA**
1	0.87	0.86	0.86	0.86
2,3,4,5	1.29	1.26	1.26	1.26
6	1.48	1.49	1.48	1.49
7	2.19	2.19	2.18	2.19
8	11.96	-	-	-
9	5.66	--	-	11.97
10	3.82	3.83	3.83	3.83
11	3.44	3.40	3.42	3.38
12,13,14	3.15	3.12	3.13	3.11

3.3.8. Piperine extraction

The amount of piperine extracted from both ground pepper and peppercorns by using microwave-assisted (MAE) and subcritical (SCE) extractions were evaluated. The chemical structure of piperine (Fig. 3.20), calibration curve by using o-terphenol as internal standard (Fig. 3.21), and chromatogram of standard piperine (Fig. 3.22) with retention time of 7.023 min is shown. The previous studies evidenced that different HDES possesses unique physicochemical properties and is expected that these properties would influence the extracting efficiency of piperine from their matrix. Thus, we selected [Ch]Cl:BA 1:2, [Ch]Cl:VA 1:2 and [Ch]Cl:CA 1:2 to test their efficacy in extracting piperine by employing MAE and SCE. The crude extract in ethyl acetate is shown in Fig. 3.23. As shown in Fig. 3.24., the HDES was able to extract piperine from *Piper nigrum* at different yields. In general, the piperine content in peppercorns was higher than in ground pepper irrespective of the HDES and the extraction technique used. The low piperine content in ground black pepper can be attributed to excessive grinding during processing. The average piperine content in ground pepper was 19.9 ± 4.9 mg/g and 14.9 ± 8.7 mg/g, respectively, for SCE and MAE. Comparatively, an average piperine content of 25.8 ± 2.1 mg/g and 26.3 ± 7.2 mg/g were found in peppercorns, respectively, for SCE and MAE. As expected, different HDES extracted piperine at different amounts. The [Ch]Cl:BA 1:2 extracted 34.6 mg/g of piperine compared to 50.78 mg/g reported to be in the fruit of *Piper nigrum*[146-147]. The lowered piperine content in may be attributed to the use of ethyl acetate for liquid-liquid extraction (LLE) rather than using a slightly polar solvent. The octanol/water partition coefficient ($\log K_{ow}$) of ethyl acetate is 0.73 whereas $\log K_{ow}$ of [Ch]Cl:BA is 0.79, [Ch]Cl:VA is 1.39 and [Ch]Cl:CA is 3.05. The partitioning of piperine into ethyl acetate

might account for the lower yield obtained. Statistically, at the 95% confidence interval, no significant difference exists between the different DES systems efficiency in extracting piperine from *Piper nigrum*. However, the increased hydrophobicity of [Ch]Cl:CA 1:2 may account for the lowered piperine yield from ground pepper.

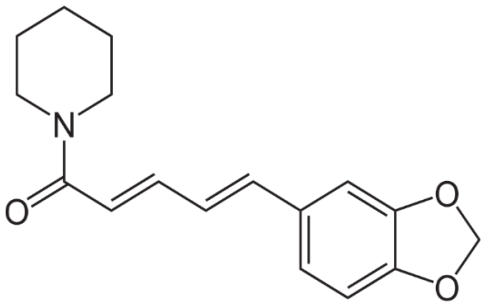

Figure 3.20. Chemical structure of piperine.

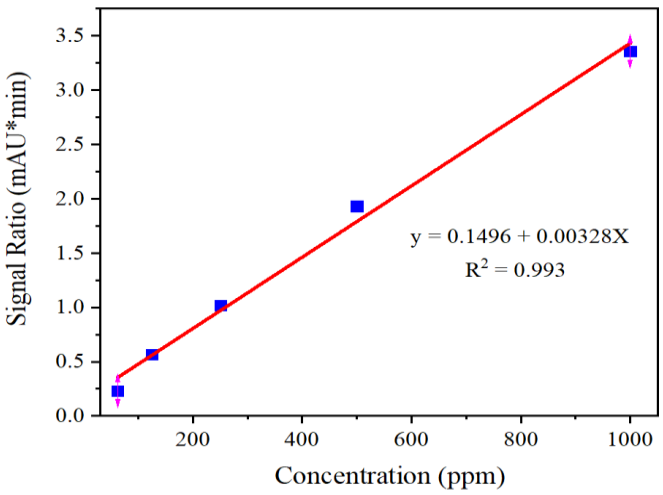

Figure 3.21. Calibration curve for piperine.

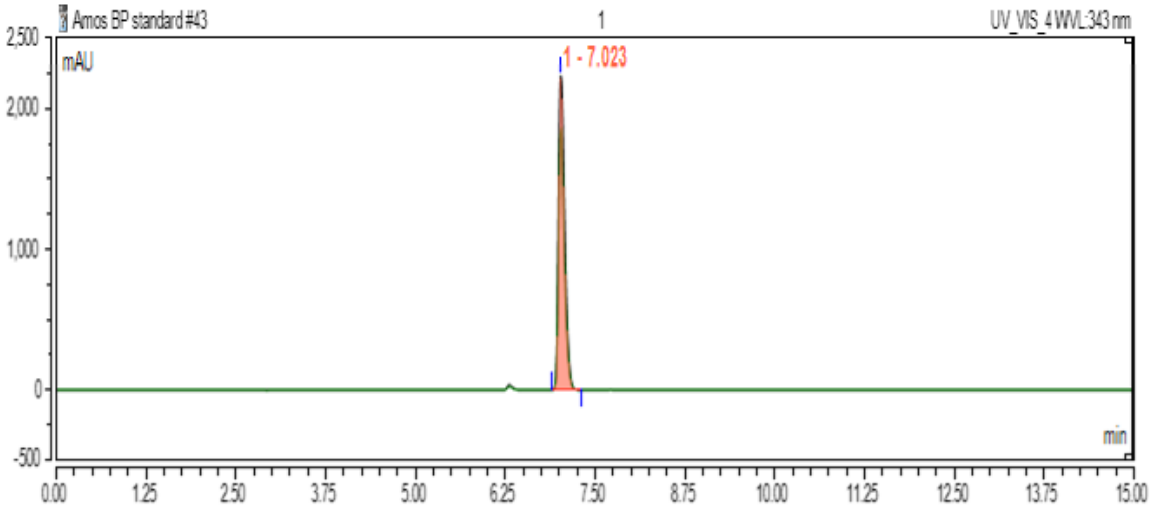

Figure 3.22. UHPLC chromatogram of piperine.

A) Extract from MAE

B) Extract from SCE

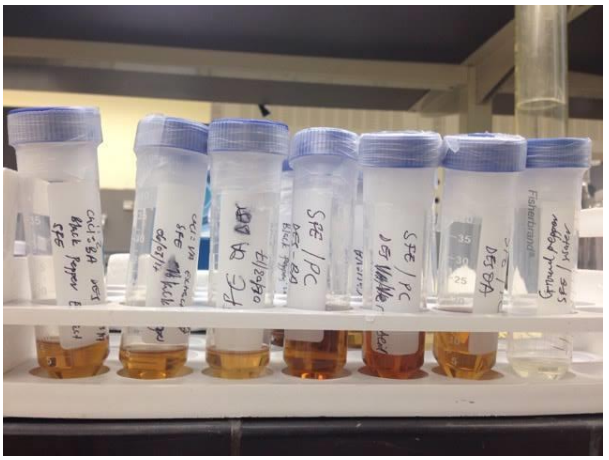

Figure 3.23. Liquid-liquid extract of piperine in ethyl acetate.

A) Piperine content from MAE **B)** Piperine content from SCE

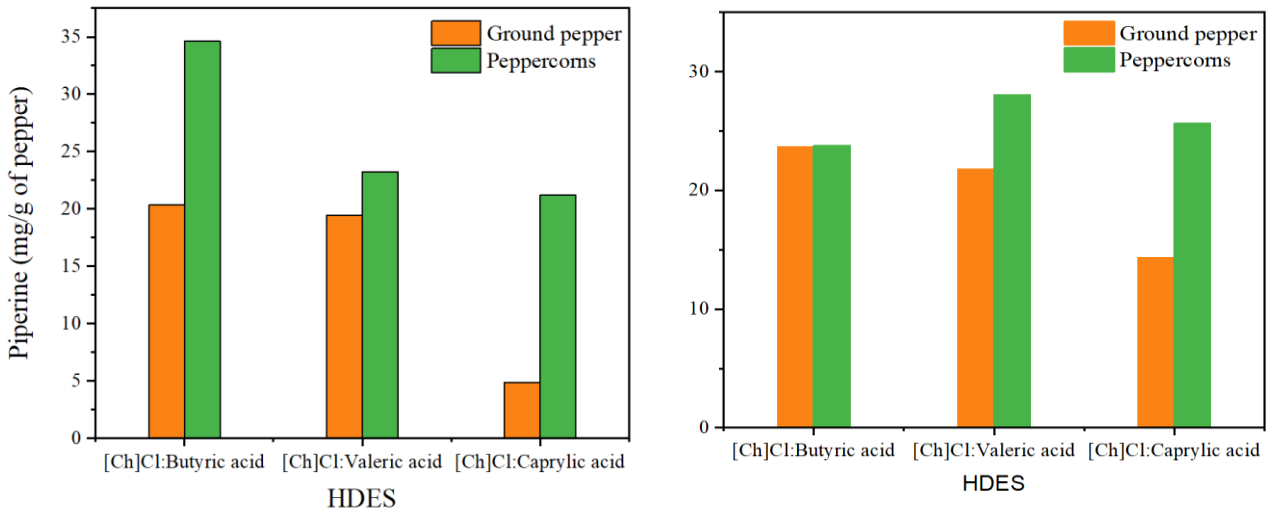

Figure 3.24. Piperine content in black pepper extracted with HDES.

Although, both MAE and SCE shows no statistical difference in yield, MAE is a preferred choice for subsequent piperine extraction and optimization process due to the short extraction time (3 min) as compared to 10 min for SCE. In summary, HDES was able to extract a moderately polar analyte, piperine, from *Piper nigrum* with excellent yield. Optimization of the process by using a more polar solvent like methanol for LLE may enhance piperine yield. In here, we have synthesized and characterized a new hydrophobic DES with tunable chemical and physical properties and was applied to extract bioactive compound, piperine, from black pepper.

CHAPTER FOUR

ELECTRONIC AND MOLECULAR PROPERTIES OF HYDROPHOBIC DEEP EUTECTIC SOLVENTS

4.1. Introduction

Deep eutectic solvents (DES) are new generation of designer solvents alternative to ionic liquids[35-36]. The term was first introduced by Abbott and his co-workers by mixing choline chloride and urea (1:2 molar ratio), with depressed melting point compared to the individual components[35-36]. The formation of DES simply involves the combination of a salt acting as a hydrogen bond acceptor (HBA) with a hydrogen bond donor (HBD) in the correct molar ratio until the eutectic point is reached. The driving force for the eutectic point between HBA and HBD is hydrogen bond interaction between the chloride anion and the HBD, resulting in charge delocalization[35, 121]. Since its inception in 2001, many independent researchers have worked with different HBAs and HBDs to understand the nature, physicochemical, and thermophysical properties of the solvent[38, 52, 148]. Choline chloride, [Ch]Cl, remains the most used salt for DES formation due to its low cost, low toxicity, biodegradability, and biocompatibility, while commonly used HBDs include urea, alcohols, sugars, amides, amino acids, and carboxylic acids[74].

Carboxylic acid-based DES have recently attracted attention due to their uniqueness in analytical extraction[41, 47], organic synthesis[39], electrochemistry[148], and as pharmaceutical ingredients[149]. Commonly used monocarboxylic and dicarboxylic acids in DES include, but not limited to, acetic acid, oxalic acid, malonic acid, malic acid, maleic acid, levulinic acid, and citric acid[40, 150]. Recently, a hydrophobic DES was synthesized

from decanoic acid and quaternary ammonium salts and was reported to have higher extraction efficiencies for volatile organic compounds (VOCs)[55].

Despite numerous physicochemical and thermochemical data on different carboxylic acid-based DES, little or no attempt has been made to understand the electronic and molecular properties of these eutectic systems. Abbott et al. [36] inferred that two carboxylic acids might be required to complex each chloride anion for eutectic point to be reached. After a decade of this speculation, detailed molecular explanations on how this complexation occur with respect to the DES frontier molecular orbitals on chemical potential, electronegativity, and charge transfer (CT) is still missing in literature.

In this work, different molar combinations of choline chloride salt with butyric acid (BA), valeric acid (VA), and caprylic acids (CA) were studied. These HBDs were selected not only because it has not been thoroughly investigated in the literature, but also to tailor the polarity of the formed DES. To date, most DES have been hydrophilic, hence studying the electronic properties of fatty acid-based DES would be the first of its kind. The longest-wavelength intermolecular charge transfer polarity scale by Kosower[151] was normalized by Nile red (NR) dye to determine electron transition (E_T or Z) (equation 4.1). The Kamlet-Taft multiparameter linear polarity parameters (hydrogen bonding acidity; α, hydrogen bonding basicity; β, and dipolarity/polarizability; π*)[152-153] were determined using 4-nitroaniline (4NA) and N, N-diethyl-4-nitroaniline (DENA) as solvatochromic probes. E_T (NR) response in kcal.mol^{-1}, α, and β values of the newly formed carboxylic acid based-DES were calculated using the equations below (equations 4.2, 4.3, and 4.4) with υ referring to the wavenumber.

E_T (NR) kcal.mol^{-1}= 28591.44/ λ_{max} (nm) (Equation 4.1)

$\alpha = 0.0649\ E_T$ (NR) – 2.03 – 0.72 π^* (Equation 4.2)

$\beta = (1.035\ \upsilon_{DENA} + 2.64 - \upsilon_{4NA})/\ 2.80$ (Equation 4.3)

$\pi^* = 0.314\ (27.52 - \upsilon_{DENA})$ (Equation 4.4)

To fully understand charge transfer, dipole moments, chemical potential, electron affinity, electronegativity, and ionization potential of the eutectic mixtures, density functional theory (DFT) employing a hybrid density functional model (B3LYP) at 6-312 (d) basis set was used to study the frontier molecular orbitals (FMOs) of the HBA, HBDs, and the DES. The FMOs are known molecular orbitals useful in chemical reactions and have been used by several researchers to study reactivity and stability of mixtures[154-157]. In this study, we combined experimental approach by solvatochromic molecular probes and computational models to explore how HBA and HBD behave during DES formation, and correlate empirical polarity indices with DFT.

4.2. Experimental

4.2.1. Chemicals

Choline chloride, butyric acid, caprylic acid, Nile red, and 4-nitroaniline were all purchased from Acros Organics and had a purity of ≥ 99%. Valeric acid (purity ≥ 99, Alfa Aesar) and N, N-diethyl-4-nitroaniline (Frinton Laboratories, Inc.) were used. All other

chemicals were of analytical grade.

4.2.2. Synthesis of DES

DES were synthesized by mixing choline chloride and HBDs at 1:2 or 1:3 molar ratios and heated at 80 ℃ for 15-30 min under constant stirring at an atmospheric pressure until a homogenous liquid was obtained. The prepared HDES were cooled to room temperature and stored in a desiccator.

4.2.3. Solvatochromic assay

A UV-Vis spectrophotometer (Synergy|H1 microplate reader, Biotek) was used to determine the maximum absorption wavelength (λ_{max}) from the absorption spectra. Absorbance readings were collected by spectral scanning of DES in Nile red (400-650 nm), N, N-diethyl-4-nitroaniline (300-450 nm), and 4-nitroaniline (300-450 nm) at 1-nm intervals in triplicate. The working concentration for all the solvatochromic probes was kept as low as 0.5×10^{-4} M in order to neglect solute-solute interaction in the observed solvent effect[158]. The effect of temperature on electron transition in the probes and on Kamlet-Taft parameters were obtained from 25-45 ± 0.2 ℃.

4.2.4. Computational

Quantum theoretical calculations were performed with Gaussian 09 software package[159] to investigate the electronic properties of HBA, HBDs, and DES. Gas-phase equilibrium geometries were fully optimized and vibrational frequencies were calculated with DFT/B3LYP; a hybrid of Beck's three-parameter exchange functional[160] and Lee-Yang-Parr correlation functional[161] with 6-31G (d) basis set. DFT/B3LYP makes correction for both gradient and exchange correlations and provide qualitative results with

comparable accuracy to *ab initio* methods at reduced CPU time. The global minima on the potential energy surface was confirmed by the absence of negative frequencies. The molecular orbital calculations were executed with same computational methods and basis sets at 298 K to obtain the highest occupied and lowest unoccupied molecular orbital energies (HOMO and LUMO), based on the optimized structures of HBA, HBDs, and DES. The chemical potential (μ), electronegativity (χ), global hardness (η), chemical softness (S), charge transfer (ΔN), and reaction energy (ΔE) were calculated.

4.3. Results and discussion

4.3.1. Physical characterization of DES

Several carboxylic acid-based DES have been reported in the literature, but data on the electronic properties of these solvents are missing. Also, no work has been done to elucidate how an increased hydrocarbon chain of fatty acids affect the molecular and electronic properties of DES. In this work, three HBDs (fatty acids) were selected to tailor the nature of the DES by increasing the alkyl chain length. Butyric acid (BA), valeric acid (VA), and caprylic acid (CA) are cheap, readily available, biodegradable, and nontoxic making them excellent HBDs for this research. From Table 4.1, DES formed by 1:3 molar ratio (HBA to HBD) are transparent liquids at room temperature except [Ch]Cl:CA 1:2 which shows cloudiness even at 1:2 molar ratio. The high viscosity of DES [Ch]Cl:BA 1:2, [Ch]Cl:VA 1:2, and [Ch]Cl:CA 1:2 are partly due to high charge transfer and strong hydrogen bonding between the cation and the chloride anion.

Table 4.1. Physical characterization of synthesized DES

HDES	Acronym	Physical characterization at room temperature **molar ratio 1:2**	**molar ratio 1:3**
Choline chloride: Butyric acid	[Ch]Cl:BA	viscous (high), white cloudy	white transparent liquid, viscous (medium)
Choline chloride: Valeric acid	[Ch]Cl:VA	viscous (high), white cloudy	white transparent liquid, viscous (medium)
Choline chloride: Caprylic acid	[Ch]Cl:CA	viscous (very high), white-yellowish	viscous (very high), white-yellowish

4.3.2. Solvatochromism

4.3.2.1. Electron transition (E_T) between solvent and solute interaction

Solvatochromism, due to its simplicity, remains the most widely used method for studying empirical solvent properties through charge transfer (CT) from donor to acceptor molecules. The use of 96-well microplate UV/Vis spectrophotometer with 4-zone^{TM} incubator made it easier to control temperature between 298-318 K. Nile red, instead of penta-tert-butyl substituted betaine dye by Dimroth and Reichardt, was used to calculate E_T values due to the acidic nature of the DES. The latter becomes protonated in acidic medium and losses its absorption band, hence not a suitable probe to study the solute-solvent solvation microsphere between the probe and the carboxylic acid-based DES. Low basicity (pK_a = 1.00 ± 0.05), photochemical stability, and solubility in solvents with diverse polarity are among the several reasons why Nile red is preferred as solvatochromic probe in acidic media[119]. From Fig. 4.1., the spectral scan of DES in Nile red shows a bathochromic shift of the maximum wavelength (λ_{max}) when the hydrocarbon chain length is decreased (increase in polarity). The λ_{max} of Nile red does not appear to shift significantly

between the various DES, most especially between 1:2 and 1:3 molar ratios of the same HBD. This data supports previous report that the λ_{max} of Nile red changes minimally in the presence of hydrogen bonding solvents[119].

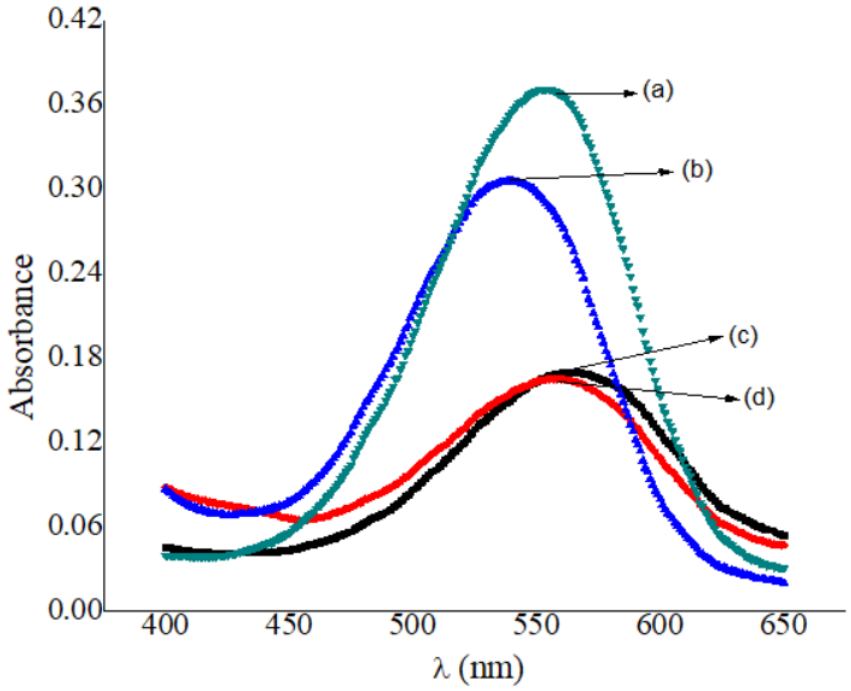

Figure 4.1. Absorption spectra of 0.5×10^{-4} M solution of Nile red dye in DES and methanol (control) at 298 K. (a) methanol, (b) [Ch]Cl:CA 1:3 (c) [Ch]Cl:BA 1:3, and (d) [Ch]Cl:VA 1:3.

In all the DES formed, electron transition stays linear between 303 K to 308K after which a modest shift in λ_{max} was observed between 308 K to 318 K (Fig. 4.2.). This behavior of the DES shows that the composition of the solvent changes at elevated temperatures and affect the empirical polarity index. The E_T (NR) value of methanol at 298 K was found to be 51.61 kcal.mol^{-1} similar to a literature value of 52.02 kcal.mol^{-1}, and

consistent to E_T (30) and E_T (26)[119] values. It can be inferred that increasing the hydrocarbon chain of the HBD affects the E_T (NR) parameter, and hence the polarity of the formed DES. This property is a good indicator for selecting appropriate HBD for DES needed for solvent-dependent chemical reactions.

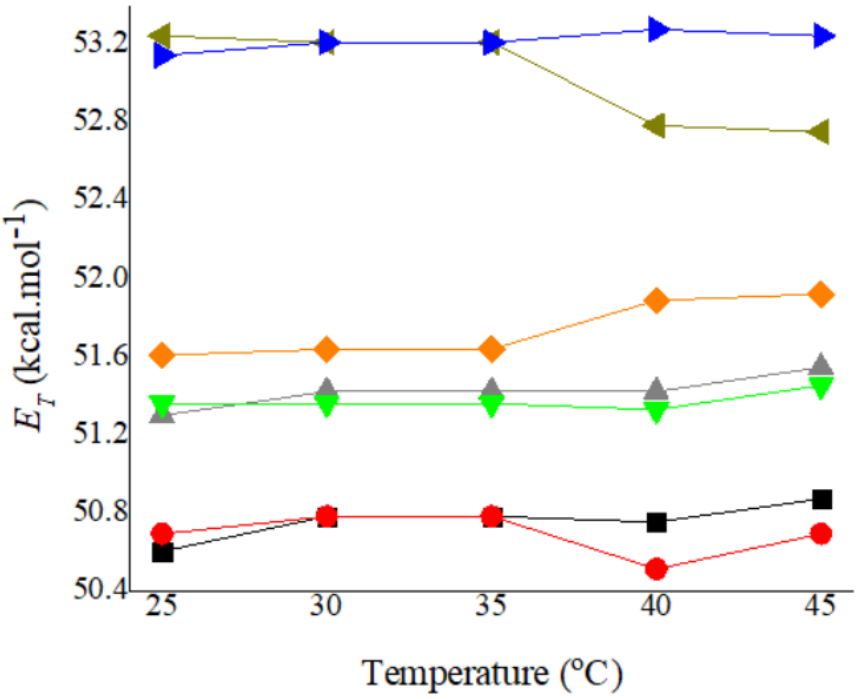

Figure 4.2. Electronic transition (π-π *) of Nile red dye in DES and methanol (control) from 25-45 ± 0.2 °C. black ([Ch]Cl:BA 1:2), red ([Ch]Cl:BA 1:3), gray ([Ch]Cl:VA1:2), (green)[Ch]Cl:VA 1:3, orange (methanol), dark yellow ([Ch]Cl:CA 1:2), and blue ([Ch]Cl:CA 1:3). E_T values were computed from average of λ_{max} readings in triplicate from 400-650 nm.

4.3.2.2. Kamlet-Taft parameters

The Kamlet-Taft parameters π* and β of the DES were determined from DENA and 4NA molecular probes using equation 3 and 4, respectively. The dipolarity/polarizability parameter (π*) measures the nonspecific interactions such as dipole-dipole and dipole-induced dipole interactions, and the polarizability occurring between the solute and the solvent. From the results, nonspecific interactions serve as an index for DES polarity and it decreases with increasing the hydrocarbon chain of the HBD. As shown in Table 4.2, nonspecific interactions in DES at 313 K decrease in the order [Ch]Cl:BA 1:2 (0.9457 ± 0.02) > [Ch]Cl:BA 1:3 (0.9136 ± 0.01) > [Ch]Cl:VA 1:2 (0.8303 ± 0.02) > [Ch]Cl:VA 1:3 (0.78472 ± 0.01) > [Ch]Cl:CA 1:2 (0.4212 ± 0.04) > [Ch]Cl:CA 1:3 (0.3270 ± 0.03), signifying that slight changes in the HBD moiety affects the KT π* parameter.

Table 4.2. Kamlet-Taft parameters of HDES at 313 K and 318 K.

DES	π*		β		α		E_T^N	
	313 K	318 K	313 K	318 K	313 K	318 K	313 K	318 K
[Ch]Cl:2BA	0.945171	0.945171	0.513754	0.513754	0.583363	0.591178	0.618928	0.622644
[Ch]Cl:3BA	0.913624	0.907259	0.525578	0.499034	0.590558	0.606767	0.611547	0.617076
[Ch]Cl:2VA	0.830303	0.830303	0.494869	0.477484	0.709513	0.717535	0.639588	0.643404
[Ch]Cl:3VA	0.784722	0.797805	0.557187	0.506937	0.736339	0.734913	0.636739	0.64054
[Ch]Cl:2CA	0.421234	0.457006	0.852714	0.846182	1.092353	1.064491	0.681586	0.680584
[Ch]Cl:3CA	0.326979	0.406926	0.954602	0.878448	1.192133	1.132424	0.696764	0.695743
Methanol	0.764949	0.823777	0.545576	0.476394	0.786852	0.746534	0.65399	0.65496

Changing the temperature to 318 K gave a similar trend indicating that HBDs significantly contribute to the non-specific interactions and polarity of the DES. This confirms a recent report by Teles et al.[162] that π* values decreases by increasing alkyl chain length between ammonium-based salts and carboxylic acids. The ionic character of [Ch]Cl:BA 1:2 DES is highest among the prepared HDES partly due to the presence of

permanent dipoles and delocalized bonds[153] giving rise to high π* value. The dipolarity/polarizability value of methanol (control) at 313 K (0.76495) and 318 K (0.82378) are closer to [Ch]Cl:VA 1:3 (0.78472) and [Ch]Cl:VA 1:2 (0.83030) DES, respectively, which means DES may replace methanol in organic reactions and synthesis.

The hydrogen-bonding basicity parameter (β) describes the ability of a solvent to accept protons or donate electron density to form hydrogen bonds and are mostly affected by the nature of the anionic part of the HBA[162]. From the results, as opposed to π* which decreases by increasing the hydrocarbon chain of the HBD, a reverse pattern is observed in the β parameter. Apart from [Ch]Cl:BA 1:2 DES which showed no change in β, a modest decrease was observed in all DES between 313 K to 318 K (Table 4.2). Reports on DES-ethaline, DES-glyceline, and DES-reline shows that β and π* do not change with increasing temperature[163]. In contrast to earlier reports, π* and β values of ionic liquids [bmim][PF_6] and [bmim][BF_4, respectively, were found to decrease with increasing temperature[164]. Surprisingly, π* tend to increase marginally from 298 K to 318 K in DES formed by using BA and VA as HBDs (Fig. S4.1). The reported data was collected within short temperature range compared to literature data (collected from 25-95 ℃) and may account for this deviation. The β values of the formed DES show their ability to accept protons for chemical reactions which is even better than some organic solvents or ionic liquids.

The Kamlet-Taft hydrogen-bonding acidity (α) describes the ability of the solvent to donate protons and is calculated from the E_T (NR) and π* values. From the results, the hydrogen-bonding acidity of DES range from 0.58336 to 1.19213 at 313 K. Comparable to methanol (0.786852), most carboxylic acid-based DES can serve as proton donors in

chemical reactions. The high acidic nature of the DES may be due to the carboxylic functional group. Increasing the alkyl chain or the molar ratio of the HBD significantly affects the α parameter.

To elucidate how α, β, and π* values calculated from our newly synthesized DES correlate with literature data, we created a ternary plot (popularly known as Snyder's Selectivity Triangle) to compare our data with KT parameters for some selected organic solvents and ionic liquids. From Fig. 4.3., the KT parameters of [Ch]Cl:BA ([Ch]Cl:BA 1:2 and [Ch]Cl:BA 1:3) are within the range of ionic liquids, while [Ch]Cl:VA ([Ch]Cl:VA 1:2 and [Ch]Cl:VA 1:3) are in close range to KT parameters of methanol. Our results were validated by comparing the experimental KT parameters of methanol (methanol*) with reported values in literature. From the ternary plot, the two appear in same quadrant and are close to each other. Depending on the HBD, KT parameters that appear to be more susceptible to change are hydrogen bonding acidity and dipolarity/polarizability.

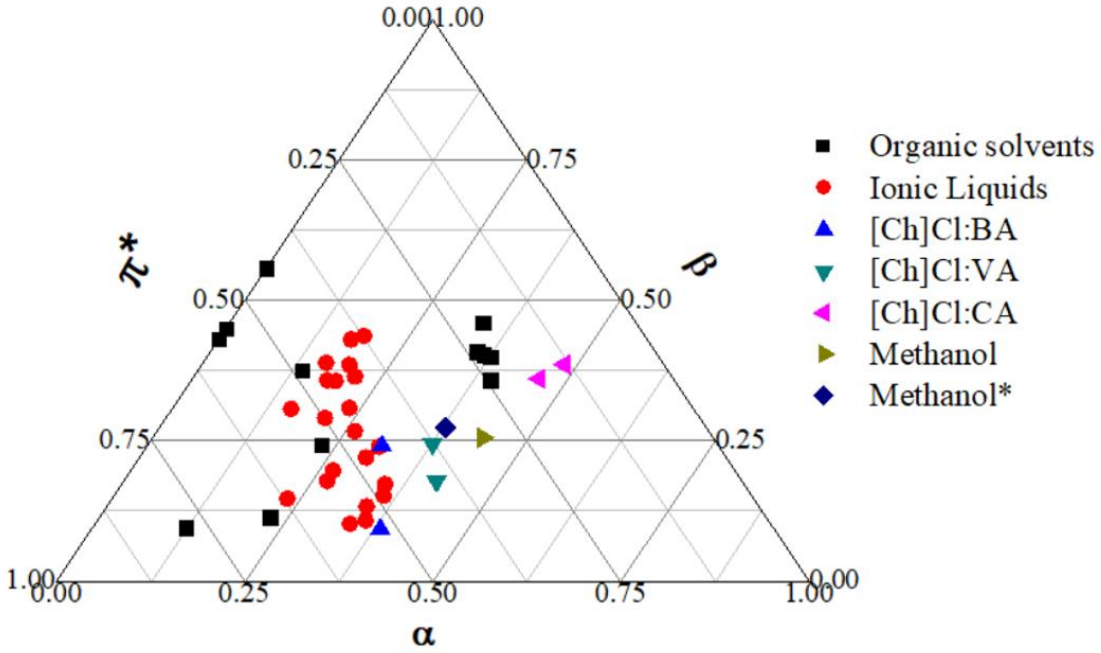

Figure 4.3. Kamlet-Taft parameters of HDES at 298 K compared to selected organic liquids and ionic liquids. The selected organic solvents and ILs are listed in appendix (Table S4.2). *experimental control

4.3.3. Density functional theory

4.3.3.1. Bond angle and distance

The electronic and molecular properties of DES were obtained from the optimized geometry of HBA and HBDs molecules through DFT/B3LYP calculation methods with 6-31G (d) basis set. DES molar ratios used for the study ranges from 1:1 to 1:3 except for [Ch]Cl:CA which we omitted the 1:3 molar ratio because of computational time. The optimized geometries, bond distance, and bond angles of [Ch]Cl:BA 1:2 DES is shown in Fig. 4.4.

Bond angles, bond distances, and optimized geometries of [Ch]Cl:BA, [Ch]Cl:VA, [Ch]Cl:CA, [Ch]Cl:VA 1:2, [Ch]Cl:CA 1:2, [Ch]Cl:BA 1:3, and [Ch]Cl:VA 1:3 are found in the supplementary data (Fig. S4.2-11). To quantitate the effect of HBDs on the choline chloride acceptor, we calculated and compared the bond angles of each DES to the optimized choline chloride acceptor. The bond angle for C15-O16-H17 and N1-C14-C15 in optimized choline chloride is 117.34º and 106.96º, respectively. These angles are more susceptible to change if molecular interactions occur in the presence of HBD. The C15-O16-H17 bond angle can help measure the degree of such molecular interaction. The [Ch]Cl:BA 1:2, [Ch]Cl:VA 1:2, and [Ch]Cl:CA 1:2 DES showed a reduced bond angle of 115.53º, 116.09 º, and 116.09 º, respectively, for C15-O16-H17 and 104.09º, 105.01º, and 105.02º, respectively, for N1-C14-C15. The lowering of bond angles for both C15-O16-H17and N1-C14-C15 in HDES shows molecular interaction between the HBA and the HBD and might be attributed to a decrease in electronegativity of the central atoms during DES formation.

Also, we measured the bond distance between the carboxylic proton of the HBD and the chloride anion of the DES to verify if they can form hydrogen bond. From the results (see appendix), all the carboxylic protons are within the bond distance of $2.04 \leq \text{Å} \leq 2.22$, which is capable to form short-strong hydrogen bond responsible for the eutectic nature of the mixture.

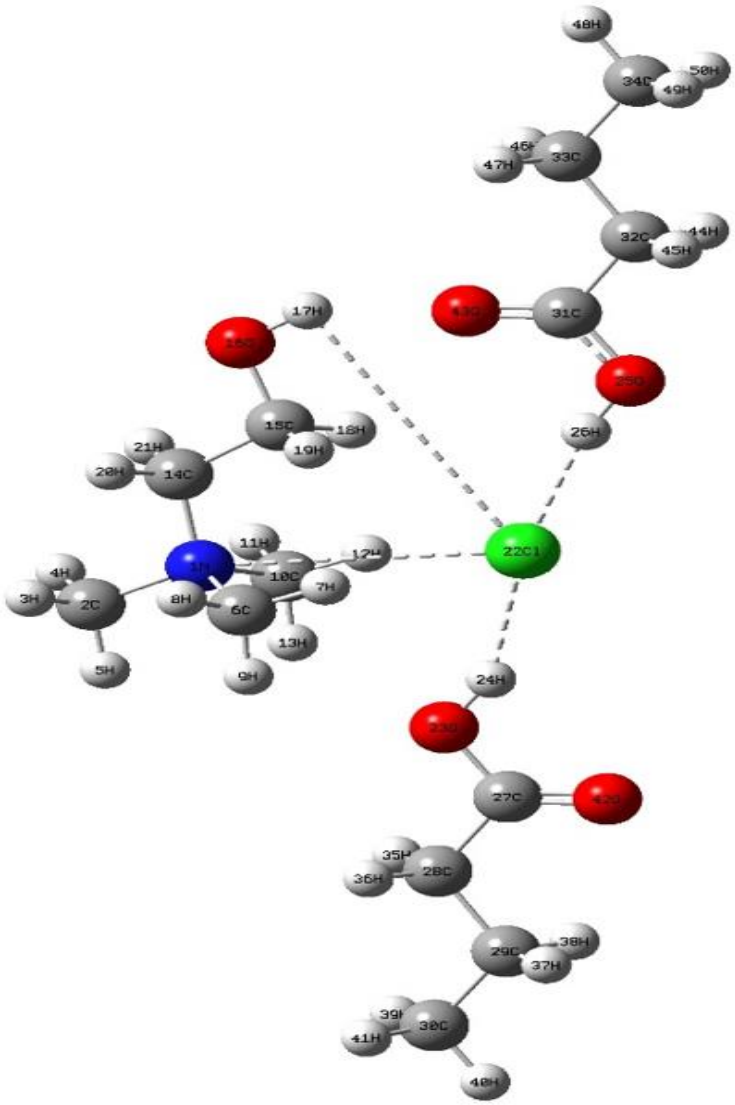

Figure 4.4. Optimized geometry of [Ch]Cl:BA 1:2 DES by DFT/B3LYP with 6-31G (d) basis set. carbon (gray), oxygen (red), nitrogen (blue), hydrogen (white), and chloride anion (light green). Bond distance between N1-Cl22 (3.95 Å), H17-Cl22 (4.64 Å), H26-Cl22 (2.12 Å), and H24-Cl22 (2.17 Å). Bond angle between C14-C15-O16 (104.44 º), C15-O16-H17 (104.09 º), C2-N1-C14 (107.99 º), and N1-C14-C15 (115.53 º).

The optimized DES bond distances and bond angles of the reactants (HBA and HBD) help to understand the existence and influence of the molecular interactions between the two in DES formation.

4.3.3.2. Electronic/Molecular properties

In addition to the solvatochromic data, quantum chemical calculations through DFT/B3LYP were used to determine the electronic and molecular properties of the carboxylic acid-based DES. The highest occupied molecular orbital (HOMO) and the lowest unoccupied molecular orbital (LUMO) were calculated for all optimized HDES including their corresponding HBA and HBD. These orbitals are important in quantum chemistry because electrons are most likely to be located there for molecular reactions to occur. The HOMO defines a region where electrons have highest energy for reaction whiles the LUMO creates a region for invading electrons from other molecules to fill-in during bonding. In other terms, the HOMO act as the ability to donate electrons (ionization potential) into the LUMO which also act as the orbitals ability to obtain electrons (electron affinity). From the results, the ionization potential of the HBDs do not change significantly as the alkyl chain length increases. As expected, the ionization potential of the HBD is greater than the HBA, and the electron affinity of the HBA is greater than the HBDs. Among the HBDs, those with 1:2 molar ratios have the highest ionization potential and follows the trend 2BA>2VA>2CA.

The difference in energy between these frontier molecular orbitals (HOMO-LUMO gap) is critical to study molecular reactivity, global hardness, electronegativity, chemical potential, and charge transfer occurring within the molecule. The higher the HOMO-

LUMO gap, the less reactive the molecule because electrons have wider distance to jump, and the molecule becomes more stable. Among the reactants simulated as given, choline chloride ([Ch]Cl) has the smallest electronic gap of 0.18477 eV which makes it the most reactive and least stable compared to the HBDs with electronic gap between 0.2688-0.28527 eV. Another molecular parameter used to describe liquids and polymers for chemical reactivity and synthesis is based on the molecular softness or hardness. Soft molecules are highly reactive with shorter HOMO-LUMO electronic gap whiles hard molecules have wider HOMO-LUMO gap. The stability of hard molecules is attributed to their wider electronic gap and do not easily involve themselves in chemical reactions. The global harness of choline chloride is 0.0924 compared to 0.143 average value for HBDs. The global hardness of DES increases as the molar ratio of the HBD increases but no apparent change occurs by increasing the alkyl chain of the HBD. The hardness and softness property of DES is necessary since most DES is employed in chemical reactions, organic synthesis, pharmaceuticals, and electrochemical applications. Understanding this phenomenon is essential to help choose the right solvent for desired industrial and pharmaceutical purpose.

4.3.3.3. Charge transfer (ΔN)

Deep eutectic solvents are formed through hydrogen bonding between HBA and HBD. Hydrogen bonding, as any covalent bond involves charge transfer (ΔN) or electron flow from one unit to the other. On this basis, we speculated that DES forming stronger hydrogen bonds (high viscous liquids) will have high degree of charge transfer compared to others. As stated by Sanderson in his electronegativity equalization principle[165-166], combination of HBA and HBD led to electron flow from the species of lower

electronegativity to species of higher electronegativity until the adduct (DES) electronegativity become equalized. The electronegativity of HBA, HBDs, and DES were calculated from the FMOs using the Mulliken's formulae[166-167] [$\chi = (I + A)/2$]. From the results (Table S4.1.), electrons flow from the HBA (χ = 0.079475) to the HBDs ($0.131845 \leq \chi \leq 0.13823$). As shown in Table 4.3, the electronegativity values of the HDES appear to be closer to the geometric mean of the two reactants (HBA and HBD) as stated by Sanderson's. The chemical potential (Lagrange multiplier, $\mu = -\chi$), a new density functional parameter by Parr et al[154, 166], were calculated as an index to measure charge transfer between the HBA and the HBD during DES formation. The electronegativity and chemical potential of DES remain similar when the same molar ratio of HBD is used irrespective of the alkyl chain. Electron flow pattern can be observed in Fig. 4.5. where the HOMO structure of [Ch]Cl:BA 1:2 DES shows electron density localized on the chloride anion (light green) whiles the LUMO electron cloud is localized on the nitrogen (blue)/hydrogen (white) of the HBA.

Table 4.3. Electronic properties of carboxylic acid-based DES.

HDES	Mole ratio	ΔЄ electronic gap (eV)	Ionization potential (I) = -HOMO	Electron affinity (A) = -LUMO	Chemical potential, μ = (ЄHOMO +Є LUMO)/2	Electronegativity, χ =(I+A)/2
[Ch]Cl:BA	1:1	0.21848	0.20929	-0.00919	-0.10005	0.10005
[Ch]Cl:BA	1:2	0.23138	0.21985	-0.01153	-0.10416	0.10416
[Ch]Cl:BA	1:3	0.24758	0.23722	-0.01036	-0.11343	0.11343
[Ch]Cl:VA	1:1	0.21846	0.20937	-0.00909	-0.10014	0.10014
[Ch]Cl:VA	1:2	0.23504	0.22225	-0.01279	-0.10473	0.10473
[Ch]Cl:VA	1:3	0.24764	0.2372	-0.01044	-0.11338	0.11338
[Ch]Cl:CA	1:1	0.21984	0.20855	-0.01129	-0.09863	0.09863
[Ch]Cl:CA	1:2	0.2345	0.22162	-0.01288	-0.10437	0.10437

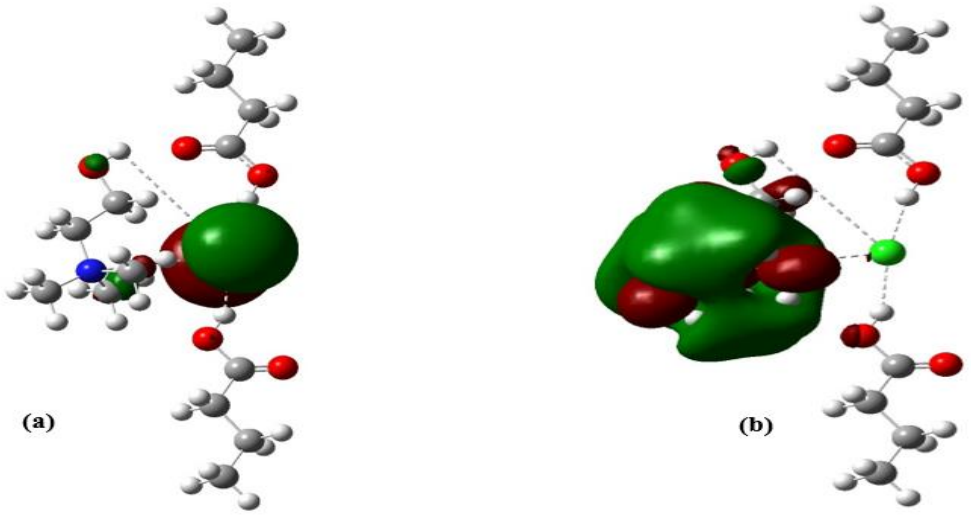

Figure 4.5. Frontier molecular orbitals of DES. (**a**) HOMO of [Ch]Cl:2BA and (**b**) LUMO of [Ch]Cl:2BA. carbon (gray), oxygen (red), nitrogen (blue), hydrogen (white), and chloride anion (light green).

Table 4.4. Molecular indices of DES by density functional theory

HDES	Mole ratio	Dipole moment (Debye)	Charge transfer, ΔN= (μB-μA)/(ηB+ηA)	Reaction energy, ΔE = -0.5*(ηAB-ηA-ηB)	Global hardness, η = (I-A)/2	Chemical softness, S = (1/2η)
[Ch]Cl:BA	1:1	10.279	0.224412	0.062865	0.10924	4.577078
[Ch]Cl:BA	1:2	11.6059	0.250806	0.059288	0.11569	4.321895
[Ch]Cl:BA	1:3	10.6744	0.239059	0.051498	0.12379	4.039098
[Ch]Cl:VA	1:1	10.381	0.223714	0.062868	0.10923	4.577497
[Ch]Cl:VA	1:2	11.9701	0.248927	0.058313	0.11752	4.254595
[Ch]Cl:VA	1:3	10.6264	0.237014	0.051533	0.12382	4.03812
[Ch]Cl:CA	1:1	9.3692	0.222832	0.06255	0.10992	4.548763
[Ch]Cl:CA	1:2	11.9343	0.246531	0.058308	0.11725	4.264392

From Table 4.4, it is not surprising that the [Ch]Cl:BA 1:2 DES has the highest charge transfer of 0.250806 followed by [Ch]Cl:VA 1:2 (0.248927) and [Ch]Cl:CA 1:2 (0.246531). Abbott et al.[35] showed that charge transport in DES controls viscosity by ionic mobility and this explains why [Ch]Cl:BA 1:2, [Ch]Cl:VA 1:2, and [Ch]Cl:CA 1:2 are highly viscous among the synthesized DES as shown in Table 4.1. Compared to the covalent adduct between BF_3 and NH_3, Ghosh and Bhattacharyya[154] used density functional theory to predict a charge transfer of 0.264178 in the F_3B-NH_3 adduct. The reaction energy involved in forming DES (ΔE) is lower compared to conventional covalent bond as seen in F_3B-NH_3 (Table 4.4). Apart from charge transfer serving as an index of solvent polarity, dipole moment (the chief quantitative descriptor of molecular charge distribution[165]), of all the raw materials and DES were calculated. Dipole moments between the hydrogen bond donors shows that, the molecules undergo conformational reorientation in the presence of the HBA in forming the DES. For example, in 2BA, 2VA, and 2CA, the dipole moment of these donors was close to zero, however, the dipole moments increase to approximately 12 Debye in [Ch]Cl:BA 1:2, [Ch]Cl:VA 1:2, and [Ch]Cl:CA 1:2 HDES (Table 4.4). This data provides the molecular basis why two carboxylic acids are required to form carboxylic acid-based DES[35].

4.4. Conclusions

A modest attempt to study the electronic and molecular properties of carboxylic acid-based DES by conventional solvatochromic assay and density functional theory was studied. A bathochromic shift was observed when [Ch]Cl:BA 1:3 DES interacts with solute (Nile red), signifying polarity of the DES. An increase in the alkyl chain in the HBD

decreases polarity making the DES an ideal candidate to be classified as hydrophobic. The Kamlet-Taft parameters of the synthesized HDES were comparable to selected ionic liquids and organic solvents in literature. We further confirmed our experimental data by using quantum theoretical calculations through DFT/B3LYP methods with 6-31G (d) basis set. The global hardness, chemical stability, and chemical reactivity gives more insight on the electronic properties of the HBA, HBDs, and the DES. The high dipole moment and charge transfer (an index of polarity) of the simulated DES show a similar trend to the experimental (solvatochromic) data. The results presented herein also gives more insight into the molecular basis as to why two carboxylic acids are necessary to form carboxylic acid-based DES.

CHAPTER FIVE

CONCLUSIONS

5.1. Summary

Solvents are invaluable media used day-to-day by textile, pharmaceutical, and chemical industries. Designing green solvents capable of replacing toxic volatile organic compounds is necessary for health and environmental sustainability. This dissertation explored how to design a new set of hydrophilic deep eutectic solvents using choline chloride, choline bromide, and choline iodide as the QAS.

In Chapter 2, we explored that anions interact with hydrogen-bond donors through hydrogen bonding to depress the melting point of the solvent. Changing the anions of the QAS affects the physical and chemical characteristics of the DES. In terms of the flow pattern, the DES formed with choline iodide appears solid at room temperature. The color of the DES usually depends on the nature of the constituents. Anions affect the intensity of the molecular vibrations occurring in the solvent. This accounts for the variation of the dipole moments due to electronegativity changes of the anion. The thermophysical parameter, density, changes as the anion changes. As expected, the bigger the size of the anion, the higher the density of the DES. DES synthesized from [Ch]Br has density $\leq$1.26 g cm^{-3} whereas DES from [Ch]Cl is $\leq$1.25 g cm^{-3}. Although traditional gravimetric method was used to determine the density of the DES, the results are comparable to simulated data which validates the accuracy of the gravimetric method. Parameters such as refractive index, polarity, viscosity-temperature relationship, pH, conductivity, and melting showed that varying anions significantly impacts on the DES. A thermal-stability studies showed

choline bromide as most stable QAS compared to choline chloride by thermogravimetric analysis. With the help computational simulations, we found that anions contribute significantly to the lowering of the DES vapor pressure. The significantly lower vapor pressure of DES compared to glycols (< 0.01 kPa), make DES a suitable solvent to implement in the industry, especially for the dehydration of natural gases. Also, the chapter concludes by showing how anions in QAS alter the thermodynamic activity coefficient at infinite dilution for both water and methanol.

Due to the increasing publications on hydrophilic DES, Chapter 3 of this dissertation looked into designing a hydrophobic DES from choline chloride and fatty acids. In addition to the already physicochemical parameters mentioned, thermodynamic water activity, chemical shift by NMR, and Kamlet-Taft polarity indices were studied. The synthesized HDES exhibited low a_w depicting the hydrophobicity of the solvent. To investigate how HDES behave at different molar ratio, in response to hydrogen bonding, we coupled the FTIR spectra with unsupervised statistical principal component analysis. The hydrogen bonding pattern of the newly synthesized HDES was compared to already known DES. The results expand our understating on why hydrogen bonding constitute a major driving force for DES formation. The synthesized HDES was applied to extract piperine from black pepper. Herein, we reported extraction yield of about 70% by using HDES from choline chloride and butyric acid. In general, peppercorns were found to have higher piperine content than ground black pepper.

In Chapter 4, we investigated the electronic and molecular properties of HDES via solvatochromic molecular probes and density functional theory. A bathochromic shift observed in Nile red molecular probe indicates [Ch]Cl:BA 1:2 as the most polar HDES

among those synthesized. Also, optimization of the HDES molecular geometry indicated a reduced bond angle between the atoms in choline chloride. These results signify that during hydrogen bonding, a change in electronegativity of the central atom (O16) in choline chloride occurs. Thus, a possible molecular reorientation occurs between the donor and the acceptor molecules during DES formation.

5.2. Challenges, Opportunities, and Perspectives

Despite the numerous advantages of HDES in analytical extraction, some of the notable limitations of the solvent are high viscosity and difficulty in phase separation during liquid-liquid extraction [55]. Since the viscosity of DES depends on the hydrogen bond strength of the solvent, understanding the electronic and molecular interaction between HBD and HBA occurring in HDES is an invaluable opportunity to explore. Also, an investigation into HDES polarity by using solvatochromic molecular probes to measure hydrogen-bonding acidity, hydrogen bonding basicity, and dipolarity/polarizability should be encouraged to curtail phase separation problems. Due to the ever-increasing applications of HDES, *in silico* models for predicting extraction efficiencies would be vital for future applications. For example, a PC-SAFT 'pseudo-pure' method was used for the modeling of CO_2 solubilities in HDES[168], a potential application in CO_2 capture. Developing such models to predict extraction efficiency and physicochemical and thermodynamic properties like viscosity, density, activity coefficient, and vapor pressure would cut-down cost and save time and labor. Also, for the first time, Dietz et al.[169] impregnated hydrophobic DES (DecA:N_{8888}-Br, DecA:thymol, DecA:menthol, and thymol:lidocaine) in a polyethylene support enhanced the separation of furfural and hydroxymethylfurfural

from aqueous solutions. A significant transport of furfural and hydroxymethylfurfural through the polymeric membrane support was obtained by using HDES supported liquid membranes made from M3202B and thymol-lidocaine (2:1)[169]. Opportunities in tunneling HDES viscosity for enhanced transport and yield would be interested to study[169].

Applications of HDES in biomass processing, drug solubilization and delivery, biofuels, and electrochemistry are underexplored hence an opportunity for researchers to tailor HDES polarity for these applications. Ternary HDES systems involving water or polar solvent addition may be worthy of exploring to meet specific challenges. For example, in electrochemistry, for the first time, Ruggeri et. al[170] demonstrated that addition of small water to tetrabutylammonium chloride and decanoic acid HDES (1:2) improved the electrical conductivity and viscosity of the solvent, and subsequently employed the HDES to extract Cr(VI) species from an aqueous environment.

Although, HDES are considered as green solvents, little has been done to monitor its toxicity, vapor pressure, and bioavailability. The measurement of octanol-water partition coefficient of HDES should be encouraged for predicting the environmental fate of the solvents. Since the hydrophobicity of HDES is relative, a clear distinction between hydrophilic and hydrophobic DES are sometimes confusing and hence a guideline for calling DES hydrophobic should be established.

REFERENCES

1. Harremoës, P.; Gee, D.; MacGarvin, M.; Stirling, A.; Keys, J.; Wynne, B.; Vaz, S. G., *The precautionary principle in the 20th century: Late lessons from early warnings*. Routledge: 2013.

2. Alfonsi, K.; Colberg, J.; Dunn, P. J.; Fevig, T.; Jennings, S.; Johnson, T. A.; Kleine, H. P.; Knight, C.; Nagy, M. A.; Perry, D. A., Green chemistry tools to influence a medicinal chemistry and research chemistry based organisation. *Green Chemistry* **2008,** *10* (1), p 31-36.

3. Sainio Sr, M. A., Neurotoxicity of solvents. In *Handb. Clin. Neurol.*, Elsevier: 2015; Vol. 131, p 93-110.

4. Trost, B. M., The atom economy--a search for synthetic efficiency. *Science* **1991,** *254* (5037), p 1471-1477.

5. Trost, B. M., Atom economy—a challenge for organic synthesis: homogeneous catalysis leads the way. *Angewandte Chemie International Edition in English* **1995,** *34* (3), p 259-281.

6. Sheldon, R. A., Organic synthesis-past, present and future. *Chem. Ind.* **1992,** (23), 903-6.

7. Anastas, P. T.; Warner, J. C., *Green chemistry: theory and practice*. Oxford university press Oxford: 2000; Vol. 30.

8. Byrne, F. P.; Jin, S.; Paggiola, G.; Petchey, T. H.; Clark, J. H.; Farmer, T. J.; Hunt, A. J.; McElroy, C. R.; Sherwood, J., Tools and techniques for solvent selection: green solvent selection guides. *Sustainable Chem. Processes* **2016,** *4* (1), p 1-24.

9. Enander, R. T.; Gute, D. M.; Cohen, H. J.; Brown, L. C.; Desmaris, A. M. C.; Missaghian, R., Chemical characterization of sanding dust and methylene chloride usage in automotive refinishing: implications for occupational and environmental health. *AIHA Journal* **2002,** *63* (6), p 741-749.

10. Wasserscheid, P.; Welton, T., *Ionic liquids in synthesis*. John Wiley & Sons: 2008.

11. Dai, Y.; van Spronsen, J.; Witkamp, G.-J.; Verpoorte, R.; Choi, Y. H., Ionic liquids and deep eutectic solvents in natural products research: mixtures of solids as extraction solvents. *J. Nat. Prod.* **2013,** *76* (11), p 2162-2173.

12. Hurley, F. H.; Wier, T. P., Electrodeposition of metals from fused quaternary ammonium salts. *Journal of the Electrochemical Society* **1951,** *98* (5), p 203-206.

13. Hurley, F. H., Electrodeposition of aluminum. Google Patents: 1948.

14. Wasserscheid, P.; Keim, W., Ionic liquids—new "solutions" for transition metal catalysis. *Angewandte Chemie International Edition* **2000,** *39* (21), p 3772-3789.

15. Rogers, R. D.; Seddon, K. R., Ionic liquids--solvents of the future? *Science* **2003,** *302* (5646), p 792-793.

16. Marsh, K. N.; Deev, A.; Wu, A. C.; Tran, E.; Klamt, A., Room temperature ionic liquids as replacements for conventional solvents–A review. *Korean Journal of Chemical Engineering* **2002,** *19* (3), p 357-362.

17. Pham, T. P. T.; Cho, C.-W.; Yun, Y.-S., Environmental fate and toxicity of ionic liquids: a review. *Water research* **2010,** *44* (2), p 352-372.

18. Pandey, S., Analytical applications of room-temperature ionic liquids: A review of recent efforts. *Anal. Chim. Acta* **2006,** *556* (1), p 38-45.

19. Blanchard, L. A.; Hancu, D.; Beckman, E. J.; Brennecke, J. F., Green processing using ionic liquids and CO 2. *Nature* **1999,** *399* (6731), p 28.

20. Carmichael, A. J.; Earle, M. J.; Holbrey, J. D.; McCormac, P. B.; Seddon, K. R., The Heck reaction in ionic liquids: a multiphasic catalyst system. *Organic Letters* **1999,** *1* (7), p 997-1000.

21. Egorova, K. S.; Ananikov, V. P., Fundamental importance of ionic interactions in the liquid phase: A review of recent studies of ionic liquids in biomedical and pharmaceutical applications. *J. Mol. Liq.* **2018**.

22. Iqbal, B.; Muhammad, N.; Jamal, A.; Ahmad, P.; Khan, Z. U. H.; Rahim, A.; Khan, A. S.; Gonfa, G.; Iqbal, J.; Rehman, I. U., An application of ionic liquid for preparation of homogeneous collagen and alginate hydrogels for skin dressing. *J. Mol. Liq.* **2017,** *243*, p 720-725.

23. Zhao, Q.; Chu, H.; Zhao, B.; Liang, Z.; Zhang, L.; Zhang, Y., Advances of ionic liquids-based methods for protein analysis. *TrAC Trends in Analytical Chemistry* **2018**.

24. Balraj, A.; Ramalingam, A.; Jayaraman, D., Potential applications of ionic liquids (IL) for the treatment of synthetic turbid water (STW). *J. Mol. Liq.* **2018,** *256*, p 121-126.

25. Meksi, N.; Moussa, A., A review of progress in the ecological application of ionic liquids in textile processes. *Journal of Cleaner Production* **2017,** *161*, p 105-126.

26. Nargotra, P.; Sharma, V.; Gupta, M.; Kour, S.; Bajaj, B. K., Application of ionic liquid and alkali pretreatment for enhancing saccharification of sunflower stalk biomass for potential biofuel-ethanol production. *Bioresource technology* **2018,** *267*, p 560-568.

27. Kim, B.-K.; Lee, E. J.; Kang, Y.; Lee, J.-J., Application of ionic liquids for metal dissolution and extraction. *Journal of industrial and engineering chemistry* **2018,** *61*, p 388-397.

28. Wilkes, J. S.; Levisky, J. A.; Wilson, R. A.; Hussey, C. L., Dialkylimidazolium chloroaluminate melts: a new class of room-temperature ionic liquids for electrochemistry, spectroscopy and synthesis. *Inorg. Chem.* **1982,** *21* (3), p 1263-1264.

29. Wilkes, J. S.; Zaworotko, M. J., Air and water stable 1-ethyl-3-methylimidazolium based ionic liquids. *Journal of the Chemical Society, Chemical Communications* **1992,** (13), p 965-967.

30. Fannin Jr, A. A.; Floreani, D. A.; King, L. A.; Landers, J. S.; Piersma, B. J.; Stech, D. J.; Vaughn, R. L.; Wilkes, J. S.; Williams, J. L., Properties of 1, 3-dialkylimidazolium chloride-aluminum chloride ionic liquids. 2. phase transitions, densities, electrical conductivities, and viscosities. *The Journal of Physical Chemistry* **1984,** *88* (12), p 2614-2621.

31. Holbrey, J. D.; Seddon, K. R., The phase behaviour of 1-alkyl-3-methylimidazolium tetrafluoroborates; ionic liquids and ionic liquid crystals. *Journal of the Chemical Society, Dalton Transactions* **1999,** (13), p 2133-2140.

32. Bonhote, P.; Dias, A.-P.; Papageorgiou, N.; Kalyanasundaram, K.; Grätzel, M., Hydrophobic, highly conductive ambient-temperature molten salts. *Inorg. Chem.* **1996,** *35* (5), p 1168-1178.

33. Abbott, A. P.; Capper, G.; Davies, D. L.; Munro, H. L.; Rasheed, R. K.; Tambyrajah, V., Preparation of novel, moisture-stable, Lewis-acidic ionic liquids containing quaternary ammonium salts with functional side chainsElectronic supplementary information (ESI)

available: plot of conductivity vs. temperature for the ionic liquid formed from zinc chloride and choline chloride (2∶ 1). *Chemical Communications* **2001,** (19), p 2010-2011.

34. Smith, E. L.; Abbott, A. P.; Ryder, K. S., Deep eutectic solvents (DESs) and their applications. *Chem. Rev.* **2014,** *114* (21), p 11060-11082.

35. Abbott, A. P.; Boothby, D.; Capper, G.; Davies, D. L.; Rasheed, R. K., Deep eutectic solvents formed between choline chloride and carboxylic acids: versatile alternatives to ionic liquids. *J. Am. Chem. Soc.* **2004,** *126* (29), p 9142-9147.

36. Abbott, A. P.; Capper, G.; Davies, D. L.; Rasheed, R. K.; Tambyrajah, V., Novel solvent properties of choline chloride/urea mixtures. *Chemical Communications* **2003,** (1), p 70-71.

37. Pena-Pereira, F.; Namieśnik, J., Ionic liquids and deep eutectic mixtures: sustainable solvents for extraction processes. *ChemSusChem* **2014,** *7* (7), p 1784-1800.

38. Francisco, M.; van den Bruinhorst, A.; Kroon, M. C., Low-transition-temperature mixtures (LTTMs): A new generation of designer solvents. *Angewandte Chemie international edition* **2013,** *52* (11), p 3074-3085.

39. Ruß, C.; König, B., Low melting mixtures in organic synthesis–an alternative to ionic liquids? *Green Chemistry* **2012,** *14* (11), p 2969-2982.

40. Florindo, C.; Oliveira, F.; Rebelo, L.; Fernandes, A. M.; Marrucho, I., Insights into the synthesis and properties of deep eutectic solvents based on cholinium chloride and carboxylic acids. *ACS Sustainable Chemistry & Engineering* **2014,** *2* (10), p 2416-2425.

41. Li, J.-j.; Xiao, H.; Tang, X.-d.; Zhou, M., Green carboxylic acid-based deep eutectic solvents as solvents for extractive desulfurization. *Energy Fuels* **2016,** *30* (7), p 5411-5418.

42. Aroso, I. M.; Craveiro, R.; Rocha, Â.; Dionísio, M.; Barreiros, S.; Reis, R. L.; Paiva, A.; Duarte, A. R. C., Design of controlled release systems for THEDES—therapeutic deep eutectic solvents, using supercritical fluid technology. *Int. J. Pharm.* **2015,** *492* (1-2), p 73-79.

43. Aroso, I. M.; Silva, J. C.; Mano, F.; Ferreira, A. S.; Dionísio, M.; Sá-Nogueira, I.; Barreiros, S.; Reis, R. L.; Paiva, A.; Duarte, A. R. C., Dissolution enhancement of active pharmaceutical ingredients by therapeutic deep eutectic systems. *Eur. J. Pharm. Biopharm.* **2016,** *98*, p 57-66.

44. Imperato, G.; Höger, S.; Lenoir, D.; Koenig, B., Low melting sugar–urea–salt mixtures as solvents for organic reactions—estimation of polarity and use in catalysis. *Green Chemistry* **2006,** *8* (12), p 1051-1055.

45. Imperato, G.; Eibler, E.; Niedermaier, J.; König, B., Low-melting sugar–urea–salt mixtures as solvents for Diels–Alder reactions. *Chemical Communications* **2005,** (9), p 1170-1172.

46. Abbott, A. P.; Capper, G.; Gray, S., Design of improved deep eutectic solvents using hole theory. *Chemphyschem* **2006,** *7* (4), p 803-806.

47. Zhao, B.-Y.; Xu, P.; Yang, F.-X.; Wu, H.; Zong, M.-H.; Lou, W.-Y., Biocompatible deep eutectic solvents based on choline chloride: characterization and application to the extraction of rutin from Sophora japonica. *ACS Sustainable Chemistry & Engineering* **2015,** *3* (11), p 2746-2755.

48. DeSimone, J. M., Practical approaches to green solvents. *Science* **2002,** *297* (5582), p 799-803.

49. Reichardt, C.; Welton, T., *Solvents and solvent effects in organic chemistry*. John Wiley & Sons: 2011.

50. Sheldon, R. A., Green solvents for sustainable organic synthesis: state of the art. *Green Chemistry* **2005,** *7* (5), p 267-278.

51. Jessop, P. G., Searching for green solvents. *Green Chemistry* **2011,** *13* (6), p 1391-1398.

52. Zhang, Q.; Vigier, K. D. O.; Royer, S.; Jérôme, F., Deep eutectic solvents: syntheses, properties and applications. *Chem. Soc. Rev.* **2012,** *41* (21), p 7108-7146.

53. Lozano, P.; Bernal, J. M.; Vaultier, M., Towards continuous sustainable processes for enzymatic synthesis of biodiesel in hydrophobic ionic liquids/supercritical carbon dioxide biphasic systems. *Fuel* **2011,** *90* (11), p 3461-3467.

54. Zhao, H.; Baker, G. A., Ionic liquids and deep eutectic solvents for biodiesel synthesis: a review. *J. Chem. Technol. Biotechnol.* **2013,** *88* (1), p 3-12.

55. van Osch, D. J.; Zubeir, L. F.; van den Bruinhorst, A.; Rocha, M. A.; Kroon, M. C., Hydrophobic deep eutectic solvents as water-immiscible extractants. *Green Chemistry* **2015,** *17* (9), p 4518-4521.

56. Shishov, A.; Bulatov, A.; Locatelli, M.; Carradori, S.; Andruch, V., Application of deep eutectic solvents in analytical chemistry. A review. *Microchem. J.* **2017,** *135*, p 33-38.

57. Patil, U. B.; Shendage, S. S.; Nagarkar, J. M., One-pot synthesis of nitriles from aldehydes catalyzed by deep eutectic solvent. *Synthesis* **2013,** *45* (23), p 3295-3299.

58. Wang, L.; Dai, D. Y.; Chen, Q.; He, M. Y., Rapid, Sustainable, and Gram-Scale Synthesis of Phenols Catalyzed by a Biodegradable Deep Eutectic Mixture in Water. *Asian Journal of Organic Chemistry* **2013,** *2* (12), p 1040-1043.

59. Avalos, M.; Babiano, R.; Cintas, P.; Jimenez, J. L.; Palacios, J. C., Greener media in chemical synthesis and processing. *Angewandte Chemie International Edition* **2006,** *45* (24), p 3904-3908.

60. Hayyan, M.; Mjalli, F. S.; Hashim, M. A.; AlNashef, I. M., A novel technique for separating glycerine from palm oil-based biodiesel using ionic liquids. *Fuel Processing Technology* **2010,** *91* (1), p 116-120.

61. Shahbaz, K.; Mjalli, F.; Hashim, M.; AlNashef, I., Using deep eutectic solvents based on methyl triphenyl phosphunium bromide for the removal of glycerol from palm-oil-based biodiesel. *Energy Fuels* **2011,** *25* (6), p 2671-2678.

62. Francisco, M.; van den Bruinhorst, A.; Kroon, M. C., New natural and renewable low transition temperature mixtures (LTTMs): screening as solvents for lignocellulosic biomass processing. *Green Chemistry* **2012,** *14* (8), p 2153-2157.

63. Dai, Y.; Witkamp, G.-J.; Verpoorte, R.; Choi, Y. H., Natural deep eutectic solvents as a new extraction media for phenolic metabolites in Carthamus tinctorius L. *Analytical chemistry* **2013,** *85* (13), p 6272-6278.

64. Nam, M. W.; Zhao, J.; Lee, M. S.; Jeong, J. H.; Lee, J., Enhanced extraction of bioactive natural products using tailor-made deep eutectic solvents: application to flavonoid extraction from Flos sophorae. *Green Chemistry* **2015,** *17* (3), p 1718-1727.

65. Tang, B.; Zhang, H.; Row, K. H., Application of deep eutectic solvents in the extraction and separation of target compounds from various samples. *Journal of separation science* **2015,** *38* (6), p 1053-1064.

66. Karimi, M.; Dadfarnia, S.; Shabani, A. M. H.; Tamaddon, F.; Azadi, D., Deep eutectic liquid organic salt as a new solvent for liquid-phase microextraction and its application in

ligandless extraction and preconcentraion of lead and cadmium in edible oils. *Talanta* **2015,** *144*, p 648-654.

67. Radošević, K.; Ćurko, N.; Srček, V. G.; Bubalo, M. C.; Tomašević, M.; Ganić, K. K.; Redovniković, I. R., Natural deep eutectic solvents as beneficial extractants for enhancement of plant extracts bioactivity. *LWT-Food Science and Technology* **2016,** *73*, p 45-51.

68. Hizaddin, H. F.; Ramalingam, A.; Hashim, M. A.; Hadj-Kali, M. K., Evaluating the performance of deep eutectic solvents for use in extractive denitrification of liquid fuels by the conductor-like screening model for real solvents. *J. Chem. Eng. Data* **2014,** *59* (11), p 3470-3487.

69. Brett, C. M., Deep eutectic solvents and applications in electrochemical sensing. *Current Opinion in Electrochemistry* **2018,** *10*, p 143-148.

70. Nkuku, C. A.; LeSuer, R. J., Electrochemistry in deep eutectic solvents. *The Journal of Physical Chemistry B* **2007,** *111* (46), p 13271-13277.

71. Durand, E.; Lecomte, J.; Baréa, B.; Piombo, G.; Dubreucq, E.; Villeneuve, P., Evaluation of deep eutectic solvents as new media for Candida antarctica B lipase catalyzed reactions. *Process biochemistry* **2012,** *47* (12), p 2081-2089.

72. Choi, Y. H.; van Spronsen, J.; Dai, Y.; Verberne, M.; Hollmann, F.; Arends, I. W.; Witkamp, G.-J.; Verpoorte, R., Are natural deep eutectic solvents the missing link in understanding cellular metabolism and physiology? *Plant Physiol.* **2011,** *156* (4), p 1701-1705.

73. Dai, Y.; van Spronsen, J.; Witkamp, G.-J.; Verpoorte, R.; Choi, Y. H., Natural deep eutectic solvents as new potential media for green technology. *Anal. Chim. Acta* **2013,** *766*, p 61-68.

74. Paiva, A.; Craveiro, R.; Aroso, I.; Martins, M.; Reis, R. L.; Duarte, A. R. C., Natural deep eutectic solvents–solvents for the 21st century. *ACS Sustainable Chemistry & Engineering* **2014,** *2* (5), p 1063-1071.

75. Dai, Y.; Witkamp, G.-J.; Verpoorte, R.; Choi, Y. H., Natural deep eutectic solvents as a new extraction media for phenolic metabolites in Carthamus tinctorius L. *Analytical chemistry* **2013,** *85* (13), p 6272-6278.

76. Dai, Y.; Verpoorte, R.; Choi, Y. H., Natural deep eutectic solvents providing enhanced stability of natural colorants from safflower (Carthamus tinctorius). *Food chemistry* **2014,** *159*, p 116-121.

77. Liu, Y.; Friesen, J. B.; McAlpine, J. B.; Lankin, D. C.; Chen, S.-N.; Pauli, G. F., Natural deep eutectic solvents: properties, applications, and perspectives. *J. Nat. Prod.* **2018,** *81* (3), p 679-690.

78. Satlewal, A.; Agrawal, R.; Bhagia, S.; Sangoro, J.; Ragauskas, A. J., Natural deep eutectic solvents for lignocellulosic biomass pretreatment: Recent developments, challenges and novel opportunities. *Biotechnology advances* **2018**.

79. de los Ángeles Fernández, M.; Boiteux, J.; Espino, M.; Gomez, F. V.; Silva, M. F., Natural Deep Eutectic Solvents-Mediated Extractions: the way forward for sustainable analytical developments. *Anal. Chim. Acta* **2018**.

80. Lynam, J. G.; Kumar, N.; Wong, M. J., Deep eutectic solvents' ability to solubilize lignin, cellulose, and hemicellulose; thermal stability; and density. *Bioresource technology* **2017,** *238*, p 684-689.

81. Vanda, H.; Dai, Y.; Wilson, E. G.; Verpoorte, R.; Choi, Y. H., Green solvents from ionic liquids and deep eutectic solvents to natural deep eutectic solvents. *Comptes Rendus Chimie* **2018,** *21* (6), p 628-638.

82. Morrison, H. G.; Sun, C. C.; Neervannan, S., Characterization of thermal behavior of deep eutectic solvents and their potential as drug solubilization vehicles. *Int. J. Pharm.* **2009,** *378* (1-2), p 136-139.

83. Rajabi, M.; Ghassab, N.; Hemmati, M.; Asghari, A., Emulsification microextraction of amphetamine and methamphetamine in complex matrices using an up-to-date generation of eco-friendly and relatively hydrophobic deep eutectic solvent. *Journal of Chromatography A* **2018**.

84. Cao, J.; Yang, M.; Cao, F.; Wang, J.; Su, E., Well-designed hydrophobic deep eutectic solvents as green and efficient media for the extraction of artemisinin from Artemisia annua leaves. *ACS Sustainable Chemistry & Engineering* **2017,** *5* (4), p 3270-3278.

85. Phelps, T. E.; Bhawawet, N.; Jurisson, S. S.; Baker, G. A., Efficient and Selective Extraction of 99mTcO4–from Aqueous Media using Hydrophobic Deep Eutectic Solvents. *ACS Sustainable Chemistry & Engineering* **2018**.

86. Deng, W.; Yu, L.; Li, X.; Chen, J.; Wang, X.; Deng, Z.; Xiao, Y., Hexafluoroisopropanol-based hydrophobic deep eutectic solvents for dispersive liquid-liquid microextraction of pyrethroids in tea beverages and fruit juices. *Food Chemistry* **2019,** *274*, p 891-899.

87. Makoś, P.; Przyjazny, A.; Boczkaj, G., Hydrophobic deep eutectic solvents as “green” extraction media for polycyclic aromatic hydrocarbons in aqueous samples. *Journal of Chromatography A* **2018**.

88. Florindo, C.; Romero, L.; Rintoul, I.; Branco, L. C.; Marrucho, I. M., From phase change materials to green solvents: hydrophobic low viscous fatty acid–based deep eutectic solvents. *ACS Sustainable Chemistry & Engineering* **2018,** *6* (3), p 3888-3895.

89. Florindo, C.; Branco, L.; Marrucho, I., Development of hydrophobic deep eutectic solvents for extraction of pesticides from aqueous environments. *Fluid Phase Equilibria* **2017,** *448*, p 135-142.

90. Martins, M. A. R.; Crespo, E. A.; Pontes, P. V.; Silva, L. P.; Bülow, M.; Maximo, G. J.; Batista, E. A. C.; Held, C.; Pinho, S. P.; Coutinho, J. A., Tunable hydrophobic eutectic solvents based on terpenes and monocarboxylic acids. *ACS Sustainable Chemistry & Engineering* **2018**.

91. Ribeiro, B., Poster presentation at the 3rd International Symposium on Green Chemistry. *La Rochelle, France* **2015**.

92. Kislik, V. S., *Solvent extraction: classical and novel approaches*. Elsevier: 2011.

93. Zhu, S.; Zhou, J.; Jia, H.; Zhang, H., Liquid–liquid microextraction of synthetic pigments in beverages using a hydrophobic deep eutectic solvent. *Food chemistry* **2018,** *243*, p 351-356.

94. Laitinen, O.; Suopajärvi, T.; Österberg, M.; Liimatainen, H., Hydrophobic, superabsorbing aerogels from choline chloride-based deep eutectic solvent pretreated and silylated cellulose nanofibrils for selective oil removal. *ACS applied materials & interfaces* **2017,** *9* (29), p 25029-25037.

95. Gilmore, M.; McCourt, E.; Connolly, F.; Nockemann, P.; Swadzba-Kwasny, M.; Holbrey, J. D., Hydrophobic deep eutectic solvents incorporating trioctylphosphine oxide: Advanced liquid extractants. *ACS Sustainable Chemistry & Engineering* **2018**.

96. Gilmore, M.; McCourt, E.; Connolly, F.; Nockemann, P.; Swadzba-Kwasny, M.; Holbrey, J. D., Hydrophobic deep eutectic solvents incorporating trioctylphosphine oxide: Advanced liquid extractants. *ACS Sustainable Chemistry & Engineering* **2018**.

97. Křížek, T.; Bursová, M.; Horsley, R.; Kuchař, M.; Tůma, P.; Čabala, R.; Hložek, T., Menthol-based hydrophobic deep eutectic solvents: Towards greener and efficient extraction of phytocannabinoids. *Journal of Cleaner Production* **2018,** *193*, p 391-396.

98. Cao, J.; Yang, M.; Cao, F.; Wang, J.; Su, E., Tailor-made hydrophobic deep eutectic solvents for cleaner extraction of polyprenyl acetates from Ginkgo biloba leaves. *Journal of Cleaner Production* **2017,** *152*, p 399-405.

99. Tereshatov, E.; Boltoeva, M. Y.; Folden, C., First evidence of metal transfer into hydrophobic deep eutectic and low-transition-temperature mixtures: indium extraction from hydrochloric and oxalic acids. *Green Chemistry* **2016,** *18* (17), p 4616-4622.

100. van Osch, D. J.; Parmentier, D.; Dietz, C. H.; van den Bruinhorst, A.; Tuinier, R.; Kroon, M. C., Removal of alkali and transition metal ions from water with hydrophobic deep eutectic solvents. *Chemical Communications* **2016,** *52* (80), p 11987-11990.

101. Dwamena, A. K., Recent Advances in Hydrophobic Deep Eutectic Solvents for Extraction. *Separations* **2019,** *6* (1), p 9.

102. de María, P. D.; Maugeri, Z., Ionic liquids in biotransformations: from proof-of-concept to emerging deep-eutectic-solvents. *Curr. Opin. Chem. Biol.* **2011,** *15* (2), p 220-225.

103. Garcia, G.; Aparicio, S.; Ullah, R.; Atilhan, M., Deep eutectic solvents: physicochemical properties and gas separation applications. *Energy Fuels* **2015,** *29* (4), 2616-2644.

104. Ma, W.; Row, K. H., Optimized extraction of bioactive compounds from Herba Artemisiae Scopariae with ionic liquids and deep eutectic solvents. *Journal of Liquid Chromatography & Related Technologies* **2017,** *40* (9), p 459-466.

105. Olivier-Bourbigou, H.; Magna, L.; Morvan, D., Ionic liquids and catalysis: Recent progress from knowledge to applications. *Applied Catalysis A: General* **2010,** *373* (1-2), p 1-56.

106. Klamt, A.; Eckert, F., COSMO-RS: a novel and efficient method for the a priori prediction of thermophysical data of liquids. *Fluid Phase Equilibria* **2000,** *172* (1), p 43-72.

107. Eckert, F.; Klamt, A., Fast solvent screening via quantum chemistry: COSMO-RS approach. *AIChE J.* **2002,** *48* (2), p 369-385.

108. Eckert, F.; Klamt, A., COSMOtherm User's Manual, version C2. 1, Release 01.05; COSMOlogic GmbH & Co. *KG: Leverkusen, Germany* **2005**.

109. Klamt, A., Conductor-like screening model for real solvents: a new approach to the quantitative calculation of solvation phenomena. *The Journal of Physical Chemistry* **1995,** *99* (7), p 2224-2235.

110. Reinisch, J.; Klamt, A.; Eckert, F.; Diedenhofen, M., Prediction of the temperature dependence of a polyether–water mixture using COSMOtherm. *Fluid Phase Equilibria* **2011,** *310* (1-2), p 7-10.

111. Klamt, A.; Jonas, V.; Bürger, T.; Lohrenz, J. C., Refinement and parametrization of COSMO-RS. *The Journal of Physical Chemistry A* **1998,** *102* (26), p 5074-5085.

112. Anantharaj, R.; Banerjee, T., COSMO-RS-based screening of ionic liquids as green solvents in denitrification studies. *Ind. Eng. Chem. Res.* **2010,** *49* (18), p 8705-8725.

113. Klamt, A.; Schüürmann, G., COSMO: a new approach to dielectric screening in solvents with explicit expressions for the screening energy and its gradient. *Journal of the Chemical Society, Perkin Transactions 2* **1993,** (5), p 799-805.

114. Klamt, A., The COSMO and COSMO-RS solvation models. *Wiley Interdisciplinary Reviews: Computational Molecular Science* **2018,** *8* (1).

115. Aissaoui, T., Novel contribution to the chemical structure of choline chloride based deep eutectic solvents. *Pharm Anal Acta* **2015,** *6*, 11.

116. Mjalli, F. S.; Naser, J.; Jibril, B.; Alizadeh, V.; Gano, Z., Tetrabutylammonium chloride based ionic liquid analogues and their physical properties. *J. Chem. Eng. Data* **2014,** *59* (7), 2242-2251.

117. Liu, Y.; Daum, P. H., Relationship of refractive index to mass density and self-consistency of mixing rules for multicomponent mixtures like ambient aerosols. *Journal of Aerosol Science* **2008,** *39* (11), p 974-986.

118. Reichardt, C., Pyridinium N-phenolate betaine dyes as empirical indicators of solvent polarity: Some new findings. *Pure Appl. Chem.* **2004,** *76* (10), p 1903-1919.

119. Deye, J. F.; Berger, T. A.; Anderson, A. G., Nile Red as a solvatochromic dye for measuring solvent strength in normal liquids and mixtures of normal liquids with supercritical and near critical fluids. *Analytical Chemistry* **1990,** *62* (6), p 615-622.

120. Martinez, V.; Henary, M., Nile Red and Nile Blue: applications and syntheses of structural analogues. *Chemistry-A European Journal* **2016,** *22* (39), p 13764-13782.

121. Rengstl, D.; Fischer, V.; Kunz, W., Low-melting mixtures based on choline ionic liquids. *Phys. Chem. Chem. Phys.* **2014,** *16* (41), p 22815-22822.

122. Bandrés, I.; Montaño, D. F.; Gascón, I.; Cea, P.; Lafuente, C., Study of the conductivity behavior of pyridinium-based ionic liquids. *Electrochimica Acta* **2010,** *55* (7), p 2252-2257.

123. Vila, J.; Gines, P.; Pico, J.; Franjo, C.; Jimenez, E.; Varela, L.; Cabeza, O., Temperature dependence of the electrical conductivity in EMIM-based ionic liquids: evidence of Vogel–Tamman–Fulcher behavior. *Fluid Phase Equilibria* **2006,** *242* (2), p 141-146.

124. García, G.; Atilhan, M.; Aparicio, S., An approach for the rationalization of melting temperature for deep eutectic solvents from DFT. *Chem. Phys. Lett.* **2015,** *634*, p 151-155.

125. Chen, W.-L.; Lin, S.-T., Explicit consideration of spatial hydrogen bonding direction for activity coefficient prediction based on implicit solvation calculations. *Phys. Chem. Chem. Phys.* **2017,** *19* (31), p 20367-20376.

126. Hayyan, M.; Mbous, Y. P.; Looi, C. Y.; Wong, W. F.; Hayyan, A.; Salleh, Z.; Mohd-Ali, O., Natural deep eutectic solvents: cytotoxic profile. *SpringerPlus* **2016,** *5* (1), p 913.

127. Putnam, R.; Taylor, R.; Klamt, A.; Eckert, F.; Schiller, M., Prediction of infinite dilution activity coefficients using COSMO-RS. *Ind. Eng. Chem. Res.* **2003,** *42* (15), p 3635-3641.

128. Sasidharan, S.; Chen, Y.; Saravanan, D.; Sundram, K.; Latha, L. Y., Extraction, isolation and characterization of bioactive compounds from plants' extracts. *African Journal of Traditional, Complementary and Alternative Medicines* **2011,** *8* (1).

129. Majors, R. E., Practical aspects of solvent extraction. *LC GC North America* **2008,** *26* (12).

130. Cunha, S. C.; Fernandes, J., Extraction techniques with deep eutectic solvents. *TrAC Trends in Analytical Chemistry* **2018**.

131. Zubeir, L. F.; Van Osch, D. J.; Rocha, M. A.; Banat, F.; Kroon, M. C., Carbon dioxide solubilities in decanoic acid-based hydrophobic deep eutectic solvents. *J. Chem. Eng. Data* **2018,** *63* (4), 913-919.

132. Srinivasan, K., Black pepper and its pungent principle-piperine: a review of diverse physiological effects. *Crit. Rev. Food Sci. Nutr.* **2007,** *47* (8), p 735-748.

133. Gorgani, L.; Mohammadi, M.; Najafpour, G. D.; Nikzad, M., Piperine—the bioactive compound of black pepper: from isolation to medicinal formulations. *Comprehensive Reviews in Food Science and Food Safety* **2017,** *16* (1), p 124-140.

134. Butt, M. S.; Pasha, I.; Sultan, M. T.; Randhawa, M. A.; Saeed, F.; Ahmed, W., Black pepper and health claims: a comprehensive treatise. *Crit. Rev. Food Sci. Nutr.* **2013,** *53* (9), p 875-886.

135. Meghwal, M.; Goswami, T., Piper nigrum and piperine: an update. *Phytother. Res.* **2013,** *27* (8), p 1121-1130.

136. Epstein, W. W.; Netz, D. F.; Seidel, J. L., Isolation of piperine from black pepper. *J. Chem. Educ.* **1993,** *70* (7), p 598.

137. Cao, X.; Ye, X.; Lu, Y.; Yu, Y.; Mo, W., Ionic liquid-based ultrasonic-assisted extraction of piperine from white pepper. *Anal. Chim. Acta* **2009,** *640* (1-2), p 47-51.

138. Rathod, S. S.; Rathod, V. K., Extraction of piperine from Piper longum using ultrasound. *Industrial Crops and Products* **2014,** *58*, p 259-264.

139. Yu, G.-W.; Cheng, Q.; Nie, J.; Wang, P.; Wang, X.-J.; Li, Z.-G.; Lee, M.-R., DES-based microwave hydrodistillation coupled with GC-MS for analysis of essential oil from black pepper (Piper nigrum) and white pepper. *Analytical Methods* **2017,** *9* (48), p 6777-6784.

140. Raman, G.; Gaikar, V. G., Microwave-assisted extraction of piperine from Piper nigrum. *Ind. Eng. Chem. Res.* **2002,** *41* (10), p 2521-2528.

141. Finizio, A.; Vighi, M.; Sandroni, D., Determination of n-octanol/water partition coefficient (Kow) of pesticide critical review and comparison of methods. *Chemosphere* **1997,** *34* (1), p 131-161.

142. Velezmoro, C. E.; Meirelles, A. J., Water activity in solutions containing organic acids. *Drying technology* **1998,** *16* (9-10), p 1789-1805.

143. Durand, E.; Lecomte, J.; Villeneuve, P., Are emerging deep eutectic solvents (DES) relevant for lipase-catalyzed lipophilizations? *OCL* **2015,** *22* (4), p D408.

144. Lever, J.; Krzywinski, M.; Altman, N., Points of significance: Principal component analysis. Nature Publishing Group: 2017.

145. Kamil, M.; Asri, M. N. M.; Desa, W. N. S. M.; Ismail, D., Fourier Transform Infrared (FTIR) Spectroscopy and Principal Component Analysis (PCA) of Unbranded Black Ballpoint Pen Inks.

146. Kulkarni, D.; Apte, S. P.; Mary, F.; Sane, R., High performance thin layer chromatographic method for the determination of piperine from *Piper nigrum Linn*. *Indian Drugs-Bombay*- **2001,** *38* (6), p 323-326.

147. Santosh, M.; Shaila, D.; Rajyalakshmi, I.; Rao, I. S., RP-HPLC method for determination of piperine from *Piper longum Linn.* and *Piper nigrum Linn. Journal of Chemistry* **2005,** *2* (2), p 131-135.

148. Carriazo, D.; Serrano, M. C.; Gutiérrez, M. C.; Ferrer, M. L.; del Monte, F., Deep-eutectic solvents playing multiple roles in the synthesis of polymers and related materials. *Chem. Soc. Rev.* **2012,** *41* (14), p 4996-5014.

149. Griffin, P. J.; Cosby, T.; Holt, A. P.; Benson, R. S.; Sangoro, J. R., Charge Transport and Structural Dynamics in Carboxylic-Acid-Based Deep Eutectic Mixtures. *The Journal of Physical Chemistry B* **2014,** *118* (31), p 9378-9385.

150. Maugeri, Z.; de María, P. D., Novel choline-chloride-based deep-eutectic-solvents with renewable hydrogen bond donors: levulinic acid and sugar-based polyols. *Rsc Advances* **2012,** *2* (2), p 421-425.

151. Kosower, E. M., The effect of solvent on spectra. I. A new empirical measure of solvent polarity: Z-values. *J. Am. Chem. Soc.* **1958,** *80* (13), p 3253-3260.

152. Hu, J.; Zhu, W.; Yang, Q.; Qian, G.; Xing, H., Solvatochromic parameters of the binary mixtures of imidazolium chloride ionic liquid plus molecular solvent. *Journal of Applied Solution Chemistry and Modeling* **2014,** *3* (4), p 223-230.

153. Ab Rani, M.; Brant, A.; Crowhurst, L.; Dolan, A.; Lui, M.; Hassan, N. H.; Hallett, J.; Hunt, P.; Niedermeyer, H.; Perez-Arlandis, J., Understanding the polarity of ionic liquids. *Phys. Chem. Chem. Phys.* **2011,** *13* (37), p 16831-16840.

154. Ghosh, D. C.; Bhattacharyya, S., Molecular orbital and density functional study of the formation, charge transfer, bonding and the conformational isomerism of the boron trifluoride (BF3) and ammonia (NH3) donor-acceptor complex. *Int. J. Mol. Sci.* **2004,** *5* (8), p 239-264.

155. Rahman, M. S.; Hossain, S. M.; Rahman, M. T.; Halim, M. A.; Ishtiak, M. N.; Kabir, M., Determination of trace metal concentration in compost, DAP, and TSP fertilizers by neutron activation analysis (NAA) and insights from density functional theory calculations. *Environ. Monit. Assess.* **2017,** *189* (12), p 618.

156. Amalraj, A.; Pius, A., Chemosensor for fluoride ion based on chromone. *J. Fluor. Chem.* **2015,** *178*, p 73-78.

157. Atay, Ç. K.; Kara, Y.; Gökalp, M.; Kara, I.; Tilki, T.; Karci, F., Disazo dyes containing pyrazole and indole moieties: Synthesis, characterization, absorption characteristics, theoretical calculations, structural and electronic properties. *J. Mol. Liq.* **2016,** *215*, p 647-655.

158. Mehranpour, A.; Hashemnia, S., Solvatochromism in Binary Solvent Mixtures by Means of a Penta-tert-butyl Pyridinium N-Phenolate Betaine Dye. *Journal of the Chinese Chemical Society* **2006,** *53* (4), p 759-765.

159. Frisch, M.; Trucks, G.; Schlegel, H.; Scuseria, G.; Robb, M.; Cheeseman, J.; Montgomery, J.; Vreven, T.; Kudin, K.; Burant, J., Gaussian 03, revision C. 02. **2008**.

160. Becke, A. D., A new mixing of Hartree–Fock and local density-functional theories. *The Journal of chemical physics* **1993,** *98* (2), p 1372-1377.

161. Lee, C.; Yang, W.; Parr, R. G., Development of the Colle-Salvetti correlation-energy formula into a functional of the electron density. *Physical review B* **1988,** *37* (2), p 785.

162. Teles, A. R. R.; Capela, E. V.; Carmo, R. S.; Coutinho, J. A.; Silvestre, A. J.; Freire, M. G., Solvatochromic parameters of deep eutectic solvents formed by ammonium-based salts and carboxylic acids. *Fluid Phase Equilibria* **2017**.

163. Pandey, A.; Pandey, S., Solvatochromic probe behavior within choline chloride-based deep eutectic solvents: effect of temperature and water. *The Journal of Physical Chemistry B* **2014,** *118* (50), p 14652-14661.

164. Trivedi, S.; Malek, N. I.; Behera, K.; Pandey, S., Temperature-dependent solvatochromic probe behavior within ionic liquids and (ionic liquid+ water) mixtures. *The Journal of Physical Chemistry B* **2010,** *114* (24), p 8118-8125.

165. Sanderson, R., Partial charges on atoms in organic compounds. *Science* **1955,** *121* (3137), p 207-208.

166. Parr, R. G.; Donnelly, R. A.; Levy, M.; Palke, W. E., Electronegativity: the density functional viewpoint. *The Journal of Chemical Physics* **1978,** *68* (8), p 3801-3807.

167. Gordy, W.; Thomas, W. O., Electronegativities of the elements. *The Journal of Chemical Physics* **1956,** *24* (2), p 439-444.

168. Dietz, C. H.; van Osch, D. J.; Kroon, M. C.; Sadowski, G.; van Sint Annaland, M.; Gallucci, F.; Zubeir, L. F.; Held, C., PC-SAFT modeling of CO2 solubilities in hydrophobic deep eutectic solvents. *Fluid Phase Equilibria* **2017,** *448*, p 94-98.

169. Dietz, C. H.; Kroon, M. C.; Di Stefano, M.; van Sint Annaland, M.; Gallucci, F., Selective separation of furfural and hydroxymethylfurfural from an aqueous solution using a supported hydrophobic deep eutectic solvent liquid membrane. *Faraday Discuss.* **2017,** *206*, p 77-92.

170. Ruggeri, S.; Poletti, F.; Zanardi, C.; Pigani, L.; Zanfrognini, B.; Corsi, E.; Dossi, N.; Salomäki, M.; Kivelä, H.; Lukkari, J., Chemical and electrochemical properties of a hydrophobic deep eutectic solvent. *Electrochimica Acta* **2018**.

171. Crowhurst, L.; Mawdsley, P. R.; Perez-Arlandis, J. M.; Salter, P. A.; Welton, T., Solvent–solute interactions in ionic liquids. *Phys. Chem. Chem. Phys.* **2003,** *5* (13), p 2790-2794.

172. Zhang, S.; Qi, X.; Ma, X.; Lu, L.; Deng, Y., Hydroxyl ionic liquids: the differentiating effect of hydroxyl on polarity due to ionic hydrogen bonds between hydroxyl and anions. *The Journal of Physical Chemistry B* **2010,** *114* (11), p 3912-3920.

173. Khupse, N. D.; Kumar, A., Delineating solute− solvent interactions in binary mixtures of ionic liquids in molecular solvents and preferential solvation approach. *The Journal of Physical Chemistry B* **2010,** *115* (4), p 711-718.

174. Chiappe, C.; Pieraccini, D., Determination of Ionic Liquids Solvent Properties Using an Unusual Probe: The Electron Donor−Acceptor Complex between 4, 4 '-bis (Dimethylamino)-benzophenone and Tetracyanoethene. *The Journal of Physical Chemistry A* **2006,** *110* (14), p 4937-4941.

175. Buhvestov, U.; Rived, F.; Ràfols, C.; Bosch, E.; Rosés, M., Solute–solvent and solvent–solvent interactions in binary solvent mixtures. Part 7. Comparison of the enhancement of the water structure in alcohol–water mixtures measured by solvatochromic indicators. *J. Phys. Org. Chem.* **1998,** *11* (3), p 185-192.

APPENDIX

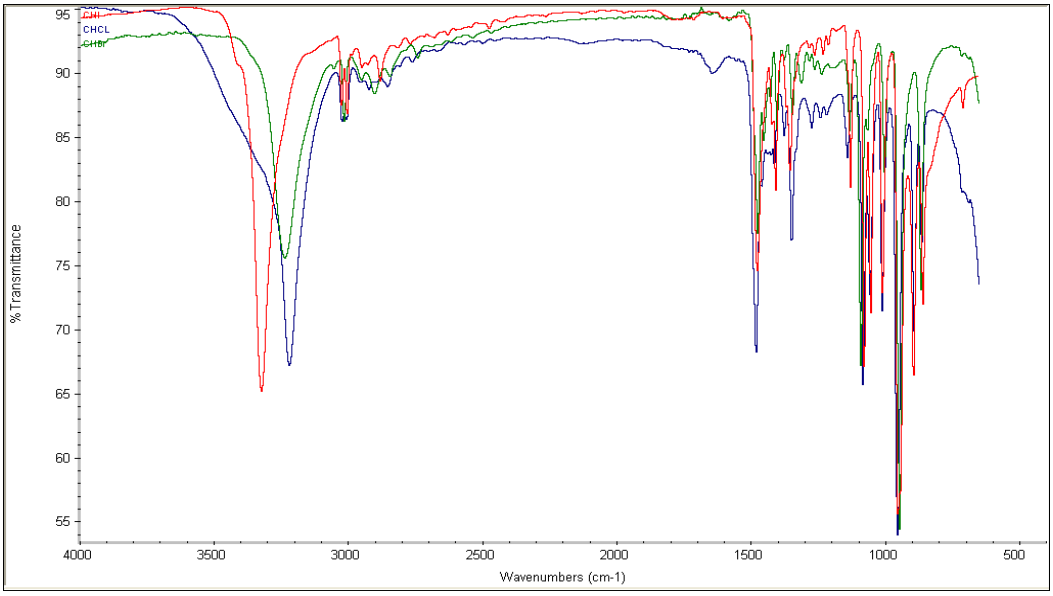

Fig. S2.1. Overlay FTIR spectra of [Ch]Cl (blue), [Ch]Br (green), and [Ch]I (red).

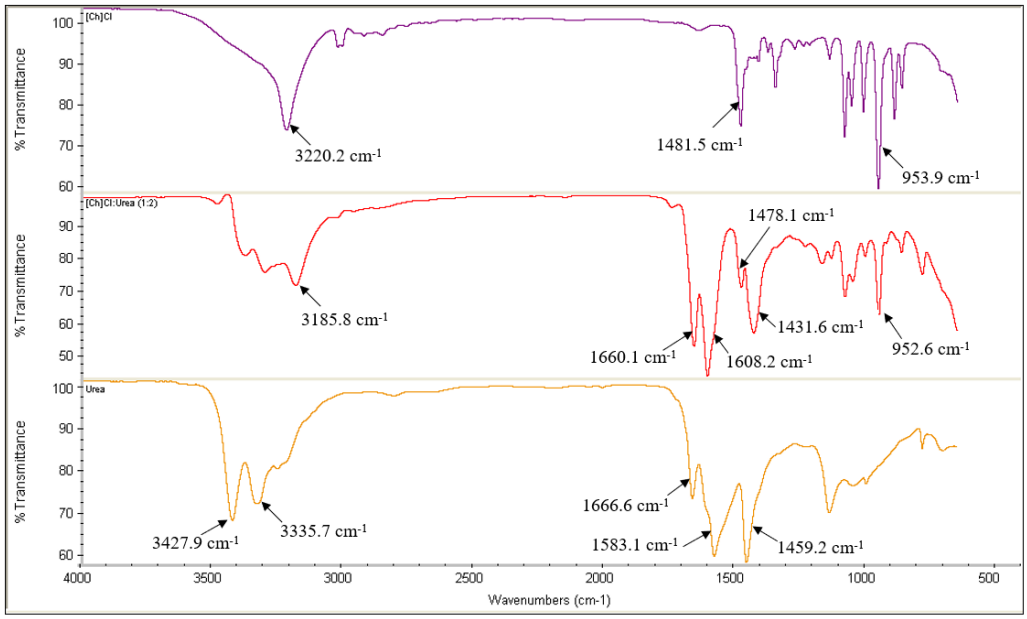

Fig. S2.2. FTIR spectra of [Ch]Cl (pink), [Ch]Cl: urea (red), and urea (orange).

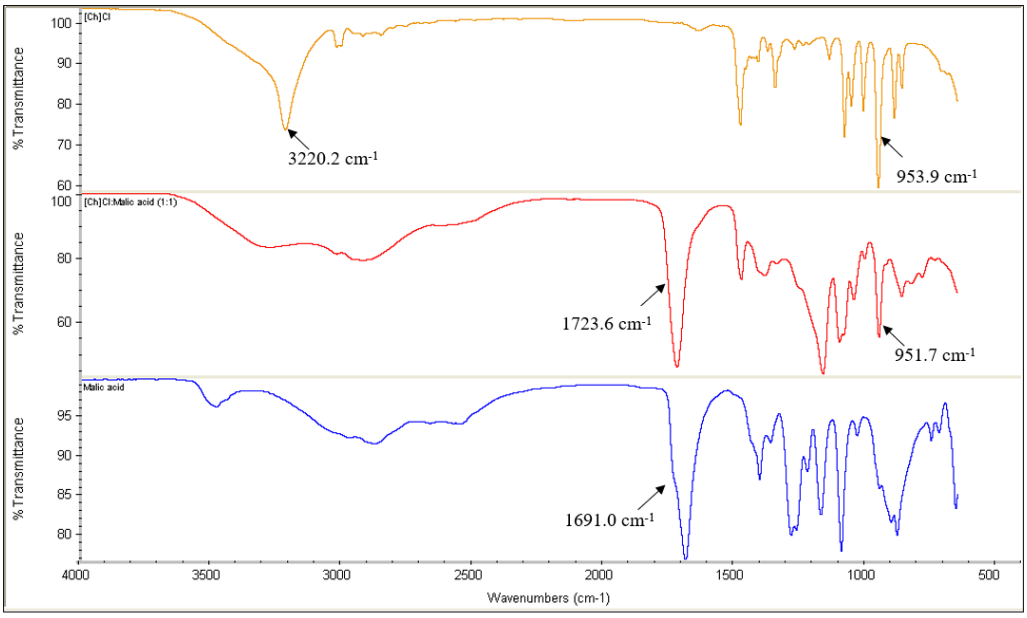

Fig. S2.3. FTIR spectra of [Ch]Cl (orange), [Ch]Cl: malic acid (red), and malic acid (blue).

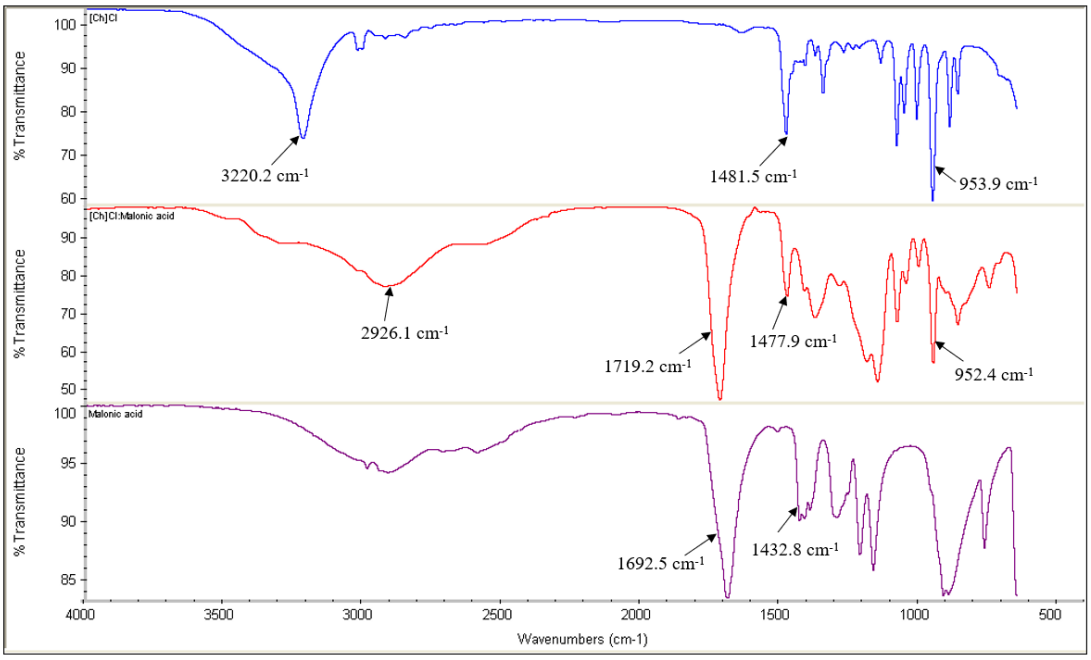

Fig. S2.4. FTIR spectra of [Ch]Cl (blue), [Ch]Cl: malic acid (red), and malic acid (magenta).

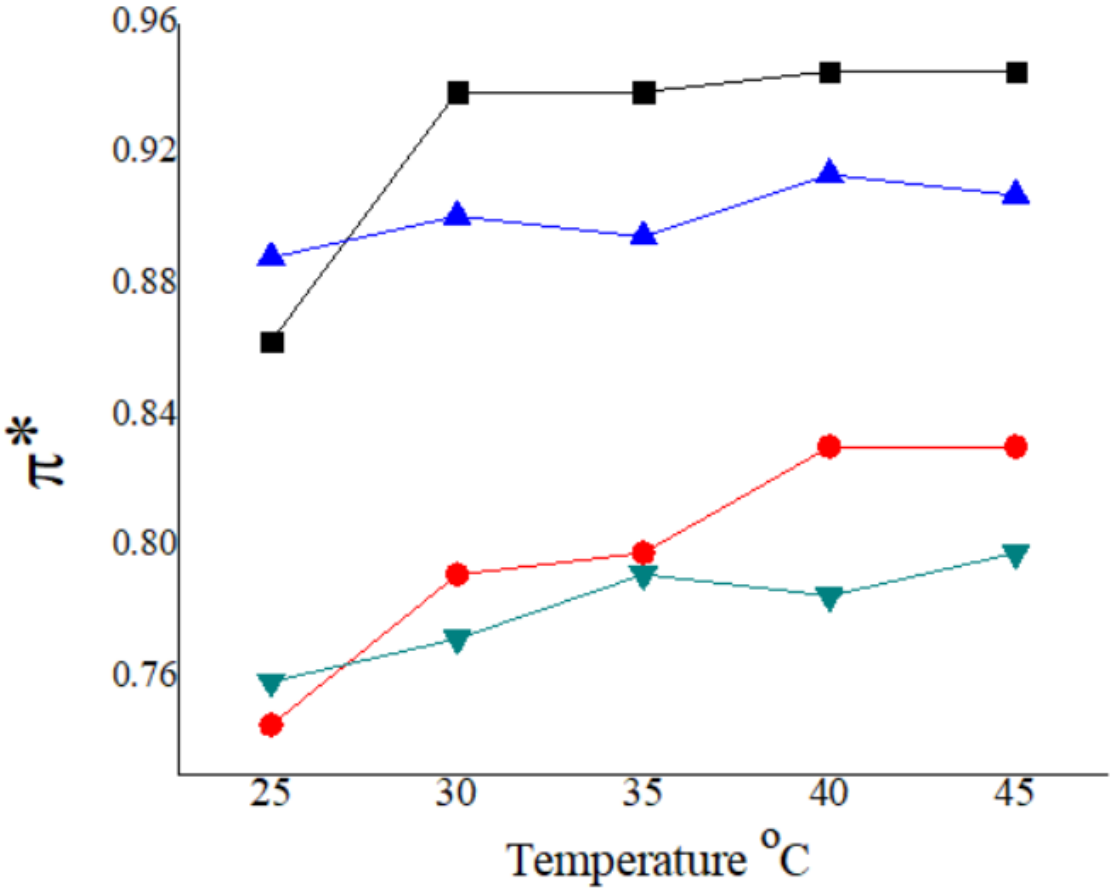

Fig. S4.1. Dipolarity/Polarizability of HDES from 298 K to 318 K. [Ch]Cl:BA 1:2 (black), [Ch]Cl:BA 1:3 (blue), [Ch]Cl:VA 1:2 (red), and [Ch]Cl:VA 1:3 (dark cyan).

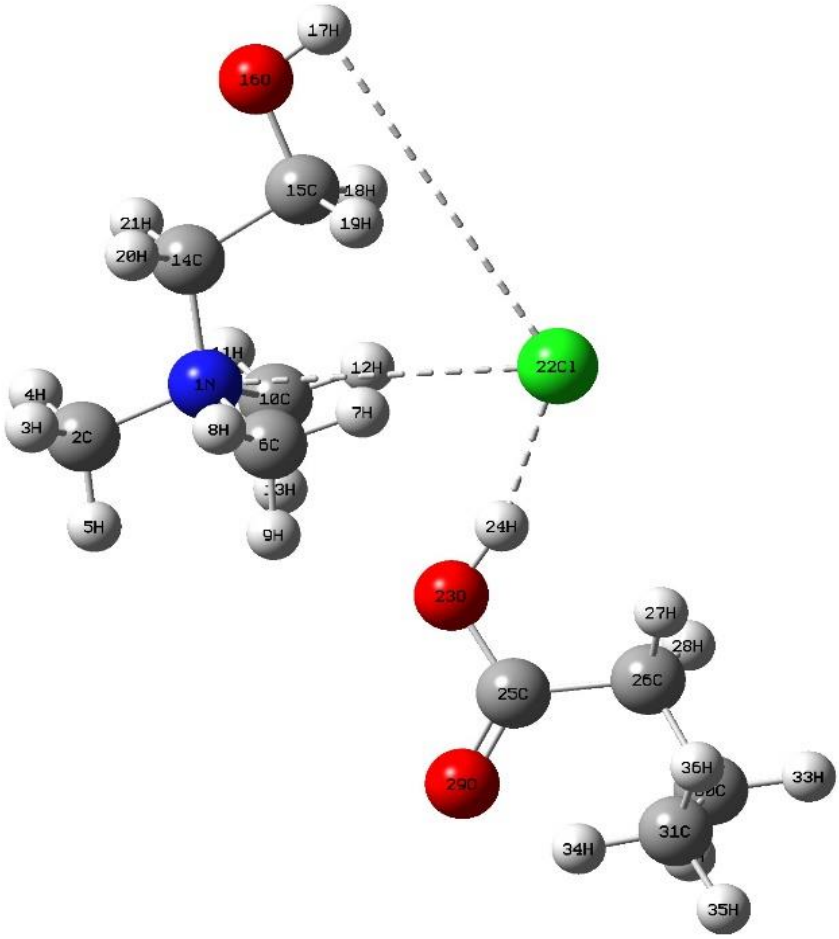

Fig. S4.2. Optimized equilibrium geometry structure of [Ch]Cl:BA by density functional theory (B3LYP). Bond distance between H17-Cl22 (4.81 Å), N1-Cl22 (3.91 Å), and H24-Cl22 (2.04 Å). Bond angle between C14-C15-O16 (102.69 º), C15-O16-H17 (107.40 º), C2-N1-C14 (107.94 º), and N1-C14-C15 (116.54 º).

A)

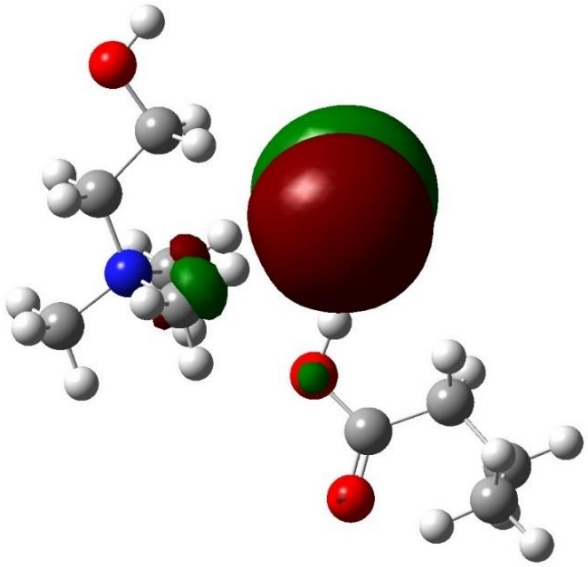

B)

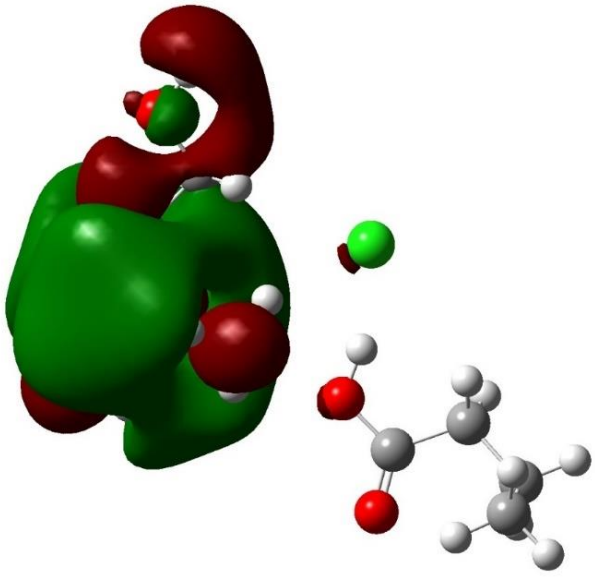

Fig. S4.3. Frontier molecular orbitals of [Ch]Cl:BA HDES*:* **A**) HOMO and **B**) LUMO

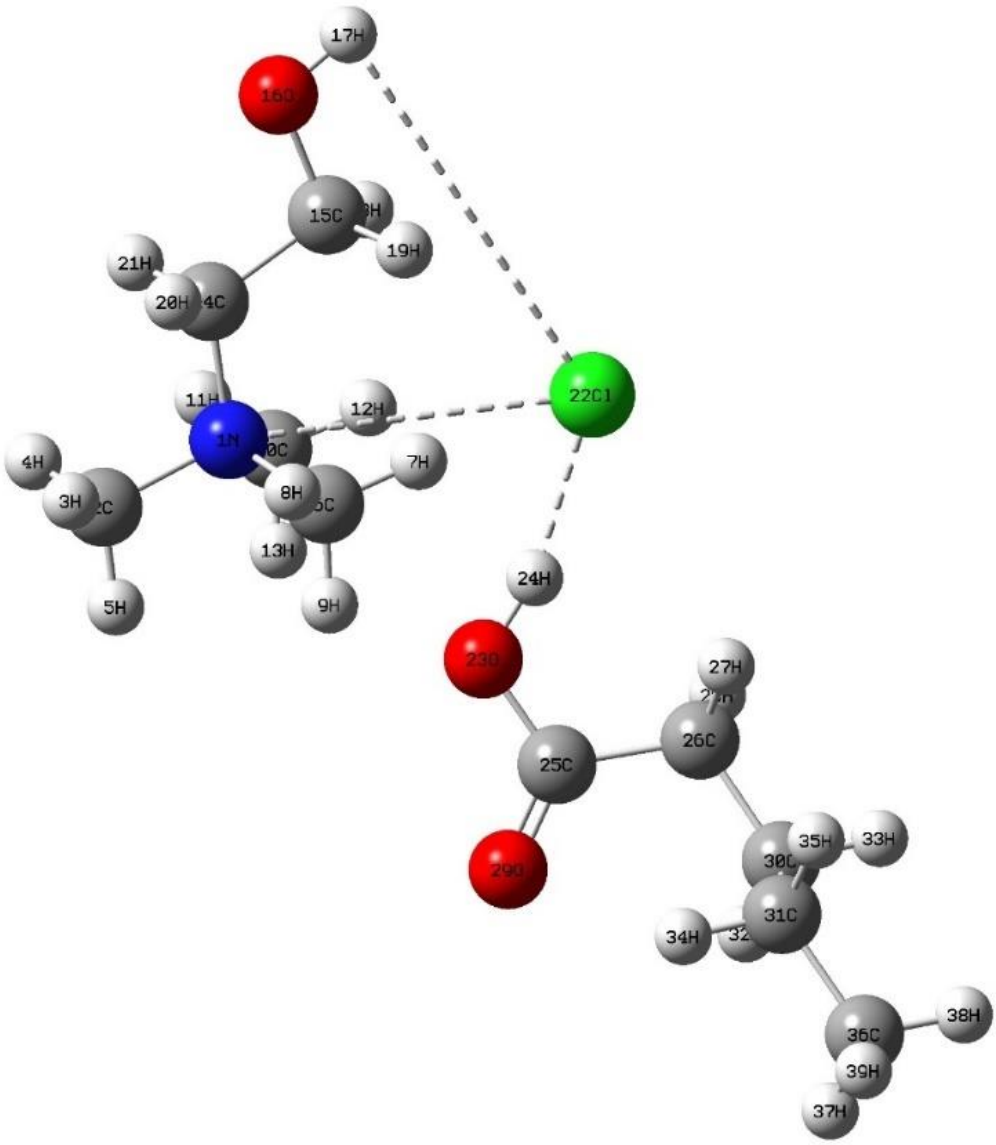

Fig. S4.4. Optimized equilibrium geometry structure of [Ch]Cl:VA by density functional theory (B3LYP). Bond distance between H17-Cl22 (4.80 Å), N1-Cl22 (3.91 Å), and H24-Cl22 (2.04 Å). Bond angle between C14-C15-O16 (102.69 º), C15-O16-H17 (107.40 º), C2-N1-C14 (107.96 º), and N1-C14-C15 (116.53 º).

A)

B)

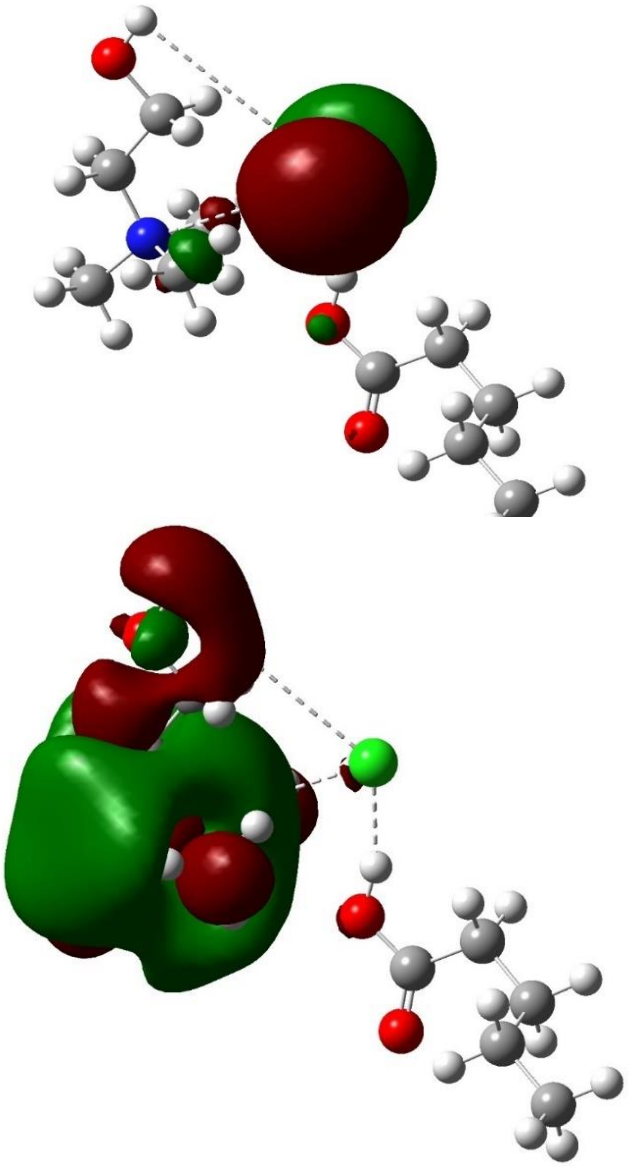

Fig. S4.5. Frontier molecular orbitals of [Ch]Cl:VA HDES: **A**) HOMO and **B**) LUMO

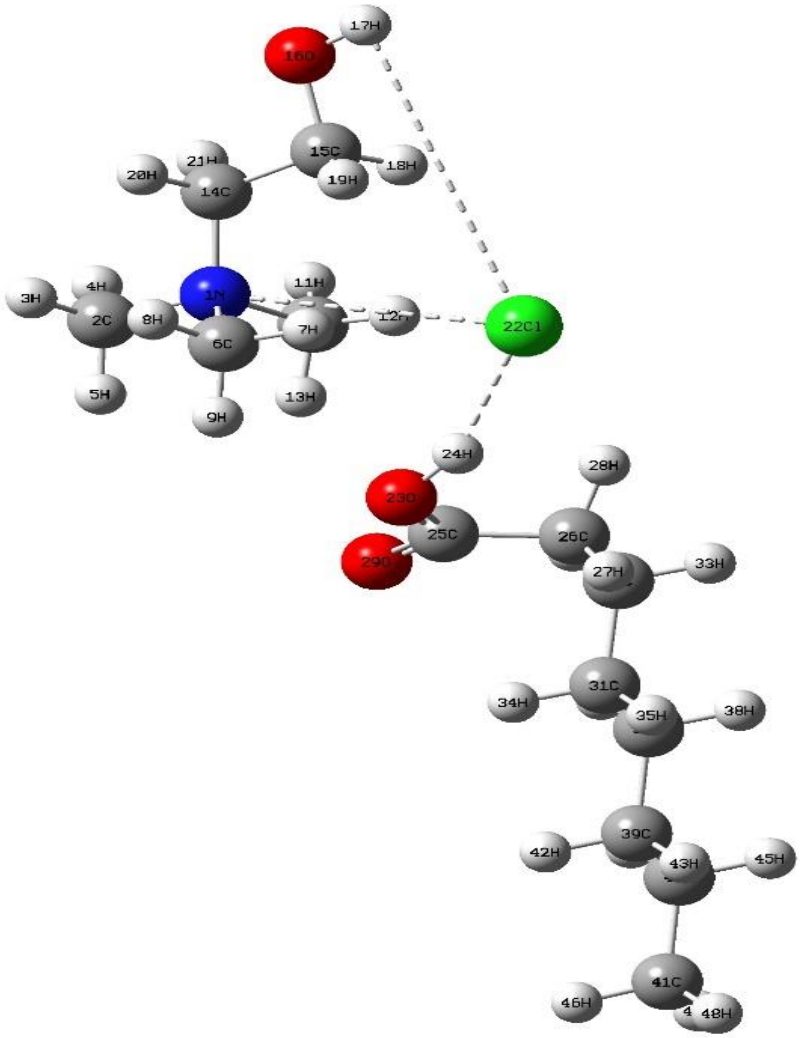

Fig. S4.6. Optimized equilibrium geometry structure of [Ch]Cl:CA by density functional theory (B3LYP). Bond distance between H17-Cl22 (4.77 Å), N1-Cl22 (3.96 Å), and H24-Cl22 (2.05 Å). Bond angle between C14-C15-O16 (102.77 º), C15-O16-H17 (107.33 º), C2-N1-C14 (108.00 º), and N1-C14-C15 (116.44 º).

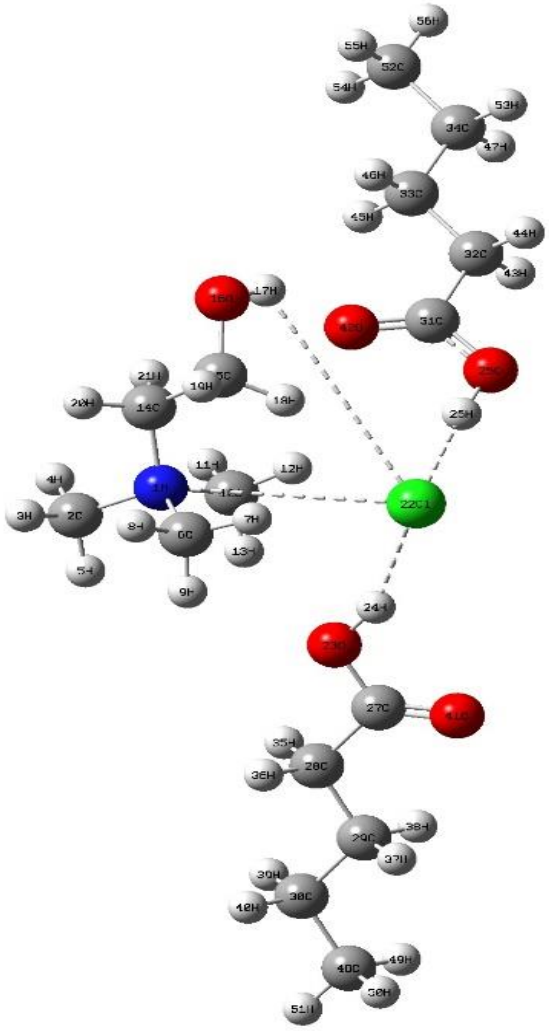

Fig. S4.7. Optimized equilibrium geometry structure of [Ch]Cl:VA 1:2 by density functional theory (B3LYP). Bond distance between H17-Cl22 (4.53 Å), N1-Cl22 (3.99 Å), H24-Cl22 (2.15 Å), and H26-Cl22 (2.05 Å). Bond angle between C14-C15-O16 (107.99 º), C15-O16-H17 (105.01 º), C2-N1-C14 (108.72 º), and N1-C14-C15 (116.09 º).

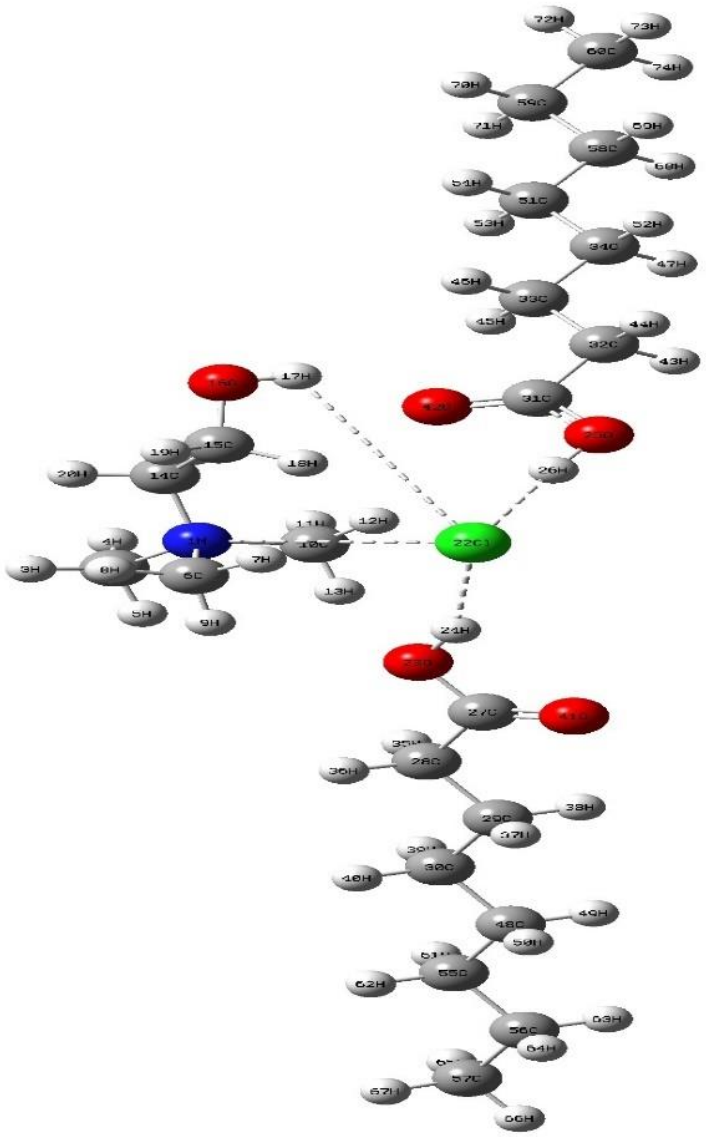

Fig. S4.8. Optimized equilibrium geometry structure of [Ch]Cl:CA 1:2 by density functional theory (B3LYP). Bond distance between H17-Cl22 (4.54 Å), N1-Cl22 (4.00 Å), H24-Cl22 (2.16 Å), and H26-Cl22 (2.05 Å). Bond angle between C14-C15-O16 (108.05 º), C15-O16-H17 (105.02 º), C2-N1-C14 (108.76 º), and N1-C14-C15 (116.09 º).

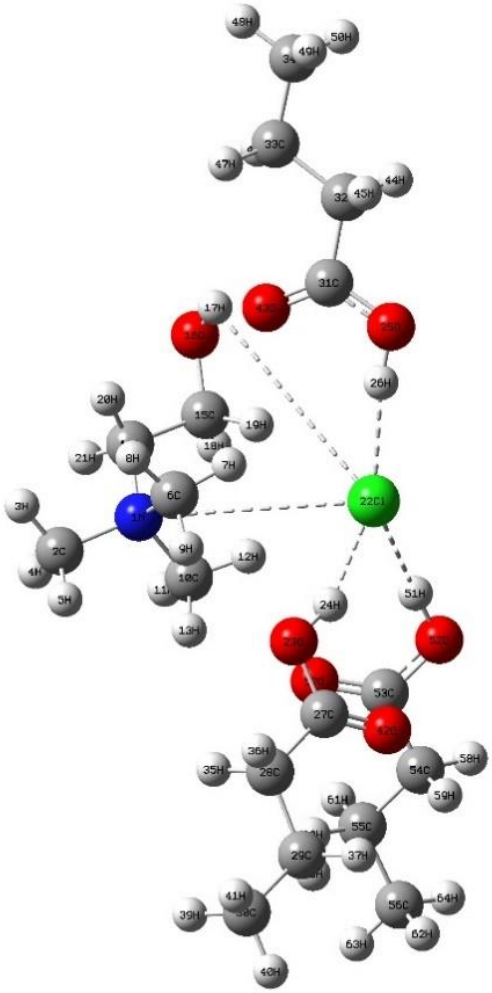

Fig. S4.9. Optimized equilibrium geometry structure of [Ch]Cl:BA 1:3 by density functional theory (B3LYP). Bond distance between H17-Cl22 (4.59 Å), N1-Cl22 (4.08 Å), H24-Cl22 (2.21 Å), H26-Cl22 (2.05 Å), and H51-Cl22 (2.20 Å). Bond angle between C14-C15-O16 (107.96 º), C15-O16-H17 (105.16 º), C2-N1-C14 (108.79 º), and N1-C14-C15 (116.01 º).

A)

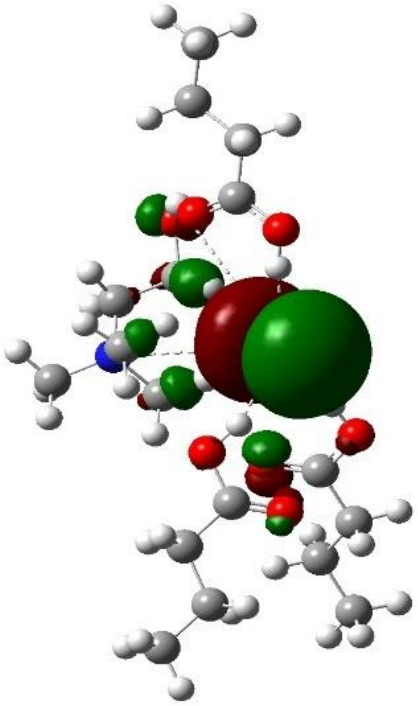

B)

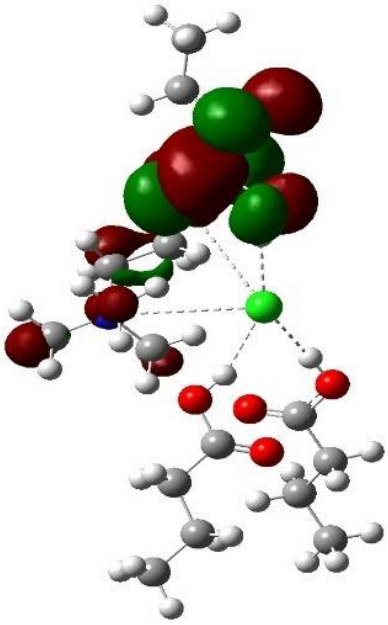

Fig. S4.10. Frontier molecular orbitals of [Ch]Cl:BA 1:3 HDES: **A**) HOMO and **B**) LUMO

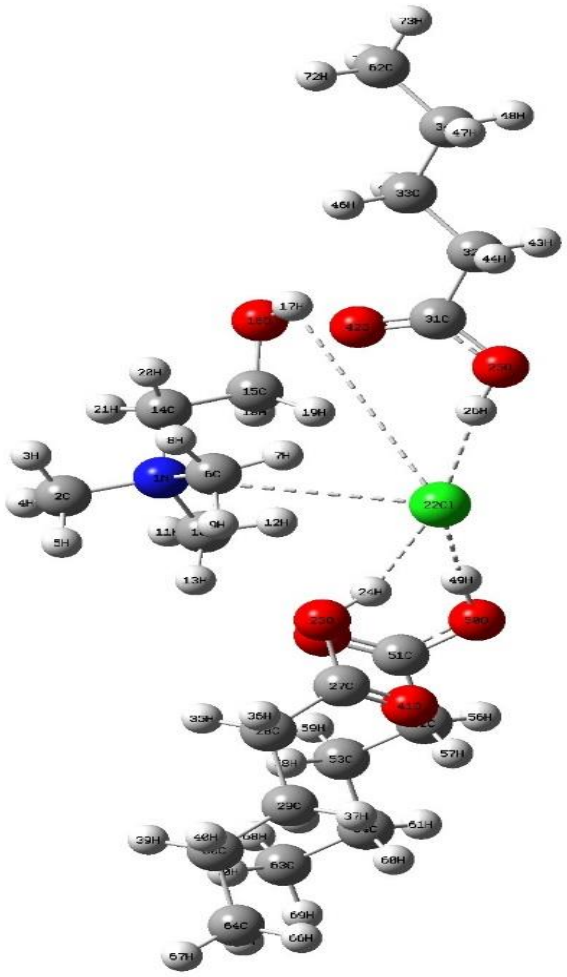

Fig. S4.11. Optimized equilibrium geometry structure of [Ch]Cl:BA 1:3 by density functional theory (B3LYP). Bond distance between H17-Cl22 (4.58 Å), N1-Cl22 (4.08 Å), H24-Cl22 (2.20 Å), H26-Cl22 (2.10 Å), and H49-Cl22 (2.20 Å). Bond angle between C14-C15-O16 (108.04 º), C15-O16-H17 (105.19 º), C2-N1-C14 (108.83 º), and N1-C14-C15 (115.97 º).

Table S4.1. Molecular parameters of choline chloride and carboxylic acids.

HBA and HBDs	Є HOMO (eV)	Є LUMO (eV)	ΔЄ (eV)	μ	χ	η	S	Dipole moment (Debye)
[Ch]Cl	-0.17186	0.01291	0.18477	-0.07948	0.079475	0.092385	5.412134	11.5653
BA	-0.27479	0.01038	0.28517	-0.13221	0.132205	0.142585	3.50668	1.3672
2BA	-0.28011	0.00365	0.28376	-0.13823	0.13823	0.14188	3.524105	0.0002
3BA	-0.26809	0.00071	0.2688	-0.13369	0.13369	0.1344	3.720238	2.294
VA	-0.27462	0.01054	0.28516	-0.13204	0.13204	0.14258	3.506803	1.3438
2VA	-0.27952	0.004	0.28352	-0.13776	0.13776	0.14176	3.527088	0.0245
3VA	-0.26775	0.00125	0.269	-0.13325	0.13325	0.1345	3.717472	2.3368
CA	-0.27448	0.01079	0.28527	-0.13185	0.131845	0.142635	3.505451	1.3059
2CA	-0.27861	0.00435	0.28296	-0.13713	0.13713	0.14148	3.534068	0.0606

Table S4.2. Literature data of ionic liquids and organic solvents used for ternary plot

Solvent	E_T^N	α	β	π*
bmim][SbF_6][171]	0.673	0.639	0.146	1.039
[bmim][BF_4][171]	0.67	0.627	0.376	1.047
[bmim][PF_6][171]	0.669	0.634	0.207	1.032
[bmim][TfO][171]	0.656	0.625	0.464	1.006
[bmim][$N(Tf)_2$][171]	0.644	0.617	0.243	0.984
[bm2im][BF_4][171]	0.576	0.402	0.363	1.083
[bmpy][$N(Tf)_2$][171]	0.544	0.427	0.252	0.954
[bm2im][$N(Tf)_2$][171]	0.541	0.381	0.239	1.01
[EMIm][PF_6][171]	0.676	0.66	0.2	0.99
[EMIm][NTf_2][172]	0.657	0.76	0.28	0.9
[EMIm][ClO_4][172]	0.67	0.56	0.41	1.11
[EMIm][DCA][172]	0.648	0.53	0.35	1.08
[EMIm][NO_3][172]	0.642	0.48	0.66	1.13
[EMIm][AC][172]	0.59	0.4	0.95	1.09
[HOEMIm][PF_6][172]	0.957	1.17	0.15	1.11
[HOEMIm][NTf_2][172]	0.929	1.17	0.34	1.03
[HOEMIm][ClO_4][172]	0.914	1.06	0.16	1.13
[HOEMIm][DCA][172]	0.784	0.8	0.51	1.11
[HOEMIm][NO_3][172]	0.769	0.77	0.65	1.11
[HOEMIm][Cl][172]	0.769	0.73	0.68	1.16
[HOEMIm][AC][172]	0.633	0.53	0.9	1.04
[3-MBP][BF_4][173]	0.651	0.56	0.423	1.071
[4-MP][BF_4][173]	0.636	0.53	0.533	1.066
Acetonitrile[171]	0.46	0.35	0.37	0.799
Acetone[171]	0.35	0.202	0.539	0.704
Dichloromethane[173]	0.309	0.04	0.578	0.733
Toluene[171]	0.1	-0.213	0.077	0.532
Methanol[173]	0.762	1.03	0.578	0.771
1,1,2,2-Tetrachloroethane[174]	0.309	0	0	0.95
Nitrobenzene[174]	0.324	0	0.3	1.01
1,1,1-Trichloroethane[174]	0.17	0	0	0.49
Benzene[174]	0.111	0	0.1	0.59
Acetophenone[174]	0.306	0.04	0.49	0.9
Toluene [174]	0.0099	0	0.11	0.54
1,4-dioxane[174]	0.164	0	0.37	0.55
Cyclohexanone[174]	0.281	0	0.53	0.76
DMSO[174]	0.444	0	0.76	1
Ethyl acetate[174]	0.228	0	0.45	0.55
Tetrahydrofuran[174]	0.207	0	0.55	0.58
Ethanol[175]	-	0.98	0.83	0.51